Communications in

Development and Assembling of Textile Products

Publisher

Principal Contact

Prof. Dr.-Ing. habil. Yordan **Kyosev**

Head of the Chair of Development and Assembly of Textile Products
yordan.kyosev@tu-dresden.de

Support Contact

Dr. Lutz **Kowalke**

journals@qucosa.de

Editorial Team

About the Journal

Aim

The journal **"Communications in Development and Assembling of Textile Products"** (CDATP) **ISSN 2701-939X** is an international, *peer reviewed, pure open access journal.*

It has the mission to offer a forum for scientific exchange in the interdisciplinary area of the *engineering development of textile based products and the technology of their assembling*.

Scope

Topic of interests are **new, not published** research results and materials related to:

- development of products of textiles
- textile materials, their production and parameter identification
- 2D and 3D pattern design
- optimisation and body shape fitting
- 3D/4D scanning, data processing
- cutting and investigations on preparatory processes
- assembling technologies – sewing, welding, gluing, thermoforming, folding, packing
- textile logistics
- recycling of textile products
- numerical modelling of all these processes
- interaction between clothing and human body with all its aspect related to mechanical, thermal, moisture, processes and human body comfort
- biomechanics related to textile product development
- other related topics.

Article types

The journal publishes communications in two types/parts:

A) **peer reviewed journal articles** (research papers, review of state-of-the art papers)
B) *not reviewed communications* in form of reports, data sets, technique reviews, conference papers, abstracts, discussions.

Language

The language of the **peer reviewed articles** is only **English.**

The non-reviewed communications have to be preferably in English, but can be published in German or other languages, too, if the editorial team is able to check the formal level and the quality of the material on this language. In this case title and abstract in English language has to be provided.

Review process for the review articles

Each submission is reviewed from at least four persons.

1. After the submission two of the Editors-in-Chief, or Editor-in-Chief and one Member of the Editorial Board (in case the other Editor-in-Chief is co-author or related to the authors of the manuscript) check the manuscript and decide about its potential for publication.

2. If the novelty and content is suitable two independent reviewers are invited to review the material. In case that their opinion is very different, additional reviewers can be invited.

The review process is **open and transparent for author and reviewers:**

- the reviewers can see the authors of the material
- the author receives the complete feedback of the reviewers, *without their personal data* (**single blind review process**).

Discussions on previous published results are welcome and will be published without review in form of short communication with DOI, too.

The length of the reviewed papers is not limited, but only well structured materials will be considered for publication.

Publication form

The journal is a **purely online journal**, without print issues. All published papers are available as **open access papers** in PDF format under [Creative Commons Attribution-NonCommercial-NoDerivatives 4.0 International License](#).

Formally, all published manuscripts are structured in **two issues per year**.

References

The references have to be formatted following the **ACM reference stlye** https://www.acm.org/publications/authors/reference-formatting

This is available in Citavi, Zotero, Endnote and many other reference managers.

Submissions Template

[Submission template in Word can be downloaded here](www.cdatp.org) www.cdatp.org

Publication charges / Article processing charges

CDATP journal do **not** charge any fees for publication of articles. The costs for DOI and web hosting are covered by the Saxonia State and University Library (SLUB), Dresden and TU Dresden. The work of all editors and production team is voluntary.

Copyright

The authors retain the copyright of their paper without restrictions.

Licensing

All papers are published under Creative Common CC-BY-NC-ND License https://creativecommons.org/licenses/by-nc-nd/4.0/

Plagiarism and self-plagiarism

The editorial team checks first the manuscripts on google.com. In cases of any suspicion using plagiarism or self-plagiarism detection software available at TU Dresden to check the submissions. If plagiarism is detected, the COPE guidelines on plagiarism will be followed.

Publication Ethics and Publication Malpractice Statement

The CDATP journal is committed to maintaining the highest level of integrity in the content published.

This journal follows the COPE *Code of Conduct and Best Practice Guidelines for Journal Editors* and the *Code of Conduct for Journal Publishers*.

Preprint servers

Posting a manuscript on a preprint server or an author personal or institutional webpage (without DOI, publisher) does not count as previous publication. Once the manuscript is accepted and published, the author is responsible to update the preprint record with a publication reference, including the DOI and URL link to the published version.

Repository policy

The authors are encouraged to deposit a copy of their accepted manuscripts papers in an institutional or other repository of their choice, as Accepted version (Author Accepted Manuscript) and as Published version (Version of Record). Authors should provide a link from the deposited version to the DOI and URL of the publication article. The only purpose of this link is to ensure, that the journal's website is clearly identified as the definitive version of record. There is no embargo period for self archiving.

The journal is listed in Romeo Service   https://v2.sherpa.ac.uk/id/publication/39565

Preliminary report on MFM measurements on magnetic nanofiber mats

Raphael Weiss, Andrea Ehrmann*

Bielefeld University of Applied Sciences, Faculty of Engineering and Mathematics, Bielefeld, Germany
*Corresponding author *E-mail address:* andrea.ehrmann@fh-bielefeld.de

INFO

ABSTRACT

Nanofiber mats can be produced unambiguously by electrospinning. Besides pure polymers or polymer blends, such nanofibers can also contain metals, ceramics, etc., often introduced in the form of nanoparticles embedded in the spinning solution. Especially in case of magnetic nanoparticles, the physical properties of the whole nanofiber mats will strongly depend on the dispersion of the nanoparticles in the fibers – while small single nanoparticles may show superparamagnetic behavior, larger agglomerations will rather tend to showing ferromagnetic properties. Investigations of the magnetic properties of a sample with high spatial resolution are mostly performed by magnetic force microscopy (MFM). This technique, however, is usually applied on very flat surfaces of thin-film or nanostructured samples. Here, we report for the first time on MFM measurements on magnetic nanofiber mats, proving in principle that this technique can be used to investigate magnetic nanofiber mats, while the highly uneven nanofiber structure still causes large problems which have to be solved in the future.

1   Introduction

Nanofiber mats are typically produced by electrospinning, i.e. by creating fibers with diameters of some ten to some hundred nanometers in a strong electric field from a polymer solution or melt [1-3]. Such nanofiber mats can be used for diverse applications in which their large surface-to-volume ratio is important, such as wound dressings [4], tissue engineering [5,6], catalyzers [7], or filters [8-10]. Besides man-made polymers [11,12] and biopolymers [13,14], polymers blended with non-solvable materials can also be used for electrospinning [15,16].

In this way, it is also possible to prepare magnetic nanofiber mats for diverse applications [17-19]. Such magnetic nanofibers are also highly interesting for basic research and future applications in spintronics or neuromorphic computing [20-24].

For both basic and applied research, however, it is necessary to characterize the distribution of magnetic nanoparticles inside the fibers. It was shown experimentally and in simulations that modifications of average distances between the nanoparticles, either due to fiber shrinkage during carbonization [25] or due to agglomerations [26], significantly modify the magnetic properties of such nanofibers.

While transmission electron microscopy (TEM) offers the possibility to "look inside" nanofibers and to investigate the nanoparticle distribution in nanofiber mats [26], this method is highly time-consuming, complicated and necessitates expensive equipment which is not available in each university of research institute. It would be ideal to directly map the magnetic properties of such nanofiber mats with sufficient spatial resolution.

A technique which can indeed be used for this purpose is magnetic force microscopy (MFM). Opposite to atomic force microscopy (AFM) which uses a cantilever to detect a sample's topography and possibly some additional mechanical properties of the surface, the MFM uses a magnetized cantilever tip and can thus be applied in a special software mode, allowing for measuring magnetic properties in addition to the sample's topography [27]. There are even a few reports in the literature showing MFM measurements on single magnetic nanofibers or nanowires attached to flat substrates [28-32]. To the best of our knowledge, however, no report was published before on MFM measurements on completely uneven, irregular magnetic nanofiber mats.

Here we report on first results of such MFM measurements on different electrospun magnetic nanofiber mats, prepared with magnetite or nickel-ferrite. We show that MFM can in principle be used to investigate magnetic properties of magnetic nanofiber mats, but further research is necessary to gain clearer images of the spatially resolved magnetic properties.

2 Experimental

Nanofiber mats were electrospun using the wire-based system "Nanospider Lab" (Elmarco, Liberec, Czech Republic) with the following spinning parameters: voltage 80 kV, nozzle diameter 0.9 mm, carriage speed 150 mm/s, distance between lower electrode and substrate 240 mm, distance between substrate and upper electrode 50 mm, relative humidity in the chamber 32 %, temperature 22 °C.

Spinning solutions were prepared from 14 % polyacrylonitrile (PAN) (X-PAN, Dralon, Dormagen, Germany) dissolved in dimethyl sulfoxide (DMSO) (min 99.9%, purchased from S3 chemicals, Bad Oeynhausen, Germany). Fe_3O_4 (magnetite) nanoparticles (50-10 nm diameter, Merck KGaA, Darmstadt, Germany) were either applied by dip-coating from an aqueous solution after electrospinning, or added to the spinning solution in a weight ratio polymer:nanoparticles of 1:1.8, which was the largest nanoparticle concentration found spinnable in an earlier investigation [24,25]. Directly before electrospinning, the dispersion was ultrasonically stirred for 40 min at 35 °C with a frequency of 37 kHz to avoid agglomerations mostly. It should be mentioned that the distribution of the nanoparticles in the fibers is not homogeneous [26], thus no perfect magnetic signals along the whole nanofiber mat can be expected, but parts with strong signals due to agglomerations and completely nonmagnetic parts.

As a reference of a perfectly flat magnetic sample, a cobalt (Co) layer (25 nm thickness) on a silicon (Si) wafer was used. In Co thin films, former investigations found circular and elliptical magnetic bubbles at the remanent state (i.e. without external magnetic field) after saturation [33], so that some magnetic pattern can be expected to be visible here.

AFM images were taken by a FlexAFM Axiom (Nanosurf, Liestal, Switzerland), equipped with a cantilever MagneticMulti75-G (NanoAndMore GmbH, Wetzlar, Germany) and post-processed with Gwyddion 2.51.

3 Results and discussion

Firstly, Fig. 1 shows an AFM topography image and the correlated magnetic MFM image of the flat reference sample. While the topography (Fig. 1a) is nearly flat, besides some fine grains of dust, a clear structure is visible in the MFM images (Fig. 1b) which can be attributed to the magnetic properties of the thin-film sample. Such MFM images are often scaled in black-and-white to enhance the contrast; however, here we decided to use a similar contrast as typical for the topography to allow for seeing all features available in the sample on these relatively large scales.
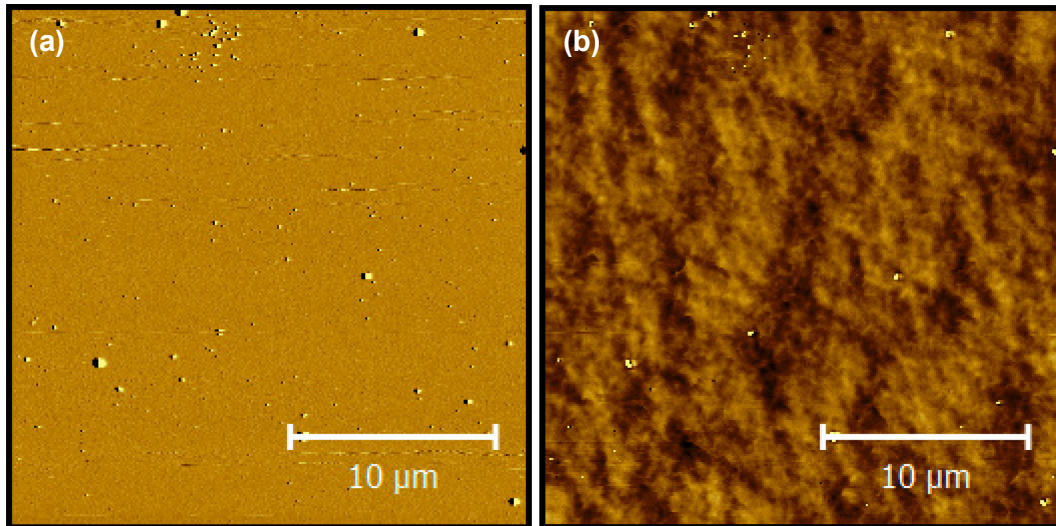
Fig. 1 (a) AFM topography image of a magnetic thin-film sample; (b) MFM phase showing the magnetic properties of the sample

Investigating nanofiber mats with MFM, however, is significantly more complicated since now topography and magnetic properties mix and have to be separated carefully. Fig. 2a shows the topography of a carbonized magnetic nanofiber mat, with some typical errors occurring when the tip touches the fibers, as it happens often when measuring such non-continuous surfaces.

Fig. 2 (a) AFM topography image of a carbonized magnetic nanofiber mat; (b) MFM phase showing the magnetic properties of the sample (tip lift height 30 nm)

The MFM phase depicted in Fig. 2b, however, mostly reflects this topography, although the "contour following" mode should mostly suppress this problem.

MFM measurements are performed in a double-scan process, e.g. by measuring the lowest line in the image from left to right to detect the topography, and then scanning the same path back with the cantilever lifted by a certain distance (here 30 nm) to detect mostly the magnetic force. Alternatively, the so-called "dual pass mode" can be used, meaning that two firstly the topography is scanned from left to right and back, and afterwards the same line is scanned from left to right and back in MFM mode, i.e. with lifted tip, making the image more accurate, but doubling the time for measuring. Generally, in MFM it is necessary to find a compromise between smaller heights during the MFM scanning time, increasing the influence of the topography and making the signals harder to interpret, and larger heights, decreasing the resolution. This is especially important in case of strongly structured surfaces, such as nanofiber mats. Here, apparently, the chosen height was not large enough so that no clear magnetic signal can be observed.

Next, samples were investigated with larger distances. Fig. 3 shows an example of a measurement with a tip lifting height of 170 nm during the MFM scanning time. Indeed, the topography becomes nearly invisible here, now allowing for evaluating the magnetic information. While this would be acceptable for large magnetic structures, as visible in Fig. 1b, it is not sufficient for the investigation of magnetic nanoparticles embedded in (or coated on) nanofibers. Thus, the next step is an optimization of the tip lifting height to enable sufficiently resolved magnetic scans of these challenging samples.
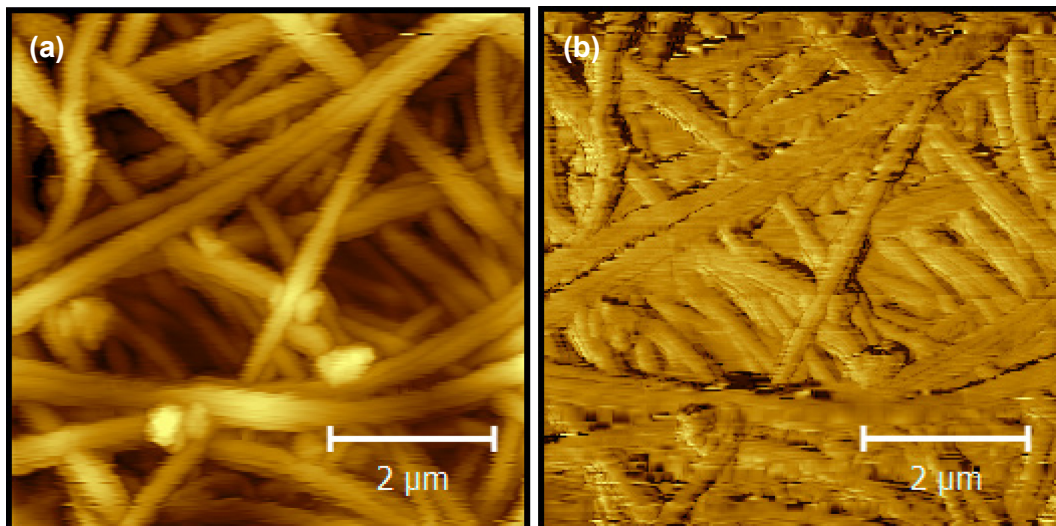

Fig. 3 (a) AFM topography image of a magnetically coated nanofiber mat; (b) MFM phase showing the magnetic properties of the sample (tip lift height 170 nm)

As an example for the influence of the tip lifting height, Fig. 4 shows measurements on the coated nanofiber mat, now again with a slightly reduced magnification, for lift heights of 300 nm (Fig. 4a) and 240 nm (Fig. 4b), respectively.

It is clearly visible that the magnetic structure becomes clearer for the lower tip lift height; but even for the relatively large lift heights chosen here, the nanofibers start becoming visible again. This example shows that while the magnetic features, here visible as large dark and bright areas, can indeed be visualized by MFM, but underline also that in spite of using the "contour follow" mode which should significantly reduce the influence of the topography, the latter cannot be ignored in magnetic investigations of electrospun nanofiber mats.

It must also be mentioned that optimizing the tip lift height is only possible for a specific situation. Fig. 5 shows the same nanofiber mat as depicted in Fig. 4 after slightly shifting the measurement position, measured with identical magnification and measurement parameters as well as with an intermediate tip lift height of 280 nm. Here, however, the topography is much stronger visible than in Fig. 4. This shows again that there is still a long way to go from this first proof-of-principle to a reliable technique which can be used to detect magnetic nanoparticles inside magnetic nanofiber mats.
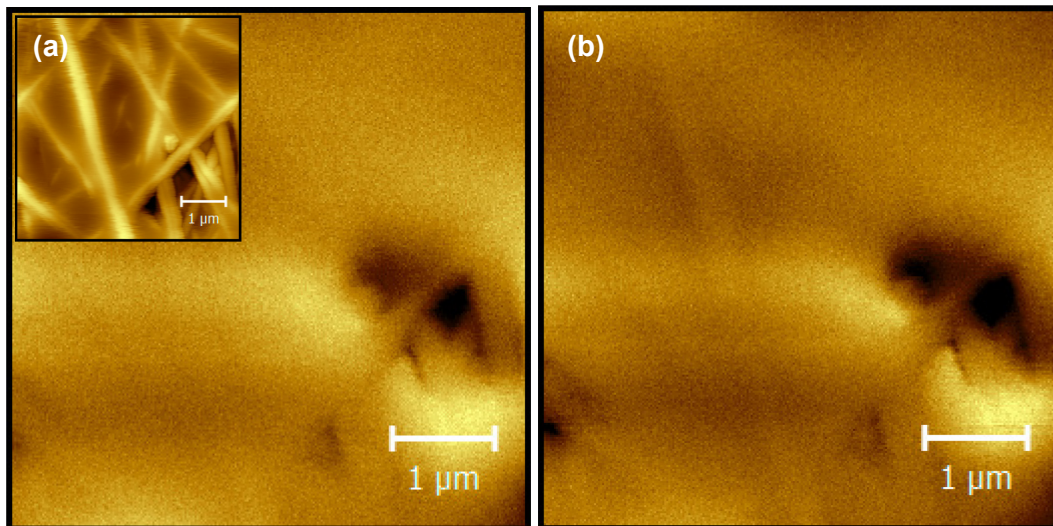
Fig. 4 MFM phases of a magnetically coated nanofiber mat with different tip lift heights: (a) 300 nm; (b) 240 nm. The inset shows the AFM topography.
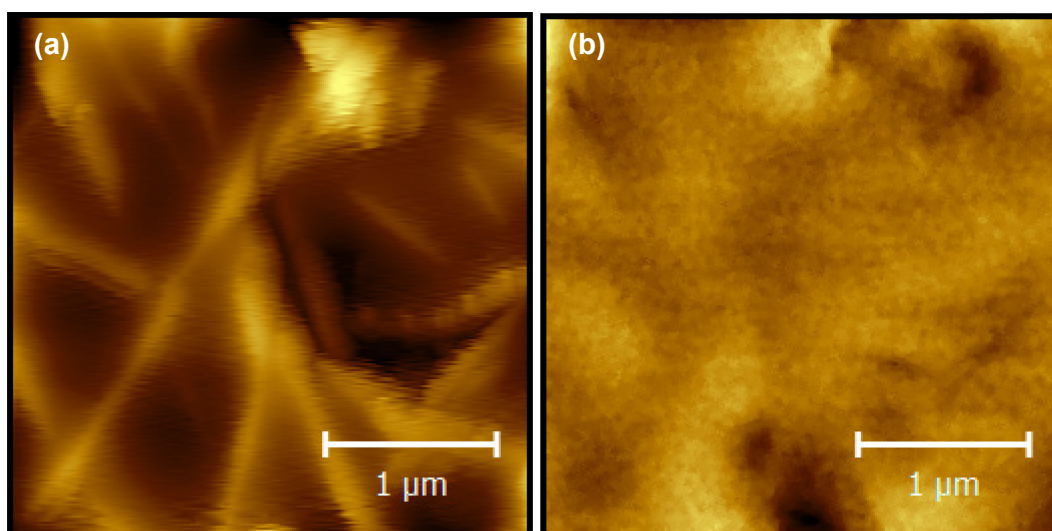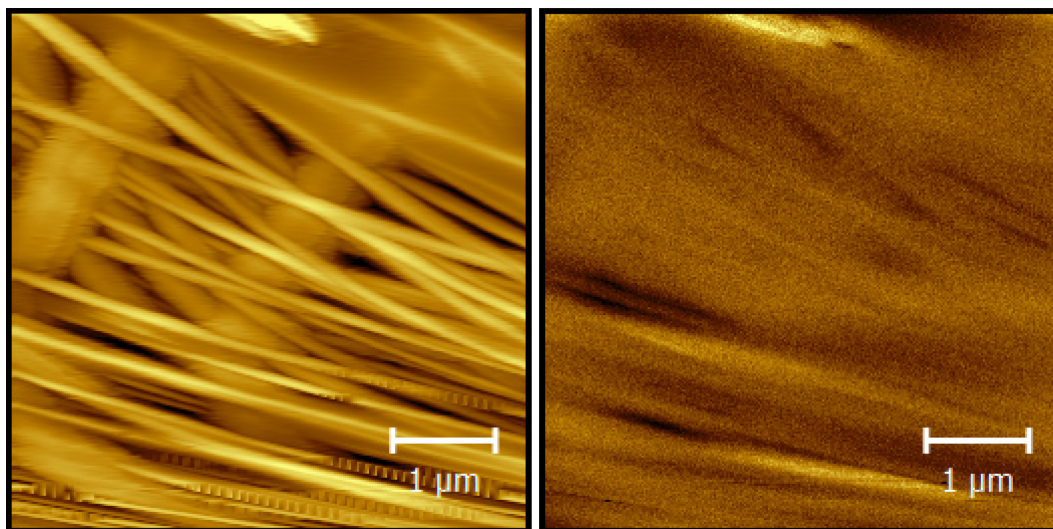

Fig. 5 (a) AFM topography image of a magnetically coated nanofiber mat; (b) MFM phase showing the magnetic properties of the sample (tip lift height 280 nm)

Besides, several further questions, especially related to the possible dimensions of nanoparticle agglomerations which are directly connected with their magnetic properties [26], must be investigated to develop this technique further and to enable a reliable interpretation of MFM images of magnetic nanofiber mats.

4   Conclusions

While magnetic force microscopy (MFM) is a typical tool for the evaluation of magnetic thin-film samples or nanostructures on flat surfaces, no previous attempts were found in the literature to use MFM for the investigation of magnetic nanofiber mats. Here we present first MFM measurements on such magnetic nanofiber mats, showing the general suitability of this method to investigate magnetic nanofiber mats, but also the challenges which have to be taken into account in these measurements.

Since no literature exists yet on measuring MFM on magnetic nanofiber mats, it is necessary to optimize the measurements without drawing on previous experience of other groups. Thus, as the next step it is planned to electrospin aligned magnetic nanofibers [34] to reduce the roughness und to optimize MFM

process parameters for this situation, before transferring this optimization back to isotropic (not oriented) magnetic nanofiber mats.

References

[1] T. Subbiah, G. S. Bhat, R. W. Tock, S. Parameswaran, S. S. Ramkumar. 2005. Electrospinning of nanofibers. *J. Appl. Polymer Sci.* 96, 2, 557-569. DOI: https://doi.org/10.1002/app.21481

[2] D. Li, Y. Xia. 2004. Electrospinning of nanofibers: reinventing the wheel? *Adv. Mater.* 16, 14, 1151-1170. DOI: https://doi.org/10.1002/adma.200400719

[3] A. Greiner, J. H. Wendorff. 2007. Electrospinning: a fascinating method for the preparation of ultrathin fibers. *Angew. Chem. Int. Ed.* 46, 30, 5670-5703. DOI: https://doi.org/10.1002/anie.200604646

[4] A. Mamun. 2019. Review of possible applications of nanofibrous mats for wound dressings. *Tekstilec* 62, 2, 89-100. DOI: https://doi.org/10.14502/Tekstilec2019.62.89-100

[5] N. Ashammakhi, A. Ndreu, Y. Yang, H. Ylikauppila, L. Nikkola. 2012. Nanofiber-based scaffolds for tissue engineering. *Eur. J. Plast. Surg.* 35, 2, 135-149. DOI: https://doi.org/10.1007/s00238-008-0217-3

[6] J. Bockelmann, K. Klinkhammer, A. von Holst, N. Seiler, A. Faissner, G. A. Brook, D. Klee, J. Mey. 2011. Functionalization of electrospun poly(ε-caprolactone) fibers with the extracellular matrix-derived peptide GRGDS improves guidance of Schwann cell migration and axonal growth. *Tissue Eng. A* 17, 3-4, 475-486. DOI: https://doi.org/10.1089/ten.tea.2010.0369

[7] X. Wang, Y. G. Kim, C. Drew, B. C. Ku, J. Kumar, L. A. Samuelson. 2004. Electrostatic assembly of conjugated polymer thin layers on electrospun nanofibrous membranes for biosensors. *Nano Lett.* 4, 2, 331-334. DOI: https://doi.org/10.1021/nl034885z

[8] B. Yalcinkaya, F. Yalcinkaya, J. Chaloupek. 2016. Thin film nanofibrous composite membrane for dead-end seawater desalination. *J. Nanomater.* 2016, 2694373. DOI: https://doi.org/10.1155/2016/2694373

[9] R. Roche, F. Yalcinkaya. 2019. Electrospun polyacrylonitrile nanofibrous membranes for point-of-use water and air cleaning. *ChemistryOpen* 8, 97-103. DOI: https://doi.org/10.1002/open.201800267

[10] R. Torres-Mendieta, F. Yalcinkaya, E. Boyraz, O. Havelka, W. Waclawek, J. Maryska, M. Cerník, M. Bryjak. 2020. PVDF nanofibrous membranes modified via laser-synthesized Ag nanoparticles for a cleaner oily water separation. *Appl. Surf. Sci.* 526, 146575. DOI: https://doi.org/10.1016/j.apsusc.2020.146575

[11] J. F. Pan, N. H. Liu, H. Sun, F. Xu. 2014. Preparation and characterization of electrospun PLCL/poloxamer nanofibers and dextran/gelatin hydrogels for skin tissue engineering. *PLoS ONE* 9, e112885. DOI: https://doi.org/10.1371/journal.pone.0112885

[12] T. Grothe, D. Wehlage, T. Böhm, A. Remche, A. Ehrmann. 2017. Needleless electrospinning of PAN nanofiber mats. *Tekstilec* 60, 290-295. DOI: https://doi.org/10.14502/Tekstilec2017.60.290-2

[13] T. Maver, M. Kurecic, D. M. Smrke, K. S. Kleinschek, U. Maver. 2016. Electrospun nanofibrous CMC/PEO as a part of an effective pain-relieving wound dressing. *J. Sol-Gel Sci. Technol.* 79, 475-486. DOI: https://doi.org/10.1007/s10971-015-3888-9

[14] B. Ebrahimi-Hosseinzadeh, M. Pedram, A. Hatamian-Zarmi, S. Salahshour-Kordestani, M. Rasti, Z. B. Mokhtari-Hosseini, M. Mir-Derikvand. 2016. In vivo evaluation of gelatin/hyaluronic acid nanofiber as burn-wound healing and its comparison with ChitoHeal gel. *Fibers Polym.* 17, 820-826. DOI: https://doi.org/10.1007/s12221-016-6259-4

[15] K.-H. Na, W.-T. Kim, D.-C. Park, H. G. Shin, S. H. Lee, J. S. Park, T. H. Song, W. Y. Choi. 2018. Fabrication and characterization of the magnetic ferrite nanofibers by electrospinning process. *Thin Sol. Films* 660, 358-364. DOI: https://doi.org/10.1016/j.tsf.2018.06.018

[16] R. J. R. Matos, C. I. P. Chaparro, J. C. Silva, M. A. Valente, J. P. Borges, P. I. P. Soares. 2018. Electrospun composite cellulose acetate/iron oxide nanoparticles non-woven membranes for magnetic hyperthermia applications. *Carbohydr. Polym.* 198, 9-16. DOI: https://doi.org/10.1016/j.carbpol.2018.06.048

[17] H. H. Liu, Y. J. Li, M. W. Yuan, G. B. Sun, Q. L. Liao, Y. Zhang. 2018. Solid and macroporous Fe_3C/N-C nanofibers with enhanced electromagnetic wave absorbability. *Sci. Rep.* 8, 16832. DOI: https://doi.org/10.1038/s41598-018-35078-z

[18] K.-Y. A. Lin, M.-T. Yang, J.-T. Lin, Y. C. Du. 2018. Cobalt ferrite nanoparticles supported on electrospun carbon fiber as a magnetic heterogeneous catalyst for activating peroxymonosulfate. *Chemosphere* 208, 502-511. DOI: https://doi.org/10.1016/j.chemosphere.2018.05.127

[19] Y. Q. Zhan, Z. H. Long, X. Y. Wan, J. M. Zhang, S. J. He, Y. He. 2018. 3D carbon fiber mats/nano-Fe_3O_4 hybrid material with high electromagnetic shielding performance. *Appl. Surf. Sci.* 444, 710-720. DOI: https://doi.org/10.1016/j.apsusc.2018.03.006

[20] K.-S. Ryu, L. Thomas, S.-H. Yang, S. S. P. Parkin. 2012. Appl. Current induced tilting of domain walls in high velocity motion along perpendicularly magnetized micron-sized Co/Ni/Co racetracks. *Phys. Expr.* 5, 093006. DOI: https://doi.org/10.1143/APEX.5.093006

[21] O. Alejos, V. Raposo, L. S. Tejerina, E. Martinez. 2017. Efficient and controlled domain wall nucleation for magnetic shift registers. *Sci. Rep.* 7, 11909. DOI: https://doi.org/10.1038/s41598-017-12230-9

[22] C. Garg, S.-H. Yang, T. Phung, A. Pushp, S. S. P. Parkin. Dramatic influence of curvature of nanowire on chiral domain wall velocity. *Sci. Adv*. 3, e1602804. DOI: https://doi.org/10.1126/sciadv.1602804

[23] T. Blachowicz, A. Ehrmann. 2018. Magnetization reversal in bent nanofibers of different cross-sections. *J. Appl. Phys.* 124, 152112. DOI: https://doi.org/10.1063/1.5022065

[24] C. Döpke, T. Grothe, P. Steblinski, M. Klöcker, L. Sabantina, D. Kosmalska, T. Blachowicz, A. Ehrmann. 2019. Magnetic nanofiber mats for data storage and transfer. *Nanomater*, 9, 92. DOI: https://doi.org/10.3390/nano9010092

[25] N. Fokin, T. Grothe, A. Mamun, M. Trabelsi, M. Klöcker, L. Sabantina, C. Döpke, T. Blachowicz, A. Hütten, A. Ehrmann. 2020. Magnetic properties of electrospun magnetic nanofiber mats after stabilization and carbonization. *Materials* 13, 7, 1552. DOI: https://doi.org/10.3390/ma13071552

[26] M. Wortmann, A. S. Layland, N. Frese, U. Kahmann, T. Grothe, J. L. Storck, T. Blachowicz, J. Grzybowski, B. Hüsgen, A. Ehrmann. 2020. On the reliability of highly magnified micrographs for structural analysis in materials science. *Sci. Rep.* 10, 14708. DOI: https://doi.org/10.1038/s41598-020-71682-8.

[27] J. I. Martín, J. Nogués, K. Liu, J. L. Vicent, Ivan K. Schuller. 2003. Ordered magnetic nanostructures: fabrication and properties. *J. Magn. Magn. Mater.* 256, 1-3, 449-501. DOI: https://doi.org/10.1016/S0304-8853(02)00898-3

[28] M. Donolato, C. Tollan, J. M. Porro, A. Berger, P. Vavassori. 2013. Flexible and stretchable polymers with embedded magnetic nanostructures. *Adv. Mater.* 25, 4, 623-629. DOI: https://doi.org/10.1002/adma.201203072

[29] K. Prashanthi, P. M. Shaibani, A. Sohrabi, T. S. Natarajan, T. Thundat, T. Nanoscale magnetoelectric coupling in multiferroic $BiFeO_3$ nanowires. *Phys. Stat. Sol. RRL* 6, 6, 244-246. DOI: https://doi.org/10.1002/pssr.201206135

[30] K. Prashanthi, T. Thundat. 2014. *In situ* study of electric field-induced magnetization in multiferroic $BiFeO_3$ nanowires. *Scanning* 36, 224-230. DOI: https://doi.org/10.1002/sca.21092

[31] S. Choopani, F. Samavat, E. N. Kolobova, A. M. Grishin. 2020. Ferromagnetic resonance and magnetic anisotropy in biocompatible $Y_3Fe_5O_{12}@Na_{0.5}K_{0.5}NbO_3$ core-shell nanofibers. *Ceramics International* 46, 2072-2078. DOI: https://doi.org/10.1016/j.ceramint.2019.09.187

[32] N. Liu, P. C. Du, P. Zhou, R. G. Tanguturi, Y. J. Qi, T. J. Zhang. Magnetoelectric coupling in $CoFe_2O_4$-$Pb(Zr_{0.2}Ti_{0.8})O_3$ coaxial nanofibers. *J. Am. Ceram. Soc.* 00, 1-7. DOI: https://doi.org/10.1111/jace.17494

[33] A. Lisfi, J. C. Lodder. 2001. Magnetic domains in Co thin films obliquely sputtered on a polymer substrate. *Phys. Rev. B* 63, 174441. DOI: https://doi.org/10.1103/PhysRevB.63.174441

[34] J. L. Storck, T. Grothe, A. Mamun, L. Sabantina, M. Klöcker, T. Blachowicz, A. Ehrmann. 2020. Orientation of electrospun magnetic nanofibers near conductive areas. *Materials* 13, 47. DOI: https://doi.org/10.3390/ma13010047

Investigation of metallic nanoparticle distribution in PAN/magnetic nanocomposites fabricated with needleless electrospinning technique

Marah Trabelsi[1,2,3], Al Mamun[1,2], Michaela Klöcker[2], Lilia Sabantina[1,2]

[1] Junior Research Group "Nanomaterials", Bielefeld University of Applied Sciences, 33619 Bielefeld, Germany
[2] Faculty of Engineering and Mathematics, Bielefeld University of Applied Sciences, 33619 Bielefeld, Germany
[3] Ecole Nationale d'Ingénieurs de Sfax, Sfax 3038, Tunisia
* Corresponding author E-mail address: lilia.sabantina@fh-bielefeld.de

INFO

ABSTRACT

Needleless electrospinning can be used to produce, for example, poly(acrylonitrile) (PAN) nanofibers, to which magnetic nanoparticles can additionally be added. Such composite nanofibers can then be stabilized and carbonized to produce carbon composite nanofibers. The magnetic nanoparticles have an influence not only on the structure, but also on the mechanical and electrical properties of the finished carbon nanofibers, as does the heat treatment during stabilization and incipient carbonization. The present study reports on the fabrication, heat treatment and resulting properties of PAN/magnetic nanofiber mats prepared by needleless electrospinning from polymer solutions. A variety of microscopic and thermal characterization methods were used to investigate in detail the chemical and morphological transition during oxidative stabilization (280 °C) and incipient carbonization (500 °C). PAN and PAN/magnetic nanofiber mats were analyzed during all stages of heat treatment. Compared to pure PAN nanofibers, the PAN/magnetic nanofibers showed larger fiber diameters and the presence of beads and agglomerations. In this study, magnetic nanofibers were investigated in more detail with the aim of detecting undesired agglomerations. Visual observation, for example with confocal laser scanning microscopy (CLSM) or scanning electron microscopy (SEM), does not provide conclusive evidence of agglomerations in the nanofibers. But based on the capabilities of energy-dispersive X-ray spectroscopy (EDS), many different types of samples can be easily analyzed where other analytical techniques cannot give a fast answer.

Keywords
Needleless electrospinning,
magnetic nanofibers,
carbon nanocomposites,
agglomerations

1 Introduction

The electrospinning technique is characterized by simplicity of use, versatility and adaptability [1,2]. Many variants of the electrospinning technique such as needleless and needle-based, melt, solvent and emulsion electrospinning, coaxial and co-electrospinning are known. A wide range of nano-architectures can be created using these electrospinning techniques, such as core-shell, tube-in-tube, porous, hollow, cross-linked and particle-encapsulated nanofibers [3-6]. The main components of a typical needle-based electrospinning system consist of a high-voltage power supply, a spinneret and a grounded collector plate [7-8]. Over time, needleless electrospinning has evolved into an alternative electrospinning technology with the aim of realizing large-scale nanofiber mats. There are also needleless electrospinning processes in which nanofibers are produced directly from an open liquid surface [9,10]. Poly(acrylonitrile) (PAN) is often used for the production of nanofibers because this polymer is relatively easy to handle and carbon nanofibers can be produced from it by heat treatment. Its carbon yield is relatively high which is advantageous for the production of carbon nanofibers [11].

The solvents in which PAN can be dissolved are polar solvents such as dimethylformamide (DMF) [12], dimethyl sulfoxide (DMSO) [13], dimethylacetamide (DMAc) [14], dimethyl sulfone, tetramethyl sulfide, and aqueous solutions of ethylene carbonate and some mineral salts [15,16]. This makes PAN very useful for a wide range of different applications [17,18]. According to scientific literature, most of the nanofibers are spun from toxic solvents such as DMF and DMAc [19], and only some papers report the use of the low-toxic solvent DMSO [20]. One of the advantages of PAN is its water resistance, which distinguishes it from other polymers [21]. In general, nanofiber mats can be used in a variety of fields, e.g., as filter materials [22,23], catalysts [24,25], cell growth, tissue engineering, medical dressings [26-28]. Furthermore, PAN is a typical precursor for the production of carbon nanofibers [29].

Through thermal processing, carbon nanofibers can be produced from PAN nanofiber mats in a two-stage process [30]. The first stage involves oxidative stabilization and it is an important heat treatment process to make the final yield of carbon material as large as possible. During oxidative stabilization, the PAN chains begin to cross-link. The resulting composite polymeric structure has the ability to withstand the rigors of high temperature processing in carbonization process more stably [31-33]. This process is crucial to prevent melting or fusing of the fibers. Another way to prevent nanofiber contraction during stabilization is electrospinning on metallic substrates [34]. Due to the conductivity of the metallic substrate, the nanofibers adhere to the surface and cannot shrink [35]. The oxidative stabilization reduces the volatilization of elemental carbon through the carbonization step and increases the final carbon yield. The process of carbonization helps in the formation of solid residues with increasing content of elemental carbon from organic material. The carbonization process is usually carried out in an inert gas, argon or nitrogen. Carbonization is a complex process in which dehydrogenation, condensation, hydrogen transfer and isomerization take place simultaneously [36]. The final pyrolysis temperature applied controls the degree of carbonization and the residual content of foreign elements, for example, after carbonization. Graphitization can also be carried out by heating to T ~ 1200 K. The carbon content of the residue exceeds a mass fraction of 90 wt.%, while at T ~ 1600 K more than 99 wt.% carbon can be found [37].

For some defined applications, organic or inorganic particles are added to polymer solutions [38], for example to improve the mechanical properties.

The addition of nanoparticles to PAN electrospinning solutions can, e.g., be used to produce magnetic PAN nanofiber mats. Many materials have magnetic properties, including iron [39], manganese alloys, magnetite [40] or cobalt. Sometimes magnetism is not the primary use of magnetic nanofibers, but the magnetic material can perform other functions. Recently, Wang et al. [41] manufactured $CuFe_2O_4$ fibers in which they were able to adjust the amount of CuO nanoparticles on the surface of the fibers by changing the ratio between the precursor of Co and that of Fe, thus making these fibers usable for catalytic oxidation [42]. These materials can exist as permanent magnets or be paramagnetic. This means they can be attracted by magnetic materials but not have permanent magnetism themselves.

Ferrite nanoparticles or iron oxide nanoparticles (iron oxides in the crystal structure of maghemite or magnetite) are the most commonly used magnetic nanoparticles. According to the literature, the magnetic nanoparticles become superparamagnetic when the ferrite particles become smaller than about 128 nm [43]. This prevents self-agglomeration to a certain amount because they only show their magnetic behavior when an external magnetic field is applied. Wortmann et al. [44] have examined magnetic nanofiber mats using transmission electron microscopy (TEM) and nevertheless found agglomeration of magnetic nanoparticles in nanofibers. The goal of this study is to further explore whether it is possible to detect these agglomerations in a different way without using a lengthy and expensive methods such as TEM.

2   Materials and methods

The nanofiber mats were prepared using polyacrylonitrile (PAN) (X-PAN, Dralon, Dormagen, Germany; M_n = 90,000 g/ml, M_w = 250,000 g/mol) dissolved in DMSO (min. 99.9%, obtained from S3 chemicals, Bad Oeynhausen, Germany). The ratio of 14% PAN with magnetic particles in DMSO proved to be the best ratio according to a previous study [45]. The polymer:nanoparticle weight ratio of 1:1.8 has given the highest nanoparticle concentration [45]. For the preparation of pure PAN nanofibers without beads, the ratio of 16% PAN in DMSO was found to be the most suitable [35]. As substrate, a polypropylene (PP) nonwoven (Elmarco, Czech Republic) was used as a supporting layer for collecting nanofibers.

All polymer solutions were stirred for 2 h on a magnetic stirrer. Afterwards, magnetic nanoparticles were incorporated, i.e. Fe_3O_4 (magnetite) with a particle size of 50-100 nm and Fe_2O_3/NiO (diiron nickel tetroxide) with a particle size < 50 nm (both purchased from Merck KGA, Darmstadt, Germany). The solution was then mixed manually for 10 minutes before the nanoparticles were dispersed in an ultrasonic bath for 40 minutes at 35 °C and a frequency of 37 kHz. The mixing and homogenization condition were selected based on the results of the previous study [45].

A wire-based electrospinning machine "Nanospider Lab" (Elmarco, Czech Republic) was used to produce nanofibers. This machine is easy to operate, which makes it ideal for lab-scale work. The Nanospider can spin a variety of polymers, and one of its advantages is that little polymer solution can be used to prepare nanofiber mats on a large scale. The following spinning parameters were used: high voltage 80 kV, nozzle diameter 0.9 mm, carriage speed 150 mm/s, electrode-substrate distance 240 mm, bottom-substrate distance 50 mm, temperature in the chamber was 22 °C and relative humidity in the chamber was 32 %. A spinning solution of 5 mL was used in all tests and spun during ~ 15 min.

Oxidative stabilization of nanofiber mats was carried out in an oven (Nabertherm, Lilienthal, Germany) approaching a typical stabilization temperature of 280 °C with a heating rate of 1 K/min, followed by isothermal treatment at this temperature for 1 hour. For the carbonization process, a furnace (Carbolite Gero, Neuhausen, Germany) was chosen to approach a temperature of 500 °C with a heating rate of 10 K/min in a nitrogen flow of 150 mL/min (STP), followed by isothermal treatment at the final temperature for 1 hour.

A Zeiss 1450VPSE scanning electron microscope (SEM) and a VK-8710 confocal laser scanning microscope (CLSM) (Keyence) were used for optical surface analysis of the nanofiber mats. To investigate the chemical composition of the samples, energy-dispersive X-ray spectroscopy (EDS) was used for more detailed investigations. The samples were sputtered with 20 nm of gold to avoid charging them. Table 1 shows the samples that were prepared.

Table1: Overview of the samples

16% PAN
14% PAN/magnetite
14% PAN/diiron nickel tetroxide

3 Result and discussion

The morphologies of the studied nanofiber mats are shown in the CLSM images in Figure 1. For the three samples (electrospun, stabilized and carbonized), the images are very similar, showing a relatively regular nanofiber mat with some fine fibers, but they have different colors due to the heat treatment processes. The fibers show a light brown discoloration during stabilization (Fig. 1b) and a more black discoloration when carbonization starts (Fig. 1c), differences which are easily recognizable. The heat treatment at 500 °C does not complete carbonization and therefore dark brown color is still clearly visible in the carbonized sample (Fig. 1c). In case of complete carbonization at 800 °C, the CLSM images show rather black color without brown parts [21]. CLSM images allow seeing a strong bead formation, but it is not possible to see if there are agglomerations of magnetic particles.

(a)

(b)

(c)
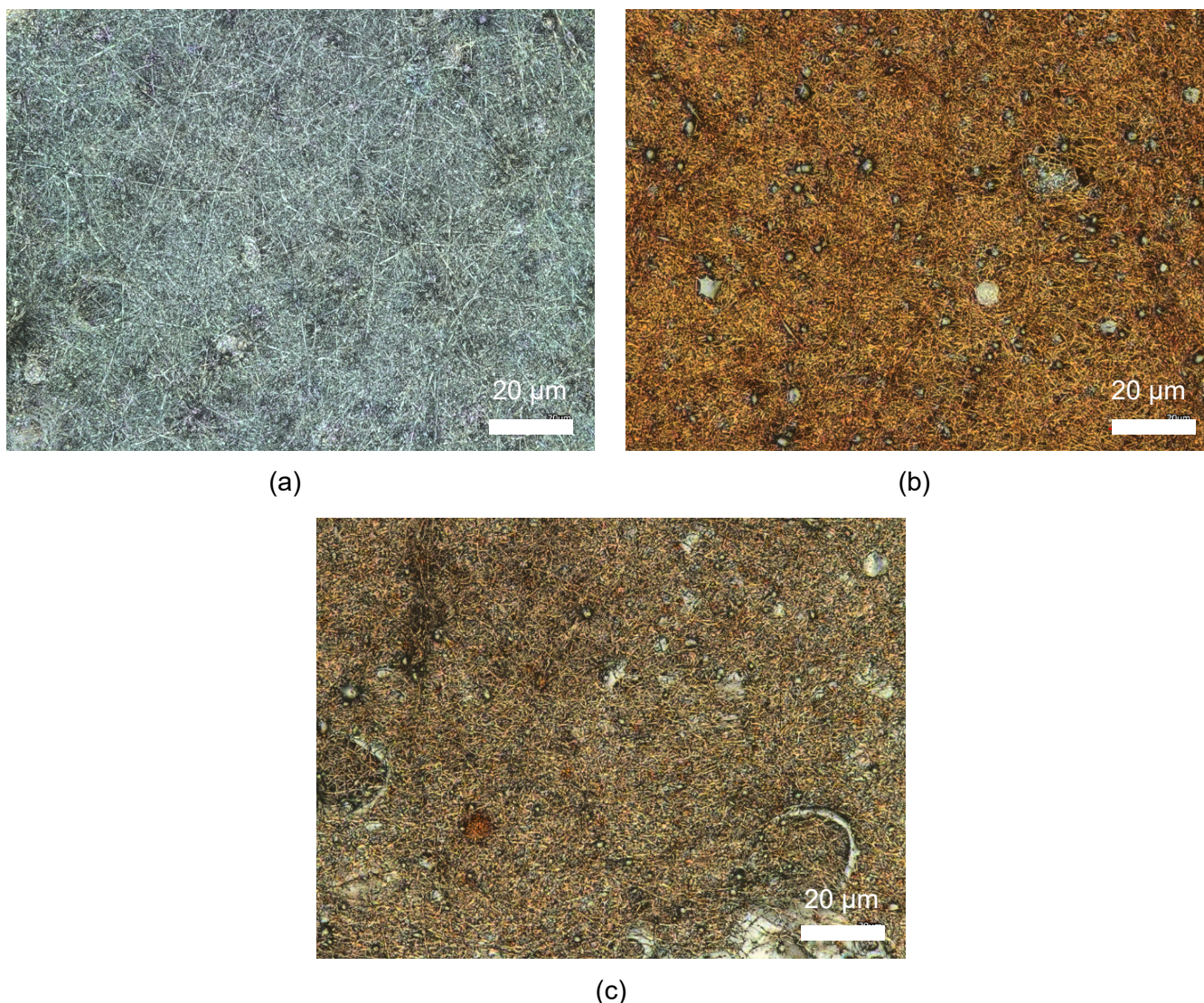
Fig 1 CLSM images of (a) PAN/magnetite after electrospinning; (b) stabilized; and (c) carbonized at 500 °C.

With optical methods it is difficult to detect agglomerations in the nanofibers. Thus, possible agglomerations of magnetic nanoparticles cannot be seen in the CLSM images (Fig. 1).

Figure 2 shows SEM images of the nanofiber mats obtained from $PAN/Fe_2O_3/NiO$ (iron nickel tetroxide) samples. After electrospinning, the nanofibers are almost straight, smooth and randomly oriented (cf. Fig. 2a). The stabilized (Fig. 2b) and carbonized (Fig. 2c) samples change their surface morphology. The nanofibers get curved and change their dimensions due to the influence of the heat treatment process. This occurs because of carbon chains that are highly flexible due to rotation around carbon-carbon single bond, allowing the molecules to take up many different configurations.
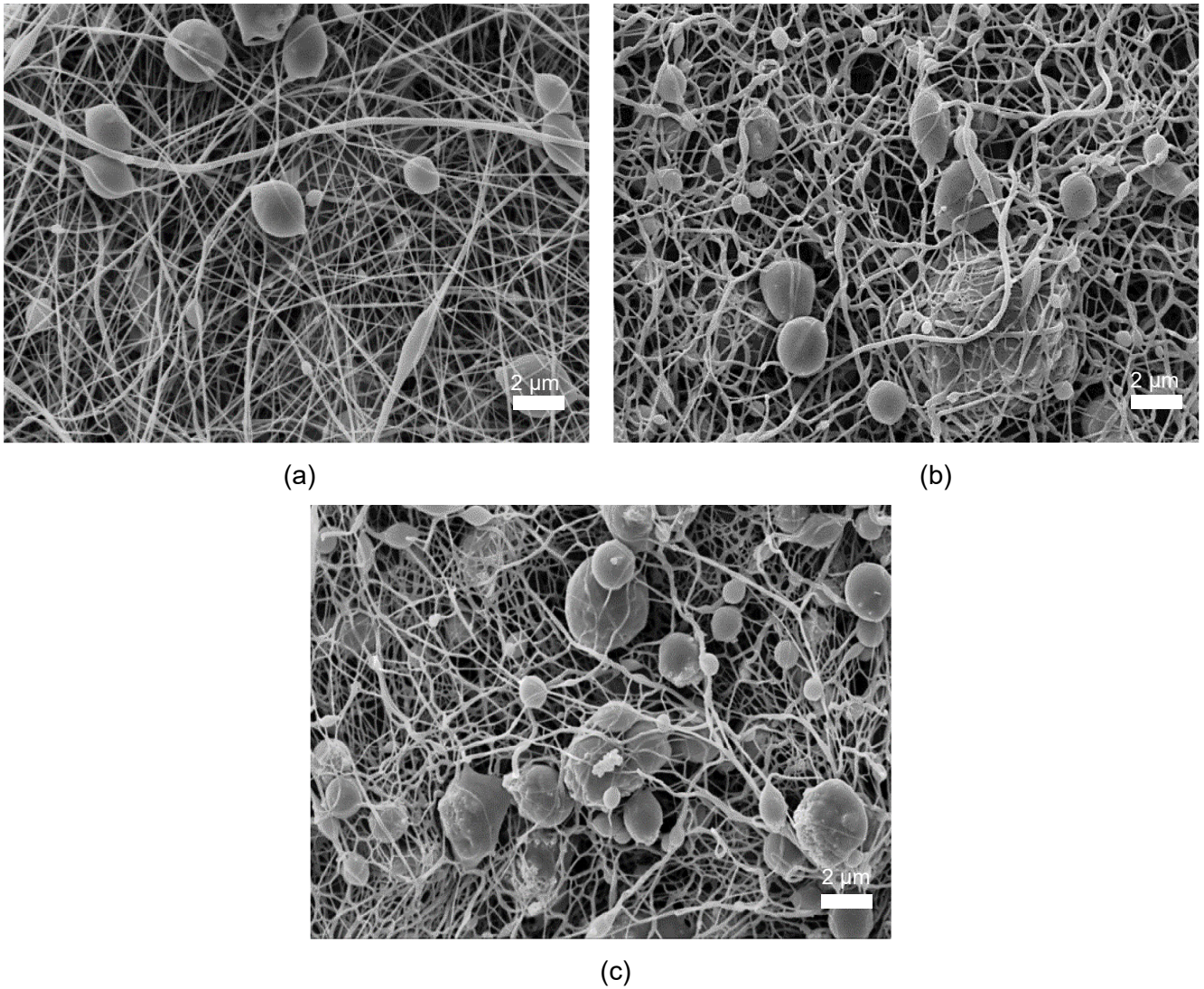
Fig. 2 SEM images of PAN/ diiron nickel tetroxide with a nominal magnification of 5000 x, (a) after electrospinning; (b) stabilized; and (c) carbonized. (a) and (b) reproduced from [46], published under a CC BY 4.0 license.

Figure 3 shows SEM images comparing pure PAN (3a) and PAN/magnetite (3b) after electrospinning.
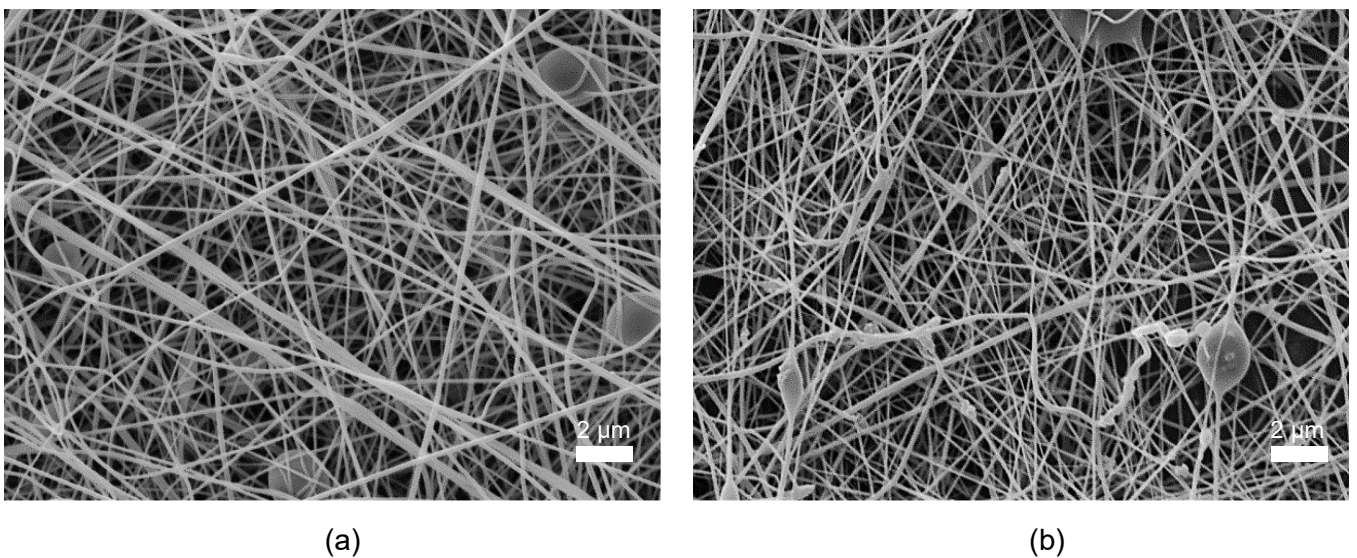
Fig. 3 SEM images of (a) pure PAN and (b) PAN/magnetite nanofiber mats, taken with a nominal magnification of 5000 x after the electrospinning process.

In pure PAN nanofibers (Fig. 3a), the nanofibers show more relatively straight orientation compared to PAN/diiron nickel tetroxide (Fig. 2a) and PAN/magnetite (Fig. 3b). In all three as-spun nanofiber mats, some nanofibers are connected with some beads and the most beads can be seen on the surface of PAN/diiron nickel tetroxide (Fig. 2a). In addition, the beads look slightly rough and a bit different from PAN/magnetite nanofibers (Fig. 3b), which can be explained by the fact that the diiron nickel tetroxide nanoparticles are concentrated in the beads due to their small size, as found later in the EDS spectra.

When particles are added to the nanofiber mats, the fiber diameters change. The distributions of nanofiber diameters are shown in Figure 4.

(a)

(b)

(c)
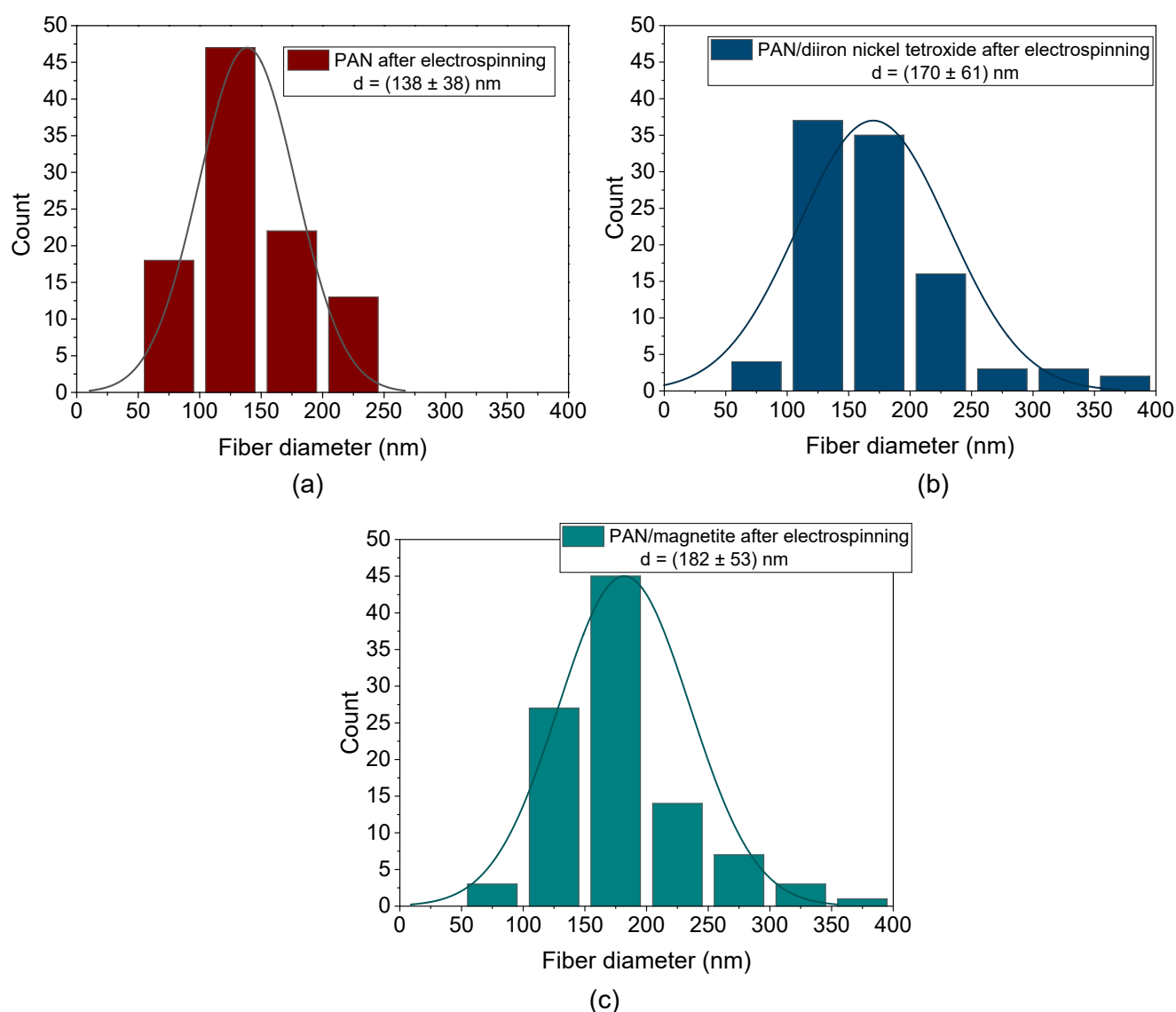
Fig. 4 Distributions of the diameters of: (a) PAN nanofibers; (b) PAN/diiron nickel tetroxide nanofibers; (c) PAN/magnetite nanofibers.

Both PAN/magnetite ((182 ± 53) nm) and PAN/diiron nickel tetroxide ((170 ± 61) nm) nanofiber mats show a higher average as well as a wider distribution of nanofiber diameters compared to pure PAN (cf. Figures 4b and 4c). Correspondingly, pure PAN nanofiber mats (4a) exhibit a lower average ((138 ± 38) nm) as well as a narrower distribution of nanofiber diameters. In addition, the PAN/magnetite nanofiber (4c) show a slightly larger average than PAN/diiron nickel tetroxide (4b) nanofiber mats.

For a closer investigation, Figure 5 depicts the surface scanned with EDS and the spectra of the materials inside this surface. The EDS spectrum was obtained in a microscopic area of the sample. As a result, the presence of carbon (C) in a large amount at 0.3 keV due to the heat treatment process and peaks at 0.5 keV, 6.4 keV and 7.1 keV related to iron (Fe) can be detected. In addition, the peaks at 0.7 keV, 0.8 keV and 7.5 keV confirm the existence of nickel (Ni).

(a)

(b)

(c)

Fig. 5 SEM images of carbonized PAN/diiron nickel tetroxide sample (a) whole surface, (b) spot on a bead; and (c) spot on a nanofibers.

As can be seen in the sub-images in Figure 5, the examined areas are marked with a green frame, and the EDS spectra are created for these areas. For the comparison of the magnetic samples, the gold peak is set as a reference in the EDS spectrum and is marked by a blue arrow (see Figures 6 a-c). The first EDS spectrum (Fig. 6a) defines the complete area of the nanofiber mat and the second (Fig. 6b) only a small area where a bead is located. A measurement of an area with fibers only is shown in Figure 6c. The iron peak (Fe) shown by the red arrow in the first EDS spectrum (Fig. 6a) is lower than the iron peak in Figure 6b. Similarly, the nickel peak (Ni) in Figure 6b is much higher than in Figure 6a and 6c. It can be noted that Figure 6c shows a significant difference from the maps with the beads (Fig. 6b), i.e. here the iron peak (Fe) is even lower than in the overall map (cf. Figure 6a).

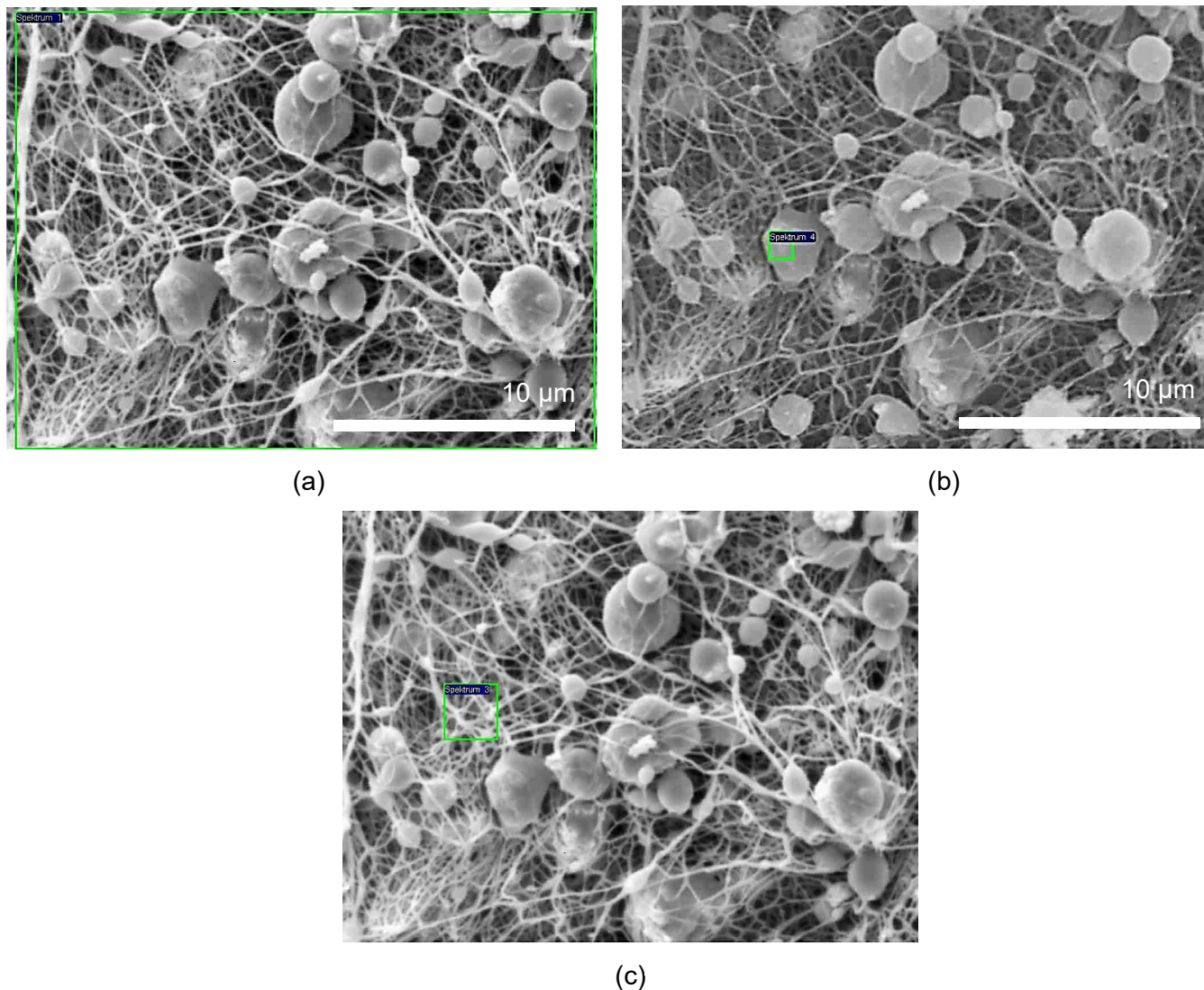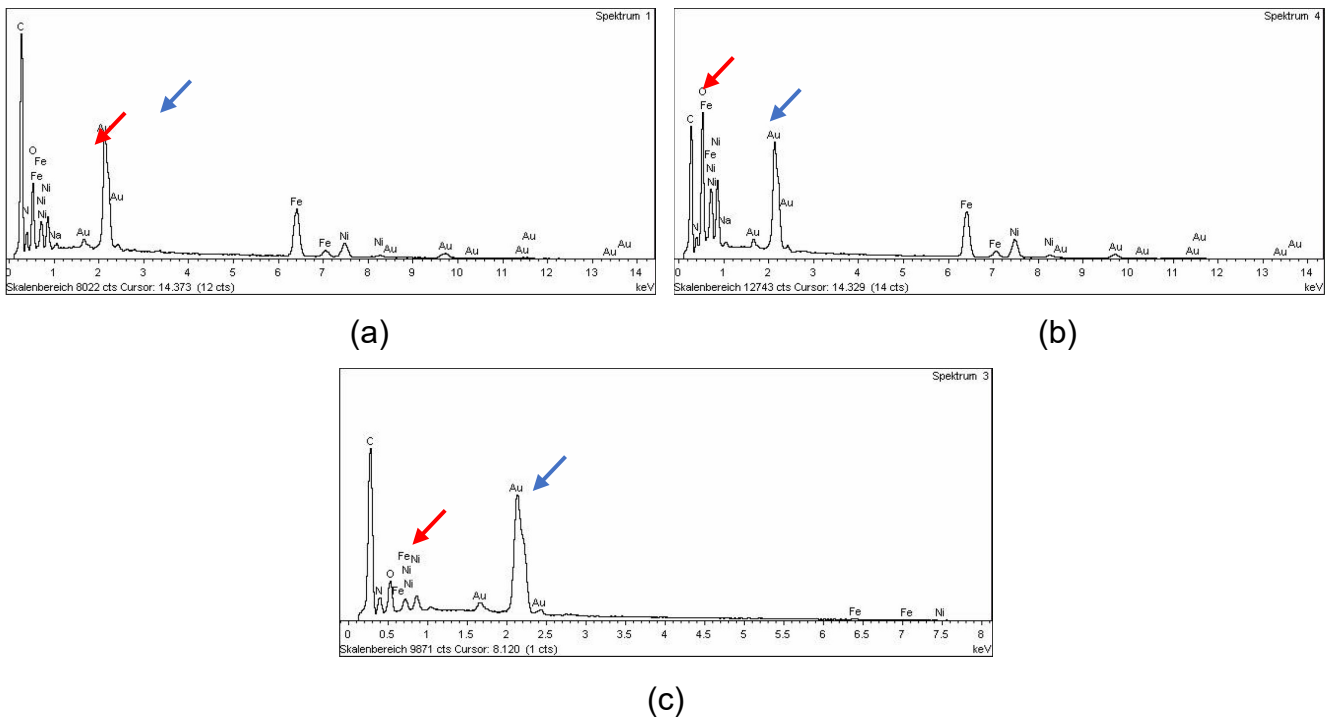*Fig. 6: EDS spectrum of carbonized PAN/diiron nickel tetroxide sample: (a) whole surface; (b) spot on a bead; and (c) spot on nanofibers.*

This suggests that the highest concentration of particles is located in the beads. Moreover, the EDS spectrum shows strong peaks of iron (Fe) and nickel (Ni) elements, which are significantly more abundant than carbon (C), confirming that the diiron nickel tetroxide nanoparticles are agglomerated within the beads.

Nanofibers or nanoparticles are certainly not the only areas of materials science in which such fundamental structural problems as agglomerations can occur. Thus, tests such as TEM analysis can be avoided when EDS is used to determine where possible agglomerations are located. TEM needs long and complex preparations, therefore it is very helpful that the agglomerates are also clearly visible in EDS. Nanofibers are used here as a substitute for practically all types of micro- and nanomaterials that are tested using microscopic images at high magnification. There are, of course, samples whose structures in question cannot be displayed at a lower magnification (such as atomic structures).

4 Conclusions

In this study, PAN/magnetic nanofibers were produced and investigated from a DMSO polymer solution using a wire-based electrospinning process. The chemical and morphological properties of the magnetic nanofibers after the heat treatment steps were examined using various characterization methods. The preparation of the samples and the acquisition of high-resolution images, for example for TEM examinations, require a lot of time and intensive preparation. For this reason, this study looked for a simpler way to find out whether nanoparticle agglomerations in the nanofibers occur, without using TEM. The results of this study lead to the conclusion that the EDS is a simpler, better manageable and more efficient technique that does not require much time to investigate the presence of agglomerations of nanoparticles in nanofiber mats.

Acknowledgements

References

[1] D. Yadav, F. Amini, A. Ehrmann. 2020. Recent advances in carbon nanofibers and their applications – A review. *Eur.Polym. J.* 138,109963. DOI: https://doi.org/10.1016/j.eurpolymj.2020.109963.

[2] F. E. C. Othman, N. Yusof, H. Hasbullah, J. Jaafar, A. F. Ismail, N. Abdullah, N. A. H. M. Nordin, F. Aziz, W. N. W. Salleh. 2017. Polyacrylonitrile/magnesium oxide-based activated carbon nanofibers with well-developed microporous structure and their adsorption performance for methane. *J. Ind. Eng. Chem.* 51, 281-287. DOI: https://doi.org/10.1063/5.0008012.

[3] I. Latsunskyi, A. Vasylenko, R. Viter, M. Kempinski, G. Mowaczyk, S. Jurga, M. Bechelany. 2017. Tailoring of the electronic properties of ZnO-polyacrylonitrile nanofibers, Experiment and theory. *Appl. Surf. Sci.* 411, 494-501. DOI: https://doi.org/10.1016/j.apsusc.2017.03.111.

[4] H. T. Niu, X. G. Wang, T. Lin. 2012. Upward Needleless Electrospinning of Nanofibers. *J. Eng. Fibers Fabr.* 7, 17-22. DOI: https://doi.org/10.1177/155892501200702S03.

[5] S. V. Lomos, K. Molnar. 2016. Compressibility of carbon fabrics with needleless electrospun PAN nanofibrous interleaves. *Express Polym. Lett.* 10, 25-35. DOI: 10.3144/expresspolymlett.2016.

[6] J. N. Zhang, M. Y. Song, D. W. Li, Z. P. Yang, J. H. Cao, Y. Chen, Y. Xu, Q. F. Wei. 2016. Preparation of self-clustering highly oriented nanofibers by needleless electrospinning methods. *Fibers Polym.* 17, 1414-1420. DOI: https://doi.org/10.1007/s12221-016-6581-x.

[7] T. Grothe, J. Brikmann, H. Meissner, A. Ehrmann. 2017. Influence of solution and spinning parameters on nanofiber mat creation of poly(ethylene oxide) by needleless electrospinning. *Mater. Sci.* 23, 342-349. DOI: 10.5755/j01.ms.23.4.17169.

[8] H. Fong, I. Chun, D. H. Reneker. 1999. Beaded nanofibers formed during electrospinning. *Polymer* 40, 4585-4592. DOI: https://doi.org/10.1016/S0032-3861(99)00068-3.

[9] N. Haitao, L. Tong. 2012. Fiber generators in needleless electrospinning. *J. Nanomater.* 2012, 725950. DOI: https://doi.org/10.1155/2012/725950.

[10] M. Zahmatkeshan, M. Adel, S. Bahrami, F. Esmaeli, S. M. Rezayat, Y. Saeedi, B. Mehravi, S. B. Jameie, K. Ashtari. 2018. Polymer Based Nanofibers: Preparation, Fabrication, and Applications. In: A. Barhoum, M. Bechelany, A. Makhlouf (Eds.) *Handbook of Nanofibers*. Springer, Cham. DOI: https://doi.org/10.1007/978-3-319-42789-8_29-2.

[11] J. Kaur, K. Millington, S. Smith. 2016. Producing high-quality precursor polymer and fibers to achieve theoretical strength in carbon fibers: A review. *J. Appl. Polym. Sci.* 133, 43963. DOI: https://doi.org/10.1002/app.43963.

[12] S. Megelski, J. S. Stephens, D. B. Chase, J. F. Rabolt. 2002. Micro- and nanostructured surface morphology on electrospun polymer fibers. *Macromolecules* 35, 22, 8456-8466. DOI: https://doi.org/10.1021/ma020444a.

[13] L. Sabantina, M. Klöcker, M. Wortmann, J. Rodríguez Mirasol, T. Cordero, E. Moritzer, K. Finsterbusch, A. Ehrmann. 2020. Stabilization of polyacrylonitrile nanofiber mats obtained by needleless electrospinning using dimethyl sulfoxide as solvent. *J. Ind. Text.* 50, 2, 224-239. DOI: https://doi.org/10.1177/1528083718825315.

[14] A. Zulfi, D. A. Hapidin, M. M. Munir, F. Iskandar, K. Khairurrijal. 2019. The synthesis of nanofiber membranes from acrylonitrile butadiene styrene (ABS) waste using electrospinning for use as air filtration media. *RSC Adv.* 9, 30741. DOI: https://doi.org/10.1039/C9RA04877D.

[15] Q. Y. Wu, X. N. Chen, L. S. Wan, Z. K. Xu. 2012. Interactions between polyacrylonitrile and solvents: Density functional theory study and two-dimensional infrared correlation analysis. *J. Phys. Chem. B* 116, 28, 8321-8330. DOI: https://doi.org/10.1021/jp304167f.

[16] M. Hattori, H. Yamazaki, M. Saito, K. Hisatani, K. Okajima. 1996. NMR study on the dissolved state of polyacrylonitrile in various solvents. *Polym. J.* 28, 594-600. DOI: https://doi.org/10.1295/polymj.28.594.

[17] A. Khajuria, P. N. Balaguru. Plastic shrinkage characteristics of fiber reinforced cement composites. 1992. In: R. N. Swamy (Ed.), *Fibre reinforced Cement and Concrete: Proceedings of the Fourth RILEM International Symposium*, 82-90.

[18] M. M. Lovleva, V. N. Smirnova, G. A. Budnitskii. 2001. The solubility of polyacrylonitrile. *Fibre Chem.* 33, 262-264. DOI: https://doi.org/10.1023/A:1012934313303.

[19] T. Marino, S. Blefari, E. Di Nicolò, A. Figoli. 2017. A more sustainable membrane preparation using triethyl phosphate as solvent. *Green Process. Synth.* 6, 3, 295-300. DOI: https://doi.org/10.1515/gps-2016-0165.

[20] L. Sabantina, J. R. Mirasol, T. Cordero, K. Finsterbusch, A. Ehrmann. 2018. Investigation of needleless electrospun PAN nanofiber mats. *AIP Conf. Proc.* 1952, 020085. DOI: https://doi.org/10.1063/1.5032047.

[21] L. Sabantina, M. A. Rodríguez-Cano, M. Klöcker, F. J. García-Mateos, J. J. Ternero-Hidalgo, A. Mamun, F. Beermann, M. Schwakenberg, A.-L. Voigt, J. Rodríguez Mirasol, T. Cordero, A. Ehrmann. 2018. Fixing PAN nanofiber mats during stabilization for carbonization and creating novel metal/carbon composites. *Polymers* 10, 735. DOI: https://doi.org/10.3390/polym10070735.

[22] S. M. Lemma, A. Esposito, M. Mason, L. Brusetti, S. Cesco, M. Scampicchio. 2015. Removal of bacteria and yeast in water and beer by nylon nanofibrous membranes. *J. Food Eng.* 157, 1-6. DOI: https://doi.org/10.1016/j.jfoodeng.2015.02.005.

[23] R. Roche, F. Yalcinkaya. 2019. Electrospun polyacrylonitrile nanofibrous membranes for point-of-use water and air cleaning. *ChemistryOpen* 8, 97-103. DOI: https://doi.org/10.1002/open.201800267.

[24] R. Ruiz-Rosas, J. M. Rosas, I. G. Loscertales, J. Rodríguez-Mirasol, T. Cordero. 2014. Electrospinning of silica sub-microtubes mats with platinum nanoparticles for NO catalytic reduction. *Appl. Catal. B Environ*. 156-157, 15-24. DOI: https://doi.org/10.1016/j.apcatb.2014.02.047.

[25] F. J. García-Mateos, R. Berenguer, M. J. Valero-Romero, J. Rodríguez-Mirasol, T. Cordero. 2018. Phosphorus functionalization for the rapid preparation of highly nanoporous submicron-diameter carbon fibers by electrospinning of lignin solutions. *J. Mater. Chem. A* 6, 1219-1233. DOI: https://doi.org/10.1039/C7TA08788H.

[26] N. Ashammakhi, A. Ndreu, Y. Yang, H. Ylikauppila, L. Nikkola. 2012. Nanofiber-based scaffolds for tissue engineering. *Eur. J. Plast. Surg.* 35, 135-149. DOI: https://doi.org/10.1007/s00238-008-0217-3.

[27] D. Wehlage, H. Blattner, L. Sabantina, R. Böttjer, T. Grothe, A. Rattenholl, F. Gudermann, D. Lütkemeyer, A. Ehrmann. 2019. Sterilization of PAN/gelatine nanofibrous mats for cell growth. *Tekstilec* 62, 78-88. DOI: https://doi.org/10.14502/Tekstilec2019.62.78-88.

[28] A. Mamun. 2019. Review of possible applications of nanofibrous mats for wound dressings. *Tekstilec* 62, 89-100. DOI: https://doi.org/10.14502/Tekstilec2019.62.89-100.

[29] E. Cipriani, M. Zanetti, P. Bracco, V. Brunella, M. P. Luda, L. Costa. 2016. Crosslinking and carbonization processes in PAN films and nanofibers. *Polym. Degrad. Stab.* 123, 178-188. DOI: https://doi.org/10.1016/j.polymdegradstab.2015.11.008.

[30] Z. Z. Zhao, J. Q. Li, X. Y. Yuan, X. Li, Y. Y. Zhang, J. Sheng. 2005. Preparation and properties of electrospun poly(vinylidene fluoride) membranes. *J. Appl. Polym. Sci.* 97, 466-474. DOI: https://doi.org/10.1002/app.21762.

[31] T. H. Ko. 1991. The influence of pyrolysis on physical properties and microstructure of modified PAN fibers during carbonization. *Appl. Polym. Sci.* 43, 589-600. DOI: https://doi.org/10.1002/app.1991.070430321.

[32] A. Shokuhfar, A. Sedghi, R. E. Farsani. 2013. Effect of thermal characteristics of commercial and special polyacrylonitrile fibres on the fabrication of carbon fibres. *Mater. Sci. Technol.* 22, 1235-1239. DOI: https://doi.org/10.1179/174328406X129887.

[33] N. Yusof, A. F. Ismail. 2011. Post spinning and pyrolysis processes of polyacrylonitrile (PAN)-based carbon fiber and activated carbon fiber: A review. *J. Anal. Appl. Pyrolysis* 93, 1-13. DOI: https://doi.org/10.1016/j.jaap.2011.10.001.

[34] J. L. Storck, B. Brockhagen, T. Grothe, L. Sabantina, K. Kaltschmidt, H. Tuvshinbayar, L. Braun, E. Tanzli, A. Hütten, A. Ehrmann. 2021. Stabilization and carbonization of PAN nanofiber mats electrospun on metal substrates. *C – Journal of Carbon Research* 7, 12. DOI: https://doi.org/10.3390/c7010012.

[35] D. Wehlage, R. Böttjer, T. Grothe, A. Ehrmann. 2018. Electrospinning water-soluble/insoluble polymer blends. *AIMS Mater. Sci.* 5, 2, 190-200. DOI: https://doi.org/10.3934/matersci.2018.2.190.

[36] J. L. Storck, T. Grothe, K. Tuvshinbayar, E. Diestelhorst, D. Wehlage, B. Brockhagen, M. Wortmann, N. Frese, A. Ehrmann. 2020. Stabilization and incipient carbonization of electrospun polyacrylonitrile nanofibers fixated on aluminum substrates. *Fibers* 8, 55. DOI: https://doi.org/10.3390/fib8090055.

[37] H. Marsh, F. Rodríguez-Reinoso. 2006. *Activated carbon (*1st ed.). Elsevier Science, Amsterdam, Netherlands. DOI: https://doi.org/10.1016/B978-0-08-044463-5.X5013-4.

[38] U. Adhikari, X. An, N. Rijal, T. Hopkins, S. Khanal, T. Chavez, R. Tatu, J. Sankar, K. L. Little, D. B. Hom, N. Bhattarai, S. K. Pixley. 2019. Embedding magnesium metallic particles in polycaprolactone nanofiber mesh improves applicability for biomedical applications. *Acta Biomater.* 98, 215-234. DOI: https://doi.org/10.1016/j.actbio.2019.04.061.

[39] D. Sudsom, A. Ehrmann. 2021. Micromagnetic simulations of Fe and Ni nanodot arrays surrounded by magnetic or non-magnetic matrices. *Nanomater.* 11, 349. DOI: https://doi.org/10.3390/nano11020349.

[40] T. Blachowicz, A. Ehrmann. 2021. Influence of clustering round magnetic nano-dots on magnetization reversal. *J. Phys. Conf. Series* 1730, 012034. DOI: https://doi.org/10.1088/1742-6596/1730/1/012034.

[41] P. Wang, T. Dong, M. Li, P. Yang. 2019. Controlling growth of CuO nanoparticles on $CuFe_2O_4$ nanotubes and their adsorption kinetics. *J. Nanosci. Nanotechnol*. 19, 8, 4474–4480. DOI: https://doi.org/10.1166/jnn.2019.16481.

[42] T. Blachowicz, A. Ehrmann. 2020. Most recent developments in electrospun magnetic nanofibers: A review. *J. Eng. Fibers Fabr.* 15, 1558925019900843. DOI: https://doi.org/10.1177/1558925019900843.

[43] A. H. Lu, E. L. Salabas, F. Schüth. 2007. Magnetic nanoparticles: synthesis, protection, functionalization, and application. *Angew. Chem. Int. Ed.* 46, 1222-1244. DOI: https://doi.org/10.1002/anie.200602866.

[44] M. Wortmann, A. S. Layland, N. Frese, U. Kahmann, T. Grothe, J. L. Storck, T. Blachowicz, J. Grzybowski, B. Hüsgen, A. Ehrmann. 2020. On the reliability of highly magnified micrographs for structural analysis in materials science. *Sci. Rep.* 10, 14708. DOI: https://doi.org/10.1038/s41598-020-71682-8.

[45] C. Döpke, T. Grothe, P. Steblinski, M. Klöcker, L. Sabantina, D. Kosmalska, T. Blachowicz, A. Ehrmann. 2019. Magnetic nanofiber mats for data storage and transfer. *Nanomater.* 9, 92. DOI: https://doi.org/10.3390/nano9010092.

[46] N. Fokin, T. Grothe, A. Mamun, M. Trabelsi, M. Klöcker, L. Sabantina, C. Döpke, T. Blachowicz, A. Hütten, A. Ehrmann. 2020. Magnetic properties of electrospun magnetic nanofiber mats after stabilization and carbonization. *Materials* 13, 1552. DOI: https://doi.org/10.3390/ma13071552.

Textile education during the 2020 pandemic: experiences in US, South Africa and Germany

Christopher M. Pastore[1],*, Yordan Kyosev[2], F. A. Fassihi[3], Becky Flax[1]

[1] *Kanbar College of Design and Engineering and Commerce, Thomas Jefferson University, Philadelphia, PA, US*
[2] *Institute of Textile Machinery and High Performance Material Technology, TU Dresden, Dresden, Germany*
[3] *Clothing and Textile Studies, Durban University of Technology, Durban, South Africa*
* Corresponding author E-mail address: Christopher.Pastore@Jefferson.edu

INFO

ABSTRACT

The Covid-19 pandemic has had a major impact on higher education across the world. In this paper we consider how textile education has been impacted and what approaches have been employed to maintain quality education and laboratory experience when traditional methods are not appropriate. This paper considers three different countries – United States, South Africa and Germany. Each has been affected in a different way, has a different sociological makeup, and has developed distinct solutions to the challenge. Methods related to HyFlex, flipped classrooms, and blending learning have been applied by all three institutions. Lectures have been presented as pre-recorded videos, synchronous video conferencing, and hybrid. Similarly, laboratory and studio experiences have been handled through pre-recorded video, guided "at home" experiments, and modified in-person experiences. This paper gives an overview of the laboratory and studio experiences, time spent in preparation, and reaction of the students to remedies. It also addresses best practices from each country in the three continents.

1. Introduction – limitations to meeting in person

The COVID pandemic situation created an unusual situation in for textile education across the planet. Textile engineering and design traditionally involve a significant amount practical training, both laboratory and studio, to enrich the theory. The pandemic kept students at home, which meant that practical training (laboratories and studios) had to be re-envisioned. The authors of this paper had intensive exchange during the period. Each country had different requirements and restrictions associated with higher education. The methods employed and evaluations of those methods were collected to create this

summary of their experience in three different countries – United States (USA), Germany and South Africa (SA).

First, we consider the restrictions applied to each university, considering national, regional, and institutional and applying the more rigorous rules. One of the restrictions associated with the pandemic was physical spacing issues for students and faculty. The formal limitations per country are summarized in Table 1.

Table 1. Comparison of limitations to in-person meeting.

Criteria	USA	Germany	SA
Maximum Occupancy	25	online only, except exceptional cases	25
Individual Spacing	2 meters	1.5 meter	2 meters
Masks	Mandatory	Mandatory	Mandatory
Students on campus	≤ 25% capacity	≤ 10% capacity	≤ 33% capacity
Additional	≤ 5 people per 90 m^2	≤ 5 people per 100 m^2	≤ 5 people per 100 m^2

It can be seen that the general criteria shown in Table 1 are quite similar for all three universities. Distinct restrictions associated with each university are explained in detail below.

1.1. USA

In the United States, specific limitations on gatherings are determined at the state or city level. Data presented in Table 1 are for Thomas Jefferson University (TJU) in Philadelphia, Pennsylvania. At TJU students who wish to stay at home and learn remotely, may. This means that each class is potentially different regarding attendance. Classes may be entirely online (if all students choose to stay at home), or a combination of in-person and online students.

In the United States, some universities opened the Fall 2020 semester with entirely in-person classes. At several institutions, outbreaks of Covid-19 resulted in them converting to online only in a matter of days or weeks.

University of North Carolina, Chapel Hill identified four coronavirus clusters, and reported that 135 students had been tested positive for Covid-19 in the first week of in-person classes. Thus one week after classes began, the university converted to online only [1]. University of Notre Dame started with in-person classes and converted to all after reporting 304 positive cases since August 3, 2020 (that number climbed to 336 cases by 21 August, 2020 [2]. North Carolina State University converted to online only after 2 weeks of classes [3].

TJU opened in a *concurrent* mode [4] where students are free to choose if they wish to attend classes in person or stay at home and participate remotely. The faculty teach the classes with video streaming so that in-person and remote students are attending simultaneously. This model is related to the Hyflex model [5] but not as robust, nor as demanding on the faculty.

1.2. Germany

In Germany, TU Dresden decided to start the Fall semester completely online. During the second half of the semester, after the situation became controlled, practical trainings were allowed to use an in-person format, if no other form was possible or suitable. This allowed for practical elements to have *hybrid* forms of learning [6], combining online materials, handouts and partial practical exercises. In the hybrid mode, classes can either meet in-person, or can be online. There is no intention of combining the two modes simultaneously.

1.3. SA

In South Africa, the minister of education has allowed 33% of students and staff to experience in-person teaching to maintain social distancing [7]. This creates a challenge in determining which students can physically attend the university, and correspondingly, which faculty. DUT has decided to meet this requirement by only allowing final year undergrad and postgraduate students to have access to the campus. The rest will be taught remotely. These 67% students who are taught online will gradually return to university as conditions improve and level of restrictions eased. Special attention will be made to opening laboratory and practica sessions for these students.

2. Technical requirements

Because of the restriction on in-person attendance, some educational components must be delivered remotely, as described above. There are technological needs associated with this requirement, both hardware and software. Of particular interest are the software requirements associated with each of the universities.

2.1. USA

Many courses will be using a simultaneous broadcast system because of the concurrent teaching model. In this mode the professor will live stream the class activity using a web camera, microphone, and broadcast software such as Zoom or Blackboard Collaborate. The university provided licenses for Blackboard Collaborate, Zoom and Microsoft Teams to all of the faculty. TJU uses Canvas as a learning management system which becomes the primary repository for digital assets for each course. Blackboard Collaborate (video conferencing software) is available as a built-in tool within Canvas. However, despite the convenience of using Collaborate, almost every faculty member has been using Zoom to run their classes.

All three video conferencing software platforms available to the faculty have the same core functionality – screen sharing, file sharing, and viewing of attendees. Collaborate is limited to showing only 4 participants simultaneously, whereas Zoom allows 49. Most of the faculty felt it important to see the entire class in one screen, so have been using Zoom.

Some classes will involve pre-recorded content that will be viewed by the students at home. These viewings are complimented by live discussions about the content using digital communications, thus creating a flipped component to the course [8]. The development of the pre-recorded content requires access to a quality digital camera as well as video editing software, both of which were provided by the university, an example of which is shown in Figure 1.

Figure 1. Setup for creating video content regarding the use of flat bed knitting machines.

Because of the high digital content demands, there were concerns about students having reliable access to the feeds. The vast majority of students had no difficulties, but occasionally a student would run into local internet outages for some period of time. One student reported driving to a McDonald's restaurant to make use of their free internet services to attend class.

2.2. Germany

TU Dresden uses the online education system OPAL developed by the state of Saxony [9]. OPAL functions as a learning management system and is available to all members of TU Dresden. Additionally TU Dresden employs the online conference platform of the German universities, DFNconf [10] for online meetings and teaching. The sudden increase in use of video conferencing resulted in significantly increased traffic for DFNconf. To accommodate the need, licenses for various platforms like Zoom and GoToMeeting were obtained for faculty.

Based on the previous experience of one of the authors as well as the possibility for converting existing slides into online content, the author preferred to install separate DokuWiki [11] instances to store the online content associated with the practical training in the assemblage of textile technologies.

No students reported they were not able to access the digital content. There were a few cases reported where the students starting looking at it only in the last two weeks of the semester.

2.3. SA

The 67% of students who are not allowed on campus will be taught using digital tools such as Moodle, Microsoft Teams, WhatsApp, etc. Therefore, a multi-modal approach has been taking place, with classes developed as either hybrid or concurrent.

One of the challenges in SA is that availability of internet access to all students [12]. Very few of the students own a computer, but most have access to a smartphone. To ensure that the students can attend virtual classes, data has been provided by university for all students who are taught remotely. There are some students living in rural areas with no internet access. For these students, printed materials and memory sticks containing lectures and videos were delivered via courier.

3. Student responsibilities

In different countries there are different student responsibilities associated with the classroom. The length of the semester, the number of hours per week spent in the classroom, whether or not it is mandatory, and the basis of grading vary. A summary of the attendance responsibilities is shown in Table 2.

Table 2. Comparison of Student Responsibilities in the Three Countries

	Germany	South Africa	United States
Semester duration:	26 Oct – 6 Feb	28 Sept – 17 Jan[1]	24 Aug – 4 Dec
Lecture attendance	Optional	Mandatory	Mandatory
Laboratory attendance	Mandatory	Mandatory	Mandatory
Mid-semester assessment	Rarely	Yes	Yes

As can be seen, all three countries have a mandatory laboratory attendance policy, which created a real challenge during this time and required creative solutions.

Also we noted that a mid-semester assessment was a very important part of the experience, as will be described later.

---

[1] This year the semester is unusual. Typically it will run July to November, but it was delayed because of the pandemic.

4. Approach

It is important to recognize at the outset the difference between *online* education and *remote* education [13,14]. In online education, students are choosing to enter into an asynchronous teaching experience. This is often because the student is working or otherwise engaged during traditional class time, and so they choose to engage the material at whatever days and times best suit their schedule.

In the case of remote education, the education remains synchronous and students are expected to maintain a specific schedule of attendance. For most of us, the emergency transition was treated in a remote education mode, at least to some degree. Many students preferred having a scheduled class time. In a recent study, Milligan [15] evaluated student preferences for synchronous vs asynchronous remote engagement based on the sudden transition to remote teaching in March of 2020 in the US. He found a distinct preference for synchronous engagement on the part of the students. Further he found that in the organic chemistry classes that were considered, student performance (as measured by exam performance) was higher in the classes with synchronous delivery compared to asynchronous delivery.

The difference between online and remote teaching is the difference between *synchronous* and *asynchronous* student engagement.

There are different ways in which the emergency transition was handled. The different techniques employed by the authors are described below.

4.1. Blended learning

In all three countries, some classes involved a version of blended learning [16] that was rapidly adapted to the current situation. A typical version of this involved dividing the class into groups, with one group being on campus while the other group(s) experienced online learning. Then on the next class meeting the cohorts changed their modality. For example, a class with 20 students that meets on Tuesdays and Thursdays would be split into two groups of 10 students each. The first group will come to campus on Tuesday and stay at home on Thursday. The second group will stay at home on Tuesday and come to class on Thursday. When on campus, the learning experience will be a traditional version of the classroom experience, but with masks and physical distancing. When possible, the in-person classes met outdoors, as shown in Figure 2. When students are at home, the learning experience will be online.

Figure 2. Students performing laboratory outdoors.

4.2. Hybrid/flexible learning

Some classes employ a variant of HyFlex (hybrid-flexible) learning [5], although not as robust as implemented in full developed Hyflex classrooms [17]. In these situations, students are free to choose if they can attend the class or not on a daily basis. The faculty prepare asynchronous elements for students who cannot attend a specific in-person class. Thus, students will be synchronous some times

and asynchronous others, as fits their schedule. The rapid solution that most schools adopted is really concurrent learning, not HyFlex (see below).

4.3. Concurrent learning

In the concurrent learning model, the classroom is simultaneously streamed online so that students may attend in-person or from home [18]. Note this is different than HyFlex in that there is no designed asynchronous element for students who cannot attend at the scheduled time. At TJU (US), during the scheduled class time of *Engineering Statics*, students either joined remotely via Zoom or showed up in the classroom (wearing masks and keeping a 2-meter spacing from each other and the instructor). The live conversations were streamed via Zoom. In these class sessions, the professor has the students solve problems and provides guidance. Sometimes the class works together, other times the class breaks into small groups using breakout rooms in Zoom. The classroom is conducive to this process as it contains a smart board and multiple video monitors throughout the room (Figure 3).
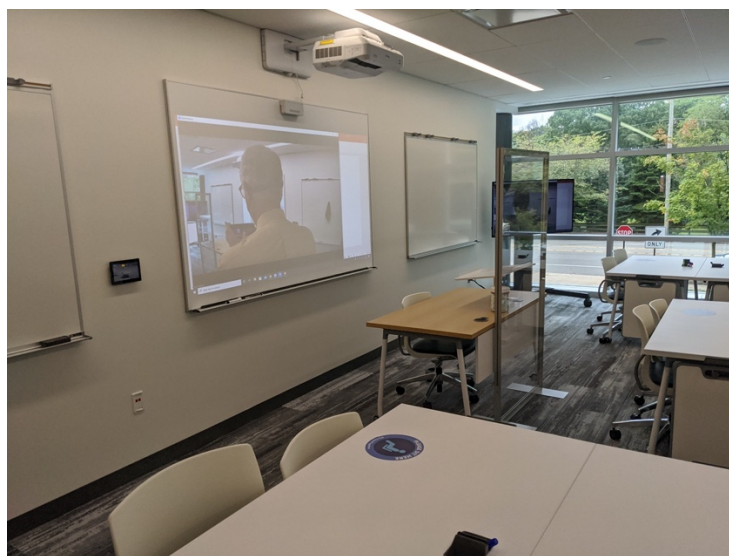

Figure 3. Classroom for Engineering Statics, showing smart board, vinyl barrier and monitor.

4.4. Flipped classrooms

A flipped classroom [8,19] has traditional lecture materials provided as online content and the synchronous activities are focused on problem solving and pursuit of activities traditionally associated with homework. Incorporating "productive failure" (wherein the students work on problems prior to receiving instruction on the topic) in the flipped classroom has been shown to increase student achievement of conceptual understanding [20]. In a flipped classroom environment, the instructor may record themselves giving a lecture, and edit that into several small pieces (5-10 minutes each). These videos are provided to the students online through a learning management system. Students are instructed to watch the videos and read assigned documents prior to joining class. There may also be problem sets for the students to engage. During the synchronous class session, students will engage in problem solving, discussions, and other active learning experiences based on their previous viewing, reading, and problem engagement.

At TJU (US), *Engineering Statics* is a flipped class that employs open educational resources. The professor developed a series of about 100 video lectures that are each about 5-10-minute length. The text book is from the Open Learning Initiative (OLI) at Carnegie Mellon University, which provides a digital course text and tests to the students at no cost. There are multiple online assessments each week. The OLI text book has a series of short questions at the end of each section. The pre-recorded videos have built-in quizzes, where the video stops until the student answers the questions, accomplished using Studio – a video tool within Canvas. There are additional quizzes embedded in

Canvas that the students must answer before they can see the next video, using the prerequisite function of Canvas. In addition to these low stakes assessments, there are monthly examinations. The students will have over 100 small assessments in addition to 4 major assessments in the course.

4.5.   Online small groups

A technique employed within a synchronous online class experience is to make use of small online groups, often called "breakout rooms", during the class. In this way the online session is varied between one large room with all students and professor participating and multiple small rooms with only a few students sharing. This can be good for performing class activities such as "think-pair-share" in an online environment [21].

Each of the universities makes use of breakout rooms during streaming classes to allow the students to process new information presented to them during the session.

5. Specific Examples
5.1.   Germany

One of the problems in the teaching of pattern making and 3D clothing simulation remotely is software licenses. Not all software vendors offer student versions of their software and the students cannot remotely access the university computer systems that have site licenses. *Grafis* (2D patterning software) has a long-term educational version, which the company extended specifically to help students during the pandemic. *CLo3D* offers a limited 30-day license version for no cost. All of the other providers have licensing fees that make the use of the software possible only in the lab on university owned hardware. The only known freeware for pattern making, *Valentina*, is not used by Germany companies yet, and also does not provide the full range of features that the commercial packages offer. Because of this, the content delivery had to be re-organized so that the CAD content could be covered within the 30-day license of *CLo3D*, allowing the students to run the software at home for no cost.

Early in the emergency teaching period, it was discovered that the topics of algorithmic thinking and programming were areas in which the students were not achieving at an acceptable level. To support student success, a separate series of independent lessons with step-by-step demonstration of writing the first lines of code in Python, creating variables and using that for the creation of 3D geometry was prepared and offered to the students. Most of the students worked very actively on these tasks during the semester. These tasks were considered part of the exam. Motivated by this, students submitted their solutions on time. At the end of the course they confirmed that they had learned the necessary skills. The students were happy with the learning software and they enjoyed creating models by doing. A sample of student work on this task is shown in Figure 4.
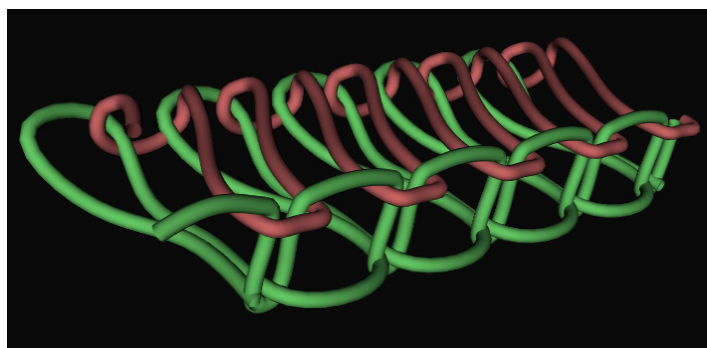

Figure 4. Parametrically generated 3D simulation of 3-thread stitch during the study using Python language and Texmind Viewer.

5.2. SA

Only 33% of total university student are permitted to be present on campus. The other 67% must participate remotely. This offered challenges in South Africa as not all students have access to quality internet connections, or can afford a data plan appropriate for remote learning (unlimited data is unusual in SA). To address this, Durban University of Technology provided sufficient data access to all students and some staff for internet connectivity. For students that have no access to the internet, physical copies of materials as well as digital copies on memory sticks were delivered to their homes.

Class schedules were adjusted to account for shutdowns (see Table 1) and new timetables were introduced and communicated to all students and staff.

Moodle is used as the primary communication and course management tool for all classes. Study materials in form of notes, PowerPoint presentations, short video recordings, YouTube clips on processes, etc. were uploaded or linked to Moodle before teaching started for each section.

Students living in remote and rural areas have very poor access to the internet. In addition, not all students have the necessary devices to communicate digitally. About 60-70% of the students do not have access to a computer of any kind except smart phones. Not all students have a smart phone. The university is in the process of providing devices to those who do not have one. At this point, including phones, about 85% of students have some level of access to the internet.

Although all classes use Moodle, several faculty also made use of WhatsApp for their courses. The DUT Clothing program uses WhatsApp very effectively. WhatsApp was loaded on staff laptops, and lecturers can (and do) record audio over power point slides or photos during lectures. These videos are shared with the students if they cannot attend synchronously.

Comparing the effectiveness of the two digital platforms, it was found that student participation was higher with WhatsApp than Moodle. Based on second year Textile Technology classes, online class attendance using Moodle was about 30-40% at best, but on WhatsApp it is about 80-90%, as illustrated in Figure 5.
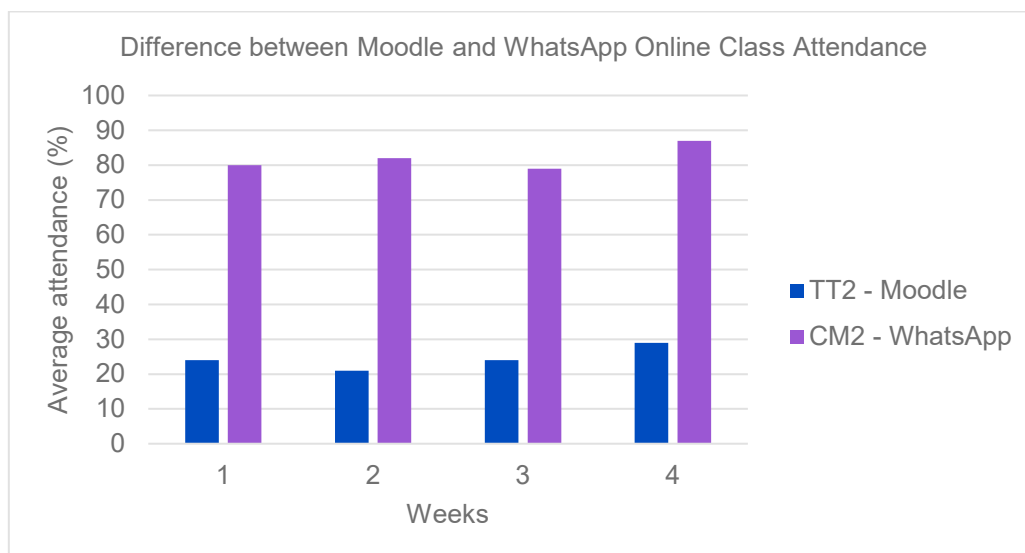

Figure 5. Second year Textile Technology student attendance as a function of distance collaboration tool: Moodle or WhatsApp at Durban University of Technology.

A comparison of first and second year students for classes using WhatsApp showed the participation of second year students was better than that of first year students, as shown in Figure 6.
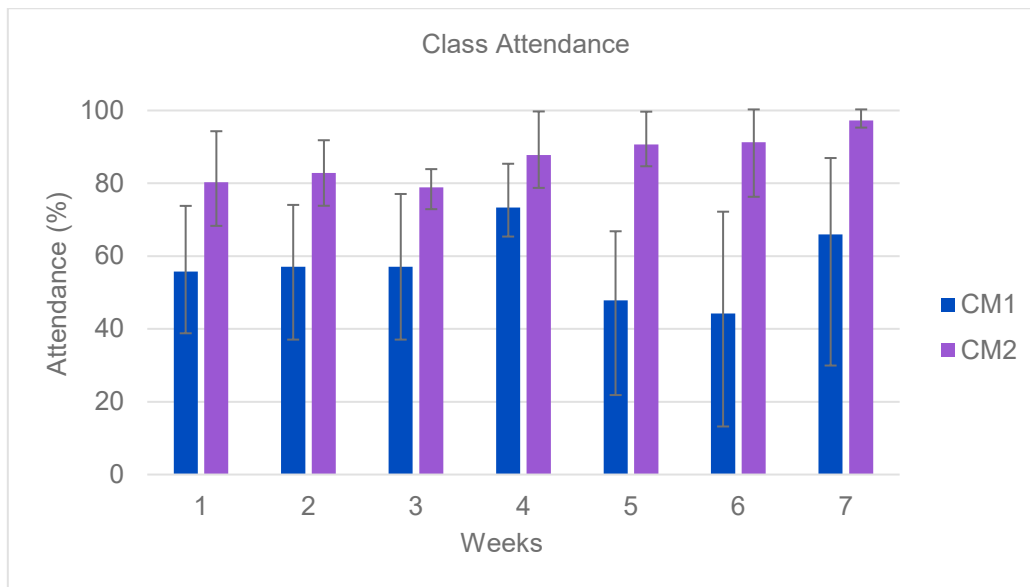
Figure 6. Comparison of Clothing Management 1 and Clothing Management 2 student attendance at DUT.

Because the majority of the students do not have access to a computer, the use of software such as Gerber and CAD as well as hands-on practical experiences were scheduled towards the end of semester when students were allowed to return to campus in smaller groups. The practical experiences were staggered so that when one group was attending laboratory work the other group was attending online classes. These online classes were recorded and uploaded for all groups to maintain safe social distancing.

5.3. USA

In preparation for a blended learning experience [22], faculty created demonstration videos using weaving, knitting, and print equipment present in the TJU laboratories and studios. Students were encouraged to view the videos before and during in-person learning experiences. Students view the pre-recorded elements and also come to the campus for in-person experiences.

Challenges arise during class time in the event of an error by the student. In traditional times, the faculty would stand beside the student to assist them in resolving the issue. During the pandemic, to maintain safe social distancing, faculty took one of two approaches:

(1) they encourage the student to analyze the situation and talk through how to resolve it, or

(2) switch physical positions with the student and address the complication.

For Computer-Aided Design (CAD) based learning in Jacquard woven, electronic knit, and digital print development, methods were developed to permit students to access terminals on campus that run the specific software via a remote desktop client. In doing this, license permissions remained with the university, and students' access to these resources is equitable. The faculty created several step-by-step procedure screen-recording videos for processes related to the software they teach. The video content is provided to the students via the university's learning management system (Canvas). Students use valuable synchronous digital learning time to ask questions and present design development for critical review.

The companies that produce this software are pushing for advanced simulation development to remove pressure from the strained supply chain. Students learn to analyze the simulation results compared to the textile goods produced on the studio's industry-grade equipment. Analytics generated from these trials allow the students to create more realistic expectations for consumers and prepare them to design more efficiently.

6. Assessment

Assessment of student work is of paramount importance. In this unusual environment, special attention was paid to the methods of assessment to ensure learning was happening. Comparisons between the traditional student performance and achievement in the emergency state was performed.

6.1. Germany

Traditionally, the courses are assessed by a final examination coupled with performance in laboratory experiences. However, with the transition to remote learning, it was decided to provide multiple assessments throughout the semester.

For example, in *Machines and processes in the clothing industry*, several pieces of homework were combined to be considered part of the final exam. The faculty developed 4 individual tasks with defined deadlines. For instance, task 1 was:

- create parametric 3D model of the sewing stiches,
- visualize these models,
- generate different human bodies with available open source software,
- prepare cross sections of the generated body with ParaView,
- calculate the circumference of the sections, and
- simulate the garment on a human body using Blender, while varying the bending, areal density, and shear properties of the fabrics. An example of student work is shown in Figure 7.

In contrast, another course, *Construction of sewing and welding machines*, used the traditional single final exam with no points awarded from homework during the semester. The participation with the online lessons was "moderate" – approx. 40-50% of the students were always online following the lectures, but the remaining students only checked the material asynchronously. The results in the exam were also "moderate". For this subject it is difficult to create realistic tasks for doing things at home, because the main phases of the machine motion and the interactions between yarns and machine elements have to be studied. These can be shown with animations and video recorded films, but this is still passive learning, and not experimental.

Figure 7. Three steps of simulation of the interaction between human body and cloth with the open source software Blender

6.2. SA

Due to the required change in teaching and learning modes from contact to blended learning, all examinable assessment methods for the Textile Science and Textile Technology programs were revised. Traditionally the assessment consisted of in-person course work with a major assessment at the end, but currently has transitioned to continuous assessment, where a number of formative assessments are graded and tallied throughout the semester to determine the final mark.

In this blended method each faculty member gives a number of graded assignments throughout the semester, with a minimum of 3-4 assessments around weeks 6, 9, 12 and 15, as well as additional assessment at the end of the course for borderline students (a make-up assessment). Students are given grades after each mid-semester assessment within a week of submission. The lecturers also provide feedback to the students regarding their performance in the class about their performance so far.

6.3. USA

The challenge of evaluating student textile work now encompasses a more extensive range of criteria. Color and texture evaluations relate to salability and market appropriateness. Scale, drape, stitch density, and other performance characteristics define end-use possibilities. Notably, the tactility of student produced textiles informs about success in student development. Removing in-person interaction with textile ideation, creation, and critique means that students and faculty had to communicate and assess those characteristics in novel and innovative ways. Documenting a collection of textiles as more than a grouping of flat surfaces, demonstrating the hand of fabric using video content, and using slide layout, color story, and typography as tools to enhance a collection are now criteria in assessing textile presentations.

The absence of in-person critiques and the ability to evaluate the fabric's qualities in hand has forced the students to research and expand their digital documentation and presentation knowledge. Using cellphone cameras and photo-processing software, students build professional presentations that demonstrate their technical textile understanding and aesthetic abilities. Within one semester, the professional progression of student work is dramatic. In each step, evidence of more significant investment in their process and documentation is clear. With an uncertain future and a rapid transition to virtual interviews, students have adjusted rapidly to exhibiting and communicating the successes of their developments and their textiles' physical attributes.

7. Student Response
7.1. US

The forced remote instruction empowered the students to think critically about their process and issues that arose. Students were responsible for continuing to develop their creative practice with whatever resources they had at their disposal. In the Spring 2020 semester, one student created a circular knitting device from a hair curler and flat metal bobby pins to achieve the required tubular knit structure, as shown in Figure 8. Another student created dress forms from household items, including a makeup brush and pool noodle, to construct and display her capstone collection.

Figure 8. Circular knitting device created at home by one of the textile students.

Students were asked to complete a voluntary survey about their experience with the classes this semester. They were asked to rate different elements of the course on a scale from 1 (very not-useful) to 5 (very useful), including overall course progress, as well as synchronous lecture, pre-class readings, quizzes, discussion boards and pre-recorded videos. For one lecture-based engineering class, the students' responses are shown in Figure 9.
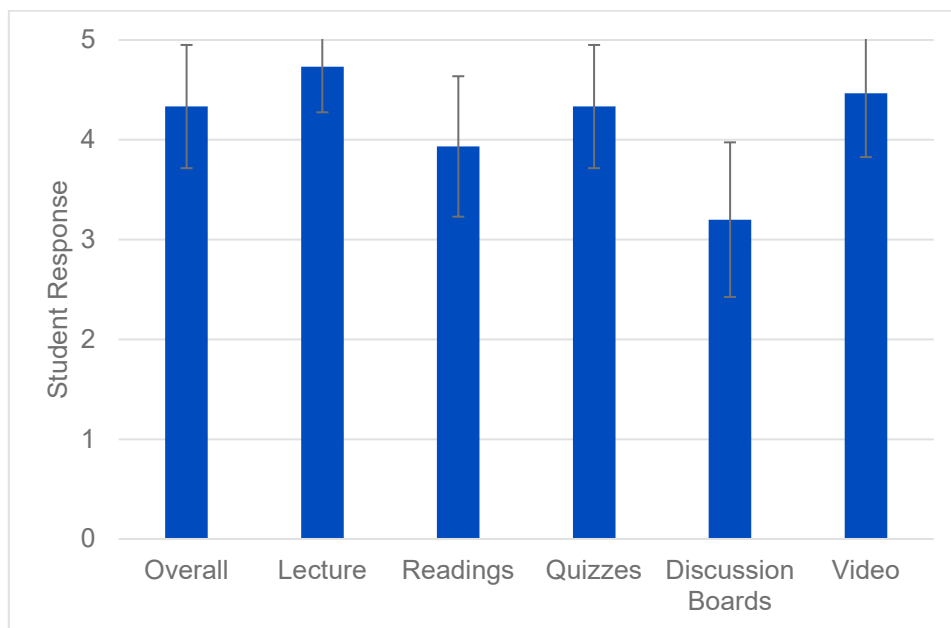
Figure 9. Student response to perception of usefulness of various elements of a lecture-based course.

Students were surveyed to evaluate their perceptions of their ability to handle the online/remote classes. The results are shown in Figure 10. It can be seen that their feelings are distributed across the spectrum of responses.
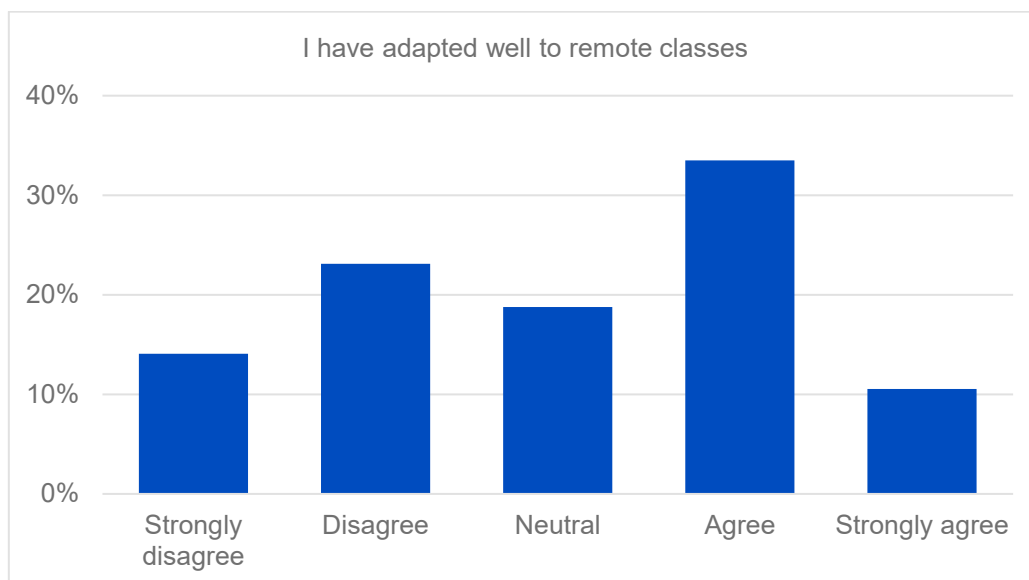
Figure 101. Students' self-assessment of their ability to adapt to remote classes.
Approximately 600 students participated in this survey.

Students were also asked to evaluate how well their instructors have dealt with the transition. The results are shown in Figure 11. It can be seen that the students had a generally favorable impression of the faculty's ability to adapt to the situation.

Figure 11. Students' perceptions of their instructors' ability to adapt to the remote teaching environment. Approximately 600 students participated in this survey.

Focusing on the students who expressed difficulties with adapting, their comments fell into seven main themes:
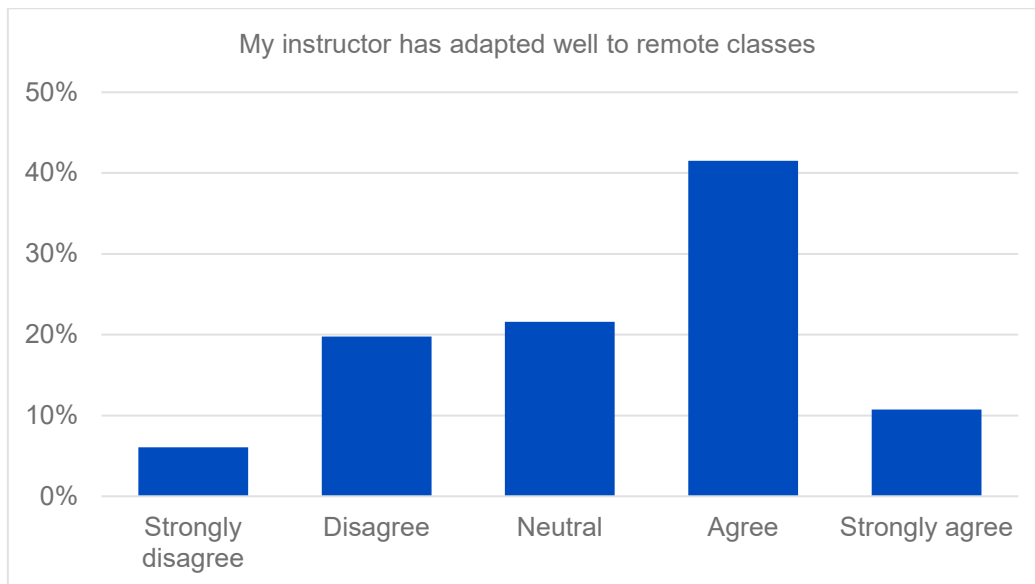
1. Lack of flexibility from professors as well as increased workload
2. Need improved online delivery (format, programs, content) vs "busy work"
3. Technology & internet issues at home
4. Difficulty concentrating off campus (distractions) and adapting to online format
5. Financial stress/unemployment/working multiple jobs
6. Caring for family while at home & family issues
7. Mental health issues/anxiety

These students offered recommendations to improve the experience:

- Partial tuition reimbursement
- Refund for services no longer provided (i.e. gym, library, housing)
- Provide further hands-on skills labs for soon to be graduate nurses
- Professors need to work on making content and lectures more concise
- Improve quality of course material delivered online
- Decrease workload and provide leniency – many professors are unaccommodating
- Improve communication from faculty to students

8. Faculty Response

The faculty response to the sudden switch to remote teaching was varied. For many faculty, the timing, restrictions regarding access to teaching spaces and limited resources created a significant challenge.

Conversely, the transition required a switch to digital assignment submissions which created a greater ease of content collection for program assessment.

The administrations in Germany and US developed robust faculty development programs, including "how to" videos, as well as online training sessions and workshops. Software licenses were provided to faculty for various digital tools.

In April, 2020, faculty in the US were asked in a survey to evaluate their level of confidence with online teaching. As can be seen in Figure 12, faculty expressed a fairly high level of confidence in their ability to teach online, which is consistent with student perceptions, although slightly more optimistic.
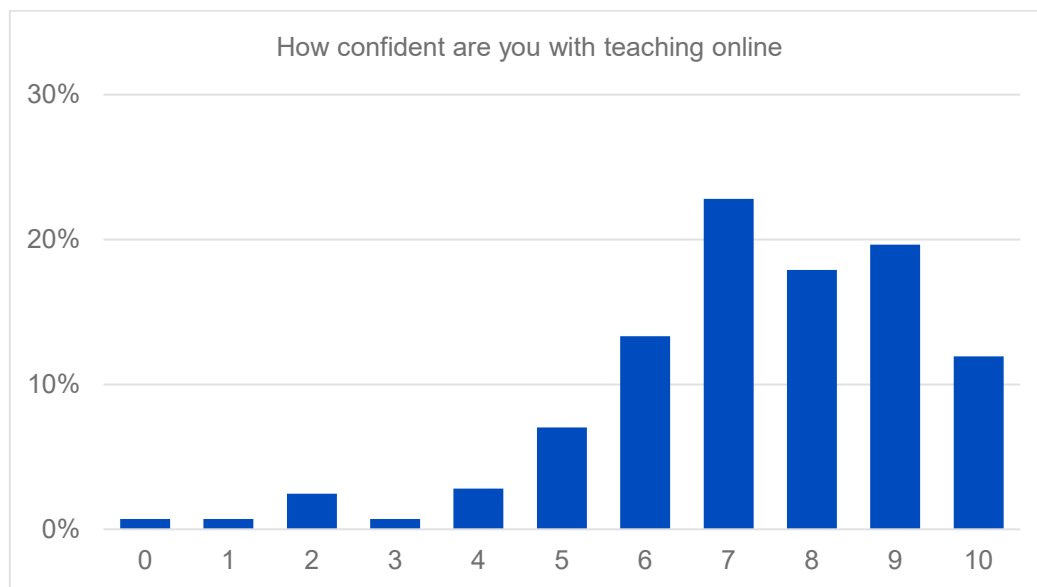

Figure 12. Faculty survey response to the question "How confident are you with teaching online."
Response ranged from 0 (no confidence at all) to 10 (completely confident).
Approximately 300 faculty members responded to the survey.

9. Discussion and Concerns

The challenges facing all of us are similar, but to different degrees. Students with no internet access (or poor-quality access) are a concern, although more common in SA than in the other countries. Even in the US, where it is mandatory for a student to own a computer while attending TJU, there are occasions where the device has failed, or a student could not afford one. In the past we would have directed such students to the public library, but those are closed.

This mode of learning has presented various challenges and required faculty to do significant work before the semester began. These dedicated instructors learned to use video-recording equipment and video-editing software on their own time to generate these teaching tools.

Learning environments are social communities. The studio/lab experience for members of the TJU textile student group solidifies the cohort's bonds and develops the open channels of communication. This genuine communication impacts critiques and feedback opportunities as well as the sharing of knowledge and peer-mentorship. Those relationships are developed during hours working and supporting one another in the communal studio/lab environment. The concern exists that the loss of that open studio freedom might result in a shift in the studio culture. Faculty are working to develop online opportunities for students to interact and bond. So far, student buy-in to these experiences has been positive, but the future will show how the blended/hybrid learning experiences affect student interactions and peer-support.

Generally, faculty felt that the transition was a heavy lift, requiring effort beyond their normal workload. At the writing of this paper, the US is in their 3rd semester of online teaching, and the faculty have adapted and have fewer complaints about the excess burden.

Several faculty have indicated that there will be positive outcomes from this experience, as they have learned to use more digital tools that will be helpful even in the "normal" classroom environment.

In the knitting classes, the instructional videos that were developed to explain the operation of the machinery to students was very successful. Students came to the lab in small groups and the instructor observed that they were able use the equipment more effectively and with greater success than previous classes. Additionally, as they were knitting they were able to refer back to those videos and zoom in to see specific elements in detail.

For labs that could not meet in person, small kits were assembled and sent to each student's home so they could perform experiments remotely. Instructors provided introductory videos and the labs were performed online synchronously. The instructor indicated that this was effective and students expressed a positive experience including student opinions that there was less pressure when they were working at home than when surrounded by classmates.

For large equipment, such as ultrasonic seaming, there was no solution for at-home explorations. It was necessary for the students to come to the university in person, but in small groups, to operate it. But for smaller equipment, some home sewing machines were purchased and sent around from student to student to experiment and develop practical skills at home. A rotating set of small equipment can be developed with students working on projects in a cyclical manner.

References

[1] Francie Diep and Andy Thomason. UNC Pulls the Plug on In-Person Fall. Will Other Campuses Follow? (August 18, 2020) Available from: https://www.chronicle.com/article/unc-pulls-the-plug-on-in-person-fall-will-other-campuses-follow

[2] University of Notre Dame. Notre Dame Covid-19 Dashboard. Available from: https://here.nd.edu/our-approach/dashboard/

[3] Randy Woodson. Fall Semester Undergraduate Classes Moving Online. (August 20, 2020) Available from: https://www.ncsu.edu/coronavirus/fall-semester-undergraduate-classes-moving-online/

[4] M. A. da Silveira and L. C. Scavarda-do-Como. 1999. Sequential and concurrent teaching: structuring hands-on methodology. *IEEE Trans Educ.* 42, 2, 103-108.

[5] Brian Beatty. 2014. Hybrid courses with flexible participation: The HyFlex course design. In: Lydia Kyei-Blankson, Esther Ntuli (Eds.). Practical Applications and Experiences in K-20 Blended Learning Environments. IGI Global, Pennsylvania, USA, pp. 153–177.

[6] N. Solihati, H. Mulyono. 2017. A hybrid classroom instruction in second language teacher education (SLTE): A critical reflection of teacher educators. *Int. J. Emerg. Technol. Learn*. 12, 5,169-180.

[7] B. Manamela. (August 26, 2020). Coronavirus COVID-19 Alert Level 2 Measures in the Post School Education and Training Sector. Retrieved June 15, 2020 from: https://www.gov.za/speeches/minister-blade-nzimande-coronavirus-covid-19-alert-level-2-measures-post-school-education.

[8] J. A. Klemens, C. Pastore, M. Hudson. 2015. Harness student creativity and expertise. In: C. Sweet, H. Blythe, R. Carpenter (Eds.). It works for me, flipping the classroom. New Forum Press, Stillwater, OK.

[9] OPAL. Available from: https://bildungsportal.sachsen.de/portal/

[10] DFN Conference. Available from: https://www.conf.dfn.de/

[11] DokuWiki. Available from: www.dokuwiki.org

[12] Laura Czerniewicz. (March 15, 2020). What we learnt from "going online" during university shutdowns in South Africa. PhilOnEdTech. Available from: https://philonedtech.com/what-we-learnt-from-going-online-during-university-shutdowns-in-south-africa/

[13] Robert M. Bernard, Philip C. Abrami, Eugene Borokhovski, C. Anne Wade, Rana M. Tamim, Michael A. Surkes, Edward Clement Bethel. 2009. A meta-analysis of three types of interaction treatments in distance education. *Review of Educational Research* 79, 3, 1243-1289.

[14] Barbara Means, Marianne Bakia, Robert Murphy. 2014. *Learning online: what research tells us about whether, when and how* (1st ed.). Routledge, London, England.

[15] John A. Milligan. 2020. What is the value of synchronous engagement in small remote organic chemistry classes? Analysis of multiple-choice polling data from the COVID-impacted spring semester of 2020. *J. Chem. Educ*. 97, 9, 3206-3210.

[16] C. J. Bonk, C. Graham (Eds.). 2006. *The handbook of blended learning: global perspectives, local designs* (1st ed.) Pfeiffer, San Francisco, USA.

[17] Lydia Kyei-Blankson, Francis Godwyll, Mohamed A. Nur-Awaleh. 2014. Innovative blended delivery and learning: exploring student choice, experience, and level of satisfaction in a hyflex course. *International Journal of Innovation and Learning* 16, 3, 243-252.

[18] D. Michele Jacobsen, Rob Kremer, Mildred L. G. Shaw, Niek J. E. Wijngaards. 1999. The learning web: a technical evaluation of webCT in concurrent classroom and distance education sections of a software engineering graduate course. In B. Collis, R. Oliver (Eds.). *Proc. of EdMedia 1999 – World Conference on Educational Multimedia, Hypermedia & Telecommunications.* Seattle, WA, USA: Association for the Advancement of Computing in Education, 1340-1341.

[19] Clyde Freeman Herreid and Nancy A. Schiller. 2013. Case studies and the flipped classroom. *Journal of College Science Teaching* 42, 5, 62-66.

[20] Yanjie Song and Manu Kapur. 2017. How to flip the classroom – "Productive Failure or traditional flipped classroom" pedagogical design? *Educational Technology & Society* 20, 1, 292-305.

[21] Adekunle Oladipupo Bamiro. 2015. Effects of Guided Discovery and Think-Pair-Share Strategies on Secondary School Students' Achievement in Chemistry. *SAGE Open* 5, 1, 2158244014564754.

[22] Nicky Hockly. 2018. Blended Learning. *ELT Journal* 72, 1, 97-101.

Influence of washing and thermal post-treatment on the adhesion between 3D-printed TPU and woven fabrics

Jannik Störmer, Daniel Görmer, Andrea Ehrmann*

Bielefeld University of Applied Sciences, Faculty of Engineering and Mathematics, Bielefeld, Germany
*Corresponding author *E-mail address:* andrea.ehrmann@fh-bielefeld.de

INFO

ABSTRACT

3D printing on textile fabrics can be used to create composites with position-dependent mechanical, water-resistant, magnetic or other properties. An important prerequisite to use such composites technologically or for design purposes is a sufficient adhesion between both materials. While previous studies revealed that soft, elastic printing polymers were advantageous to prepare connections with a high adhesion, not much research has been performed yet on the dependence of the adhesion on textile fabric structure, heat post-treatment, and the influence of washing, which is necessary for most applications of such composites. Here we investigate composites from thermoplastic polyurethane (TPU) 3D-printed on two different woven cotton fabrics. Besides the expected strong correlation of the adhesion with the distance between nozzle and printing bed, we find a higher adhesion on the thinner fabric and an increase in the adhesion after one washing cycle.

1 Introduction

During the last years, 3D printing has more and more emerged from a rapid prototyping to a rapid printing technology, allowing for producing single objects or complicated shapes which cannot be produced in a different way. One of the problems in the utilization of 3D printing techniques for a broader range of applications is the relatively low mechanical stability due to the layered production process, for which several research groups suggested different possible solutions [1-3].

Besides integrating nano- or microfibers into the filament, thermal post-treatment or inventing new polymers with improved mechanical properties [4-6], combining 3D printed objects with textile fabrics can increase the tensile properties of the 3D print and the stiffness of the fabric, respectively. While recently

a first proof-of-principle showed that this combination is possible with stereolithography (SLA) [7], most research groups investigate combinations of textile fabrics with 3D printed objects produced by fused deposition modelling (FDM).

In most cases, combining relatively dense fabrics without large pores with rigid 3D printing filaments, such as poly(lactic acid (PLA) or acrylonitrile butadiene styrene (ABS) results in severe problems with the adhesion between both parts of these composites, resulting in a large amount of research dealing with this challenge. Different groups found, e.g., an influence of the printing bed temperature [8], the textile structure [9-12] and especially the distance between nozzle and fabric [13,14] on the adhesion. In addition, chemical pretreatment of the textile fabrics [15,16] or thermal post-treatments [16,17] could alter the adhesion in a positive or also negative way.

Another way to receive a strong adhesion between both parts of the composites is using thermoplastic polyurethane (TPU) or similar elastic printing materials which can more easily penetrate into the fabric and thus build form-locking connections [17,18]. In a previous study, we found that a thermal post-treatment by ironing further increased the adhesion forces between TPU and warp-knitted fabrics [17]. Here, we report on printing TPU on two different cotton woven fabrics, partly using a heat press to perform thermal post-treatment under well-defined pressure, and testing the adhesion before and after washing to enable using such sandwiches for clothing applications.

2   Experimental

The 3D printer used is a CR-10S Pro (Creality, Shenzhen, China) with a nozzle diameter of 0.4 mm. Rectangles with dimensions of 120 mm x 25 mm x 0.8 mm were printed with a layer thickness of 0.2 mm and a printing speed of 15 mm/s for all parts of the objects (perimeters, top/bottom layers, infill). The infill density is 100 % with an orientation of ± 45°. The reference point for the printing bed leveling, performed by a feeler gauge at 5 positions, is 0.2 mm, i.e. the optimum height for printing directly on the printing bed.

The tests were carried out with the TPU filament Filaflex 82A (Recreus, Elda, Spain) and two different fabrics made of 100% cotton. Thickness measurements were taken with a caliper gauge and with a textile thickness tester J-40-T (Wolf-Messtechnik GmbH, Freiberg, Germany). While the latter gives the conventional textile thickness, the first value measured a compressed thickness which is more relevant for the situation of 3D printing on the fabric, where the nozzle is also pressed onto the fabric on a small area. One fabric is 0.2 mm (0.37 mm) thick and has a firmer fabric structure (plain weave, warp threads 22/cm, weft threads 25/cm), the other one is 0.4 mm (0.78 mm) thick and has a softer structure (twill 1/3, warp threads 18/cm, weft threads 24/cm). The textile fabric was glued onto the printing bed with green-tape, slightly stretched so that the nozzle could not move it laterally. The filament was printed at a nozzle temperature of 230 °C. The heatable print bed remained deactivated. Offsets of -0.05 mm and -0.15 mm with respect to the reference height were used for printing, i.e. printing was performed "inside" the fabrics in all cases, with the distance between nozzle and printing bed being smaller than the textile thickness. Adhesion tests were performed with samples printed with both offsets.

The heat post-treatment was performed by a heat press YF-14 (GuangZhou Amonstar Trade Co.,Ltd, London, United Kingdom). The thermopressing process was carried out for 10 seconds at 180 °C (thin fabric) and for 10 seconds at 200 °C (thick fabric), respectively, with constant pressure. The textile fabric was placed on the heated side of the press to prevent the polymer part from being heated too strongly.

Some of the samples with and without thermal post-treatment were washed using a Miele Novotronic W986 WPS (Miele & Cie. KG, Gütersloh, Germany) and the textile care product "Der Weiße Riese" (Henkel Wasch- und Reinigungsmittel, Düsseldorf, Germany). Cleaning was performed using the "Easy Care 40 °C" program for 30 minutes, plus a 30-minute spin cycle at 900 rpm. For drying, the samples were hung on a clothes rack and air dried.

The adhesion between textile fabric and imprinted polymer was investigated on a Sauter universal testing machine at a speed of 100 mm/min. The procedure was based on DIN 53530 (for a sketch of the test, cf. [17]); the tests were evaluated in accordance with ISO 6133. For each sample, one end of the filament was manually detached from the textile and clamped in the Sauter machine to perform the adhesion force test. All tests were performed with 4 replicates.

3 Results and discussion

Fig. 1 shows the results of all adhesion tests performed on the raw, unwashed specimens, untreated or after thermal post-treatment.

Firstly, comparing the untreated fabrics, it is obvious that printing at a lower nozzle position, i.e. at -0.15 mm (in other words 0.05 mm above the printing bed), is clearly advantageous for the adhesion. Unexpectedly, the highest values are here not reached for the thick woven fabric, but for the thin one.

Comparing the heat-treated samples, they show mostly an increased adhesion force, with the values of the thin sample printed at -0.15 mm being similar to the one of the untreated specimens. The smallest adhesion forces can be found for the thick samples printed at the higher nozzle position of -0.05 mm.
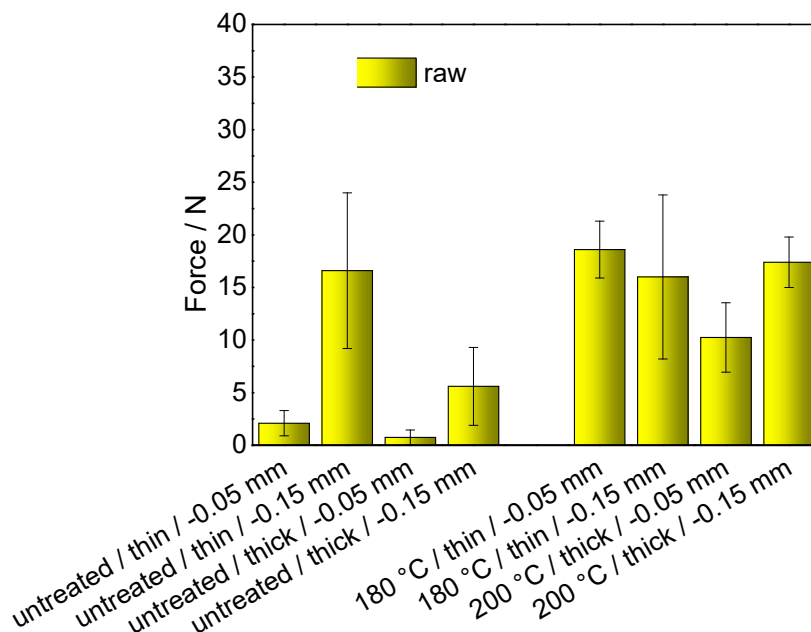

Fig. 1 Results of adhesion tests after printing and partly heat-treating.

To understand this behavior, Fig. 2 shows microscopic images of the untreated samples, comparing the back of the 3D printed parts after the adhesion tests. Interestingly, the TPU layers on the thin fabric (Fig. 2a, b) show stronger imprints of the fabric on which they were printed than the TPU on the thick fabrics (Fig. 2c, d). This finding can be correlated with the thicker fabric being "softer" due to its twill structure which allows for shifting the single threads away during printing, while the plain weave structure of the thin fabric impedes sliding of the yarns. Besides, the imprinted structure seems to have sharper edges for the samples printed at -0.15 mm, as compared to those printed at the higher nozzle position, which underlines the importance of the distance between nozzle and printing bed.

In both cases, a deeper look at the images reveals more fibers on the TPU layer, thrown out of the respective fabrics during the adhesion tests, for the lower nozzle position of -0.15 mm. This explains the clear differences between the adhesion forces of the samples printed at higher and lower nozzle position.
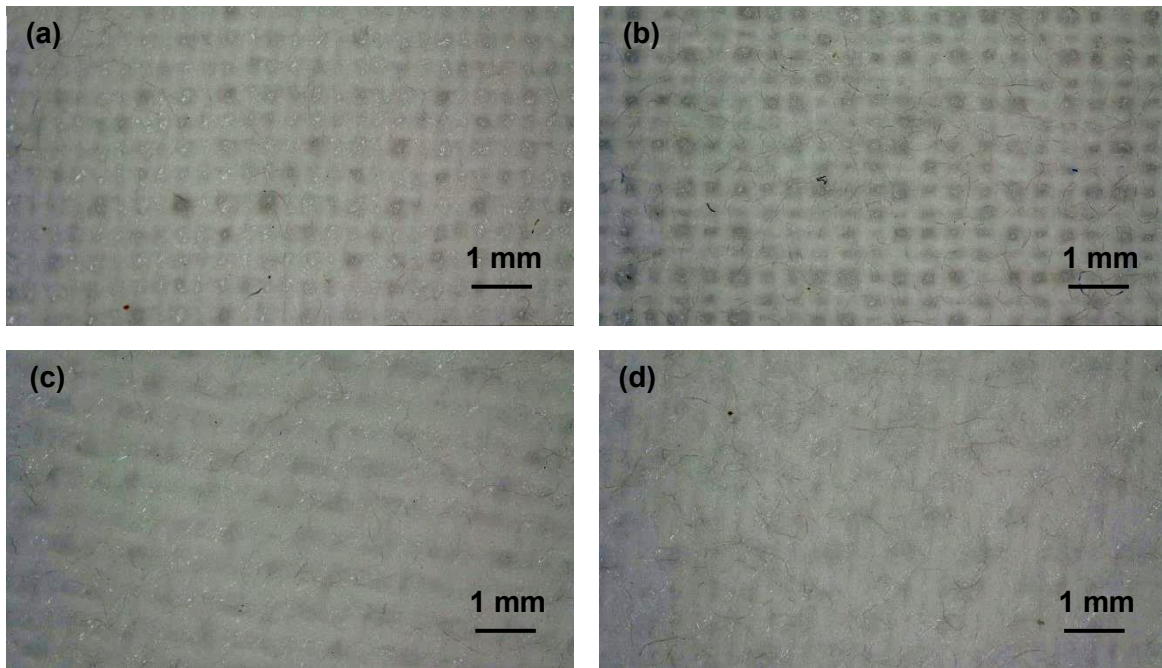
Fig. 2 Microscopic images of the back of the detached TPU after adhesion tests performed on the untreated samples. (a) thin fabric, -0.05 mm; (b) thin fabric, -0.15 mm; (c) thick fabric, -0.05 mm; (d) thick fabric, -0.15 mm

Comparing the lower side of the TPU parts of the heat-treated specimens, the imprinted structures remain unaltered, while some more fibers detached from the textile fabrics become visible (not shown here). This indicates that although the temperatures used for heat-pressing are sufficient to soften the TPU, the polymer does not melt completely, so that the penetration into the textile fabric cannot be increased. Only the attachment to the upper fibers of the textile fabrics is improved, which is, however, sufficient to increase the adhesion in most cases significantly.

Next, Fig. 3 depicts the results of the adhesion tests after washing the samples. Surprisingly, most values are larger than those measured for the unwashed samples, while the opposite behavior had been expected.
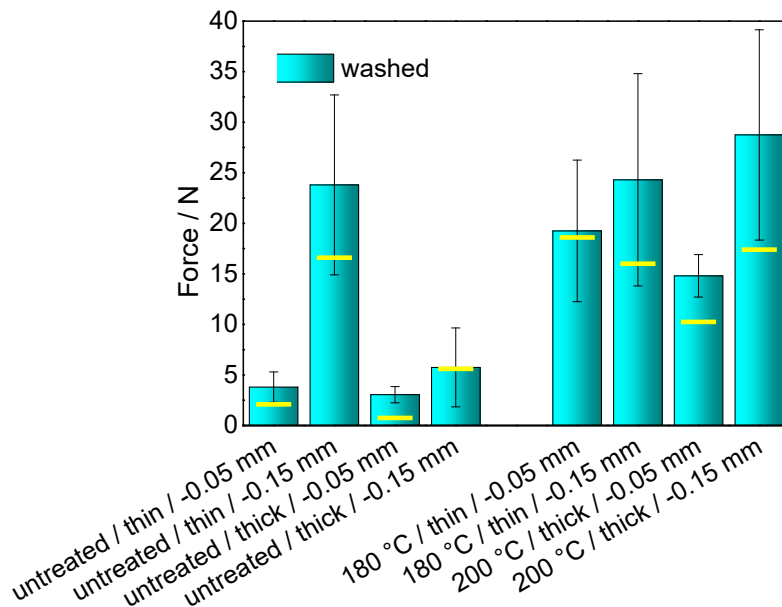

Fig. 3 Results of adhesion tests after washing the printed and partly heat-treated samples. Yellow bars indicate the average values of the raw samples, as shown in Fig. 1

Comparing the untreated samples, again the thin fabric with the lower nozzle position of -0.15 mm shows the highest adhesion. In case of the heat-treated samples, these show again mostly higher adhesion values then the untreated specimens, with a tendency to larger adhesion values for the samples printed at the lower nozzle position of -0.15 mm. Microscopic images of the back of the TPU parts do not show significant differences from the investigations of the unwashed samples.

These tests indicate that washing does not generally reduce the adhesion between 3D printed TPU parts on textile fabrics. It must be mentioned, however, that the objects used here are thin layers which are less prone to be torn off the fabric than higher object which may be printed on clothing due to design aspects. Besides, here we show the results for a first washing test, while tests with 10 or more washing cycles must follow.

The increase of the adhesion due to washing, found for most of the samples, is not easy to explain and needs further investigations. Washing was performed at 40 °C, i.e. far below the printing temperature, so that no structural modifications of the polymer layer can be expected. Thus, most probably, small changes happened inside the woven fabrics, i.e. relaxation processes as usual due to the combination of temperature, reduced yarn-yarn friction because of water and detergent, and the input of mechanical energy [19]. In this way, the fabric may become slightly denser, thus increasing the form-locking connection to the imprinted polymer layer. At the same time, the single cotton fibers may experience a better adhesion inside the yarn, so that pulling them out of the yarn, as it happens for many fibers during the adhesion test, will become harder. These assumptions, however, have to be investigated further in the future.

Another topic which must be discussed is the length of the error bars in Figs. 1 and 3. In most cases, the standard deviations are relatively large. This can be attributed to slightly varying distances between nozzle and printing bed, either due to an uneven printing bed or due to small deviations stemming from the (manual) adjustment of the printing bed.

While many printers nowadays offer the possibility to level the printing bed automatically directly before printing, this procedure is not possible if a textile fabric is already glued onto the printing bed. On the other hand, comparing the adhesion of the untreated fabrics, it is obvious that a height error of 0.1 mm already causes significant deviations of the adhesion (cf. Figs. 1 and 3). This suggests developing a procedure which enables auto-levelling in spite of textile fabrics being glued on the printing bed; a topic at which a recent study of our group is aiming.

4 Conclusions

Cotton fabrics of different thickness and woven structure were 3D-imprinted with TPU to test the adhesion between both partners of this composite. Unexpectedly, the adhesion of the untreated fabrics was higher on the thin plain weave fabric than on the thick twill fabric. On the other hand, the expected influence of the distance between nozzle and printing bed was verified. After heat-pressing the samples, these differences were largely leveled out. Washing the samples unexpectedly increased the adhesion slightly.

As the large deviations of the adhesion within one specimen or between nominally identical specimens, printed on neighboring positions of the printing bed, show, it is necessary to define a process to allow for auto-levelling the printing bed for the case of a textile fabric glued onto the printing bed.

References

[1] Arunothayan, A. R.; Nematollahi, B.; Ranade, R.; Bong, S. H.; Sanjayan, J. Development of 3D-printable ultra-high performance fiber-reinforced concrete for digital construction. *Construction and Building Materials* 2020, 257, 119546. DOI 10.1016/j.conbuildmat.2020.119546.
[2] Afshar, A.; Mihut, D. Enhancing durability of 3D printed polymer structures by metallization. *J. Mater. Sci. Technol.* 2020, 53, 185-191. DOI 10.1016/j.jmst.2020.01.072.

[3]   Oviedo, A. M.; Puente, A.H.; Bernal, C.; Perez, E. Mechanical evaluation of polymeric filaments and their corresponding 3D printed samples. *Polymer Testing* 2020, 88, 106561. DOI 10.1016/j.polymertesting.2020.106561.

[4]   Dong, J.; Mei, C. T.; Han, J. Q.; Lee, S. Y.; Wu, Q. L. 3D printed poly(lactic acid) composites with grafted cellulose nanofibers: Effect of nanofiber and post-fabrication annealing treatment on composite flexural properties. *Additive Manufacturing* 2019, 28, 621-628. DOI 10.1016/j.addma.2019.06.004.

[5]   Chalgham, A.; Wickenkamp, I.; Ehrmann, A. Mechanical properties of FDM printed PLA parts before and after thermal treatment. *Polymers* 2021, 13, 1239. DOI: 10.3390/polym13081239.

[6]   Stepashkin, A. A.; Chukowv, D. I.; Senatov, F. S.; Salimon, A. I.; Korsunsky, A. M. Kaloshkin, S. D. 3D-printed PEEK-carbon fiber (CF) composites: structure and thermal properties. *Composites Science and Technology* 2018, 164, 319-326. DOI: 10.1016/j.compscitech.2018.05.032.

[7]   Grothe, T.; Brockhagen, B.; Storck, J. L. Three-dimensional printing resin on different textile substrates using stereolithography: A proof of concept. *J. Eng. Fibers Fabrics* 2020, 1, 1558925020933440. DOI: 10.1177/1558925020933440.

[8]   Eutionnat-Diffo, P. A.; Chen, Y.; Guan, J. P.; Cayla, A.; Campagne, C.; Zeng, X. Y.; Nierstraz, V. Stress, strain and deformation of poly-lactic acid filament deposited onto polyethylene terephthalate woven fabric through 3D printing process. Sci. Rep. 2019, 9, 14333. DOI 10.1038/s41598-019-50832-7.

[9]   Narula, A.; Pastore, C.; Schmelzeisen, D.; El Basri, S.; Schenk, J.; Shajoo, S. Effect of knit and print parameters on peel strength of hybrid 3D printed textiles. J. Text. Fibrous Mater. 2018, 1: 2515221117749251. DOI 10.1177/2515221117749251.

[10]   Meyer, P.; Döpke, C.; Ehrmann, A. Improving adhesion of three-dimensional printed objects on textile fabrics by polymer coating. J. Eng. Fibers Fabrics 2019, 14, 1558925019895257. DOI 10.1177/1558925019895257.

[11]   Calvo, J.O.; Martin, A.C.; Ferradas, M.I.R.; Morcillo, P.L.F.; Munoz, L.M.; Camo, P.M. Additive manufacturing on textiles with low-cost extrusion devices: Adhesion and deformation properties. Dyna 2019, 64, 8893. DOI 10.6036/8893.

[12]   Mpofu, N. S.; Mwasiagi, J. I.; Nkiwane, L. C.; Njuguna, D. Use of regression to study the effect of fabric parameters on the adhesion of 3D printed PLA polymer onto woven fabrics. Fashion and Textiles 2019, 6, 24. DOI 10.1186/s40691-019-0180-6.

[13]   Grimmelsmann, N.; Kreuziger, M.; Korger, M.; Meissner, H.; Ehrmann, A. Adhesion of 3D printed material on textile substrates. Rapid Prototyping J. 2018, 24(1), 166-170. DOI 10.1108/RPJ-05-2016-0086.

[14]   Spahiu, T.; Al-Arabiyat, M.; Martens, Y.; Ehrmann, A.; Piperi, E.; Shehi, E. Adhesion of 3D printing polymers on textile fabrics for garment production. IOP Conf. Ser.: Mater. Sci. Eng. 2018, 459, 012065. DOI: 10.1088/1757-899X/459/1/012065.

[15]   Korger, M.; Bergschneider, J.; Lutz, M.; Mahltig, B.; Finsterbusch, K.; Rabe, M. Possible Applications of 3D Printing Technology on Textile Substrates. *IOP Conf. Ser.: Mater. Sci. Eng.* 2016, 141, 012011. DOI 10.1088/1757-899X/141/1/012011.

[16]   Kozior, T.; Döpke, C.; Grimmelsmann, N.; Juhász Junger, I.; Ehrmann, A. Influence of fabric pretreatment on adhesion of three-dimensional printed material on textile substrates. *Adv. Mech. Eng.* 2018, 10, 792316. DOI 10.1177/1687814018792316.

[17]   Görmer, D.; Störmer, J.; Ehrmann, A. The influence of thermal after-treatment on the adhesion of 3D prints on textile fabrics. *Communications in Development and Assembling of Textile Products* 2020, 1, 104-110.

[18]   Korger, M.; Glogowsky, A.; Sanduloff, S.; Steinem, C.; Huysman, S.; Horn, B.; Ernst, M.; Rabe, M. Testing thermoplastic elastomers selected as flexible three-dimensional printing materials for functional garment and technical textile applications. *J. Eng. Fibers Fabrics* 2020, 15, 1558925020924599. DOI 10.1177/1558925020924599.

[19]   Ehrmann, A.; Heimlich, F.; Brücken, A.; Weber, M.O.; Blachowicz, T. Experimental investigation of the washing relaxation of knitted fabrics from polyester yarn with stainless steel fibers. *Fibres & Textiles in Eastern Europe* 2012, 20, 90-93.

Identifying and ranking new product factors of fashion industry (case study Iranian menswear brand)

Siamak Nazemi[1,*], Roohollah Bagherzade[2]

[1] Fashion and Textile Design Department of Islamic Azad University of South Tehran, Tehran, Iran
[2] Institute for Advanced Textile Materials and Technologies (ATMT), Amirkabir University of Technology, Tehran, Iran
*Corresponding author E-mail address: nazemi.textile@gmail.com

ABSTRACT

In fashion industry, creative ideas and new products appear in new collections of brands presented in several ways, such as fashion week, exhibition etc. Iranian menswear also had the same strategy, but because of features of their customers, usually they use same designs and products in their new collections. Achieving new products in fashion industry can be related to design and technology aspect. Here we are looking for important factors affecting new products in Iranian menswear and also aiming at understanding which strategy are utilized in these product lines. Firstly this is done by gathering data from the Iranian Fashion association and 3 big Iranian menswear brands, secondly by interviews with experts from Iranian menswear brands, looking for answers of the study question. Twelve factors released from literature of study are divided in four sections: fabric sector, garment and accessories sector, and market sector. In 2010-decade, Iranian menswear brands focused on the technology factor in their new products, but during recent years, they changed their mind and now change direction to design departments. These phenomena happen due to the impact of social media on Iranian culture, with social media changing the behavior of the Iranian customer. Generally, accessing the directors of menswear brands was difficult, and during their interview they tried to hide some information. New products were an important factor in increasing market of any menswear brand. This study helps them to utilize the best strategy depending on their customers and market. This study confirms a new product's impact on customer behavior and culture which could be difference with time.

1 Introduction

Fashion industry is based on new products. The first generation of industrialization began from the weaving industry, which is related to fashion, during this time the most important factor for researchers and developers in terms of product quantity. After this time, in the 19th century haute couture was founded by the French designer Charles Fedrick Worth, also called the father of haute couture. In this time, creations of designers were most important factors for new products in fashion industries. Early in the 20th century, the famous fashion designers such as Chanel, Paul Poiret, Jeanne Lanvin, Elsa Schiaparelli, etc., changed the taste of fashion by their creative design. They also represented life style behind their fashion design. One of the famous designers was Chanel. After the Second World War, technology entered the fashion industry since one of the important materials that significantly changed this field was the newly produced polyvinylchloride (PVC). Those fabrics changed the collection atmosphere of fashion designer like Pierre Cardin [1]

Today, new products in the fashion industry appear in the design of companies or utilizing new technologies in their products. Several fashion designers work on creating their designs, such as Rei Kawakubo, Ralph & Russo, Jeremy Scott etc. Their customers engage to new collections which they launch to the market; their followers are looking for each fashion week and fashion events in which they participate, their strategy based on customer engagement. They had several departments for designing their clothes, involving markets, suppliers, and designing [2].

The Iranian fashion industry began at least 200 years ago when an Iranian king visited London and recognized the taste of fashion in European countries. After World War 2, the former Iranian regime paid attention to the fashion style, visible by the brides of the former Shah's costume in their ceremony being from Dior, but after the Islamic revolution, fashion become forbidden for people. After some reforms in the government resolution, fashion became more accessible to the people, but in Islamic form. In 2005, the Fashion Association was established, showing a first idea of attention to fashion and life style after the Islamic revolution.

Another kind of new product in fashion industries is based on new technologies, such as nanomaterials, Gore-Tex, Coolmax etc., purchased by brands such as Nike, Adidas, Puma etc. who used this kind of technology especially in sportswear. They focus on the market, suppliers, R&D centers which include scientists and designers.

For customers all around the world, some factors for choosing clothes are identical: budget, function, brand's reputation, culture, fashion trends, and quality. In the Iranian market environment, factors to choose clothes were the same, but some parameters were different during times, for example, after tight sanctions, when the budgets of people reduce, this became a major parameter. During these times, another parameter change took place by using smartphones, influencing culture and behavior of customers. Today people know more about the latest technologies launched in the world, during fashion weeks and other events.

In the 4th generation of industrialization, social media and social networks play significant roles in all aspects of our lives. The fashion industry is affected by this revolution especially in some countries like Iran, because they had a different type of culture. Social media impacted their life and changed their behavior and culture, causing different reactions especially in men society.

2 Background of the study

The background of this study is given by many previous studies. Marco Brambilla et al. [3] worked on the effect of social media on the Milan Fashion Week, investigating Instagram posts and responds of brand followers, also concluding that brands could be subdivided in four categories with respect to social media. Geissinger and Laurell [4] studied the impact of social media on the Stockholm fashion week, observing social behavior of Sweden during the fashion week by choosing seven brands and

investigated the constellation of participating companies. They concluded that social media increasingly reached consumer realm.

Bandinelli et al. [5] investigated new product developments in the fashion industry. For this purpose, eight Italian companies were analyzed by case study methodology. They concluded that three different stages were used for new product development (NPD) in fashion industry organization, process and knowledge management. In addition, customer services, roles of suppliers and competitors were important factors. Gherardi and Murgia [6] studied the staging precariousness of Milan fashion week, investigating the social movement during contemporary times and concluding that social changing affected the fashion week.

Entwistle and Rocamora [7] worked on fashion materialized in London fashion week by investigating the buying strategies and behavior of customers in the London Fashion Week. They concluded that several players are active in this field, thus relations between them were important, especially arts and commerce. Dewi et al [8] investigated the risk management during NPD in fashion industries, using data from three different fashion companies and analyzing them by Failure Mode Effect and Critically Analysis (FMECA) and House of Risk (HOR). Their study showed critical risk events, critical risks agents and risk mitigation strategies.

Goworek et al. [9] studied sustainable fashion during new product development in the UK by interviewing stockholders in the fashion sector. By analyzing thematically a range of responses, they concluded that fashion sustainability occurred through an improved knowledge, skills, process and infrastructure, if managerial decisions were taken to reduce barriers to longevity and to enhance the agency of NPD teams in this respect.

Zhang et al. [10] worked on fashions cewebrities and scales in new product development, collecting data from Chinese companies by a survey. The study indicated that fashion companies have five attributes: attractiveness, trustworthiness, expertise, interactivity, and intimacy. These attributes were found to exert varying impacts on the product design, production and commercialization, thereby influencing the purchase intention differently.

Bertola and Teunissen [11] investigated the 4th generation of industrialization and its effect on innovation in fashion industries. Using a literature review, they concluded that digital transformation, properly driven, could reshape the fashion industry into a more sustainable and truly customer-driven business. But they also underlined criticalities and slowness of adoption by traditional established brands and companies.

Cazeri et al. [1] investigated the product develop process (PDP) based on 37 academic papers related to PDP, dividing them into five main categories. They found that 27% of them were related to design performance, 5.5% to human resources, 62% were related to knowledge resources, 5.5% to financial performance and 0% related to literature review. Svendsen et al. [2] investigated marketing strategies and customer involvement in product development. They concluded that two facets of marketing strategy, i.e. product differentiation and competitor orientation, positively influenced the customer involvement. Furthermore, specific investments dedicated to the relationship were also positively related with customer involvement, and customer involvement increased customer profitability.

Lim et al. [12] investigated the strategic impact of new product development on the export involvement, and they concluded that supports of the argument that faster new product development capability must be augmented for companies looking for a higher degree of export involvement. In addition, they underlined the importance of integrating the marketing, R&D, and engineering functions to develop competitive advantages. Lindman [13] studied new product development strategies of SMEs, finding that SMEs tend to lack a long-run perspective and miss a clear role of new products in business strategy, while the goals regarding future products were not fully clear. In 2005, Pitta [14] worked on the market environmental system strategies of new products in China and concluded that information and action approach to new product developers were engaged in global marketing.

Fantazy and Salem [15] worked on the influence of strategy and flexibility in R&D on the improvement of efficiency. They revealed a direct positive effect from the strategy on NPD. Their findings also indicated a direct positive association between NPD and performance and revealed that the total effect (direct and indirect) positively influenced the performance.

Hong and Ghobakhloo [16] worked on the effect of IT and new products on the Iranian markets. They showed that IT leveraging competence in NPD and NPD effectiveness were valuable key capabilities that transformed the value of IT resources to a company's performance for Iranian small businesses. Investments in technical and human IT resources had positive effects on the development of NPD capabilities and thus a better performance in the surveyed companies.

Identifying important factors of NPD was done by literature reviewing, during this process some references were used connected with this paper. The factors investigated are illustrated in Table 1, in which all items reveal direct connections to each other [2,15]. In this paper, firstly important factors for new product development in Iran fashion industries are identified, before ranking these factors by questionnaires form experts, suppliers and customers of menswear brands using the TOPSIS method, adopted for Iranian environment, and analysing them.

3 Research methodology

In this study, three big Iranian companies in the field of menswear were chosen from data of Iran fashion association center. The important criterion considered for collecting these companies was the amount of selling in a year and the number of chain stores across the country. Table 1 shows the brands A, B, C in Iran menswear industries.

Table 1. Comparison of menswear brands A, B, C.

Name of company	Number of stores	Amount of selling per year (million dollars)
A	*30*	*40*
B	*25*	*33*
C	*21*	*26*

By interviews with the commercial director, the art director and the CEO of the three brands mentioned above, 12 factors were extracted which were important for new products. The factors in Table 2 were at least three times mentioned in the interviews.

Surveys were also sent to experts in menswear industries to collect their responses. From the 305 people asked (all menswear factories in Tehran city from data of Iran Fashion Association including SEMs and big companies), just 110 responded, i.e. the confidence level is 89% and the margin of error 6.5% for this this confidence level. On the Likert scale used in the questionnaires, each expert chose between 1 and 5 for any question (1 means low effect of that parameter on new product design in menswear and 5 means high effect of that criterion). Likert-type or frequency scales use fixed choice response formats and are designed to measure attitudes or opinions. These ordinal scales measure levels of agreement/disagreement.

A Likert-type scale considers that capability of experience is linear, i.e., on a progression from strongly agreeing to strongly disagreeing, and assumes that conditions can be measured. In this study, the questions offered a choice of five answers with the objective point being neither agree nor disagree. Then this data were used for measuring responses in questionnaires.

Table 2. Important factors extracted from interviews with brands A, B, C.

Item	Factor	Responder
1	Choosing fabric	All art directors + CEO of brand A
2	Choosing accessories	All art directors
3	R&D department	All CEOs + commercial directors of A and B
4	Fabric design	All art directors + CEOs
5	Market demand	All commercial directors + CEOs
6	Customer behavior	All commercial directors + CEOs
7	Industry equipment	All CEOs
8	Supplier ability	All CEOs + arts directors
9	Design department	All arts directors
10	Economic conditions	All commercial directors + CEOs
11	Government law & resolution	All commercial directors + CEOs
12	Social media influence	All responders

Table 3. Average evaluation of experts.

Item	Factor	Experts
1	Choosing fabric	4.5
2	Choosing accessories	4.3
3	R&D department	4.4
4	Fabric design	4.2
5	Market demand	4.2
6	Customer behavior	4.0
7	Industry equipment	3.9
8	Supplier ability	4.0
9	Design department	3.8
10	Economic condition	3.7
11	Government law & resolution	3.6
12	Social media influence	3.5

85% of the responders were female and 15% were male (most responder was female because there are more female than male workers and buyers in Iranian market). The education level of the responders was 3% PhD, 10% MBA, 10% Master of Arts, 62% Bachelor of Art and 15% without education level. Age's comparison of the responders shows that 25% of them are below 30, 30% of them are between 30 and 40 years old, 35% of them are between 40 and 50 years old, and 10% of them are above 50 years. Further, 70% of them had less than ten years of experience, 20% of them had 10-20 years of experience, 7% of them had 20-30 years of experience, and 3% of them had more than 30 years of experience. In Table 3, the average answers of the responders are illustrated.

For sorting the criteria questioned in the survey, the Technique for Order of Preference by Similarity to Ideal Solution (TOPSIS) is used. TOPSIS is used for changing quality to quantity variables and helps to understand the effects more easily. This technique is based on similarities and differences to the positive ideal solution (PIS) and negative ideal solution (NIS) [17]. In this work, multi-criterial decision analysis (MCDA) methods are used. The TOPSIS process has six steps for ranking each item [18]:

Step 1: Constructing the decision matrix which is created from 110 alternatives (amounts of experts in menswear section that responded to our questionnaires) and 12 factors (extracted from interview with arts director, commercial directors and CEOs of 3 major brands in Iran).

$$D=\begin{bmatrix} A11 & \cdots & A112 \\ A21 & \dots & A212 \\ A31 & \dots & A312 \\ A41 & \dots & A412 \\ \dots & \dots & \dots \\ \dots & \dots & \dots \\ A1101 & \cdots & A11012 \end{bmatrix} \tag{1}$$

where A_{ij} is the response of the expert *i* to question *j*, followed by rating alternative A_i with respect to criterion V_{ij} evaluated by an expert, and $A_{ij}^k=(Aa_{ij}^k, b_{ij}^k, c_{ij}^k)$.

Step 2: Calculating the normalize decision matrix, for better understanding and comparison of strategy factor all values transformed to the same scale by Eq. 2.

$$r_{ij}=\frac{x_{ij}}{\sqrt{\sum_{i=1}^{110} x_{ij}^2}} \tag{2}$$

Step 3. The weighted normalized decision matrix is shown as matrix V, calculated according to Eq. 3. In the matrix V, for each staff of the 3 major menswear brand answer (CEOs, arts directors, commercial directors) all factor are weighted that were extracted from the interviews.

$$V=[v_{ij}]_{m*n}, \quad i= I,2,3,\dots,12; \quad j=1,2,3,\dots,110 \quad V=\begin{bmatrix} 0.8 & \cdots & 0.7 \\ 0.6 & \dots & 0.6 \\ 0.8 & \dots & 0.6 \\ 0.9 & \dots & 0.7 \\ \dots & \dots & \dots \\ \dots & \dots & \dots \\ 0.8 & \cdots & 0.8 \end{bmatrix} \tag{3}$$

$$v_{ij}=r_{ij}*w_j \tag{4}$$

Step 4: Determination of the PIS and NIS. According to the weighted normalized decision matrix, normalized positive TFNs are known as the elements $\sim m_{ij}$, and their ranges belong to the closed interval [0,1]. Then, we can define the PIS A^+ and the NIS A^- as in Equations 5,6:

$$A^+=(V_1^+, V_2^+, V_3^+,\dots, V_n^+) \tag{5}$$

$$A^-=(V_1^-, V_2^-, V_3^-,\dots, V_n^-) \tag{6}$$

where $V_j^+=(1,1,1,)$ and $V_j^-=(0,0,0)$ j=1,2,3,….,n.

Step 5: Calculating the distance of each alternative from PIS and NIS. The distances (d_i^+ and d_i^-) of each alternative from A^+ and A^- can be calculated by the area compensation method.

$$d_i^+ = \sum_{j=1}^{n} d(v_{ij}, v_j^+), \quad i=1,2,....,m \quad , \quad j=1,2,......,n \qquad (7)$$

$$d_i^- = \sum_{j=1}^{n} d(v_{ij}, v_j^-), \quad i=1,2,....,m \quad , \quad j=1,2,......,n \qquad (8)$$

Step 6: Firstly, Eq. 2 is calculated, then the weight of each factor asked from experts and their average is used for Eq. 4, before finally 3 variables are calculated from Eqs. 2, 4 and 7, to obtain the closeness coefficient and rank the order of alternatives.

4   Result and discussion

In the first stage of interviews with 3 member of 3 brands with different positions, the vision of the responders was important because each responder sorted criteria due to the stages of their career, for example all art director said that design of fabric and garment is important for new products, but commercial directors told that economic conditions and customer demands were important for them, while CEOs had a middle opinion, stating that both customer and design are important criteria for new products.

This study shows that for new products in menswear industries, four main categories including design, supplier, market, and output criterion could be defined, each of which was subdivided into 3 items. The effect of government and their decisions was important; during recent decades this parameter influenced industries, but usually their obstacle decision acted like barriers, while all data indicated that the hands of government should be cut from industry. Table 4 shows the criteria sorted by d_j.

Table 4. Sorted criteria after TOPSIS calculation.

Item	Question	r_j	d_j	v_j
1	Government influence	0.021	0.0589	0.05301
2	Design department	0.024	0.0555	0.0444
3	Supplier ability	0.015	0.0532	0.03724
4	Customer need	0.016	0.0529	0.02645
5	Economic condition	0.022	0.0521	0.02084
6	Industry equipment	0.021	0.0512	0.01536
7	Market demand	0.019	0.0498	0.00996
8	Choosing fabric	0.018	0.0490	0.0049
9	Choosing accessories	0.023	0.0487	0.004383
10	Fabric design	0.020	0.0480	0.00384
11	Garment design	0.019	0.0456	0.003192
12	R&D department	0.019	0.0436	0.003052

This study was organized during the coronavirus pandemic, all menswear companies during this time faced massive problems because of the downfall of selling statistic and lockdown problem. This phenomenon affected the responses of our expert answers, where some new notion such as online

selling and 4th generation of industrialization make sense recently. All 3 brands were less affected from the pandemic just for their amount of budget, warehouse system and number of staff, in comparison with other menswear companies, but because of less ceremonies and events during this time, they were nevertheless influenced by the coronavirus pandemic (all of them produce formal clothes such as suits).

According to Fig. 1 (which illustrates important factor in menswear), another factor which affected the study was sanctions. Iran economic face strict sanction during recent years and this caused government involvement in all detailed decisions for economy, these decisions and resolutions limiting the industry for free activity. These two factors should be considered during the study.

Most of the designers believe that menswear needs less innovation in contrast to womenswear, but this research shows that experts in menswear believe that innovation and design of products have an effect on new products in this field. This suggests changes for the new generation which lives in the age of social media, nowadays people being in this environment more often than before and hence changing their behavior. Ten years ago, menswear industries demanded to produce products with special features such as nano-finishing, antibacterial finishing etc., but today most of them believe that cut and design are more important than all special features. For this change in customer and designer behavior, R&D departments become the last criterion. Life style becomes more important in recent times because of a new generation.
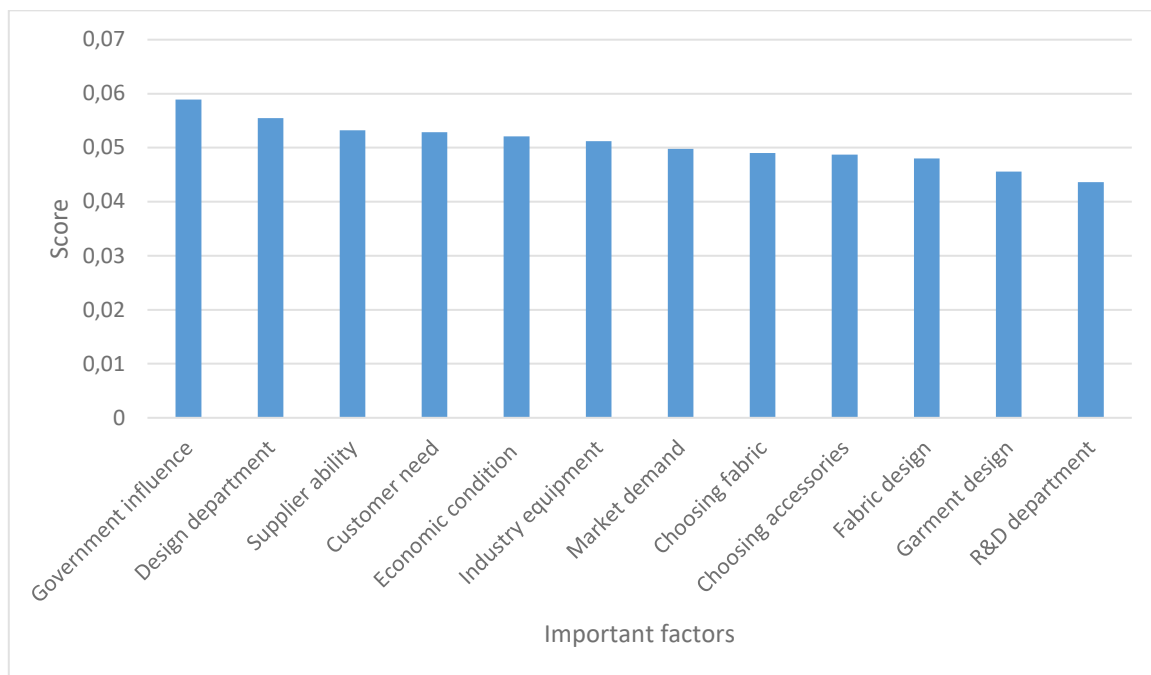

Figure 1. TOPSIS results of important factors

5 Conclusion

In this paper, important factors for new product developments in menswear are ranked. The results reveal that the influence of government is extremely high. This factor affected other factors, by changing fundamental conditions of economy which need tough political decision.

Twelve important factors were extracted in this study for improving new products in menswear industry. All factors extracted from interviews with experts were ranked by using the TOPSIS method.

On other hand, this study was done during 2020 in Tehran, facing the corona pandemic, sanctions, high inflation and reducing the Rial (Iran currency) value. These conditions make a good reason for government to put their hand in economic order and law. For further investigation we suggest the effect of the pandemic on the behavior of the government to be investigated.

References

[1] Cazeri, G. T., Ordoñez, R., Anholon, R., Pereira, C., & Rodrigues, E. Performance measurement in product development process (PDP): literature review and gaps for further research. *Brazilian Journal of Operations & Production Management* 2019, 16, 550-561. DOI: https://doi.org/10.14488/BJOPM.2019.v16.n4.a1.

[2] Svendsen, M. F., Haugland, S. A., Grønhaug, K. and Hammervoll, T. Marketing strategy and customer involvement in product development. *European Journal of Marketing* 2011, 45, 513-530.

[3] Brambilla, M., Ceri, S., Daniel, F. and Donetti, G. Spatial analysis of social media response to live events: The case of the Milano Fashion Week. *WWW'17 Companion: Proceedings of the 26th International Conference on World Wide Web Companion*, April 2017, 1457.1462. DOI: https://doi.org/10.1145/3041021.3051698.

[4] Geissinger, A., Laurell, C. Tracing brand constellations in social media: the case of Fashion Week Stockholm. *Journal of Fashion Marketing and Management* 2018, 22, 35-48. DOI: https://doi.org/10.1108/JFMM-12-2016-0115.

[5] Bandinelli, R.; Rinaldi, R.; Rossi, M; Terzi, S. New product development in the fashion industry: an empirical investigation of Italian firms. *International Journal of Engineering Business Management* 2013, 5, 31. DOI: https://doi.org/10.5772/56841.

[6] Gherardi, S.; Murgia, A. Staging precariousness: The Serpica Naro catwalk during the Milan fashion week. *Culture and Organization* 2015, 21, 174-196. DOI: https://doi.org/10.1080/14759551.2013.837051.

[7] Entwistle, J.; Rocamora, A. The field of fashion materialized: a study of London Fashion Week. *Sociology* 2006, 40, 735-751. DOI: https://doi.org/10.1177/0038038506065158.

[8] Dewi, D. S., Syairudin, B. and Nikmah, E. N. Risk management in new product development process for fashion industry: case study in hijab industry. *Procedia Manufacturing* 2015, 4, 383-391. DOI: https://doi.org/10.1016/j.promfg.2015.11.054

[9] Goworek, H.; Oxborrow, L.; Claxton, S.; McLaren, A.; Cooper, T. and Hill, H. Managing sustainability in the fashion business: Challenges in product development for clothing longevity in the UK. *Journal of Business Research* 2018, 117, 629-641. DOI: https://doi.org/10.1016/j.jbusres.2018.07.021.

[10] Zhang, H.; Liang, X.; Moon, H. Fashion cewebrity involvement in new product development: Scale development and an empirical study. *Journal of Business Research* 2020, 120, 321-329. DOI: https://doi.org/10.1016/j.jbusres.2020.01.052.

[11] Bertola, P.; Teunissen, J. Fashion 4.0. Innovating fashion industry through digital transformation. *Research Journal of Textile and Apparel* 2018, 22, 352-369. DOI: https://doi.org/10.1108/RJTA-03-2018-0023.

[12] Lim, J.-S.; Sharkey, T. W.; Heinrichs, J. H. Strategic impact of new product development on export involvement. *European Journal of Marketing* 2006, 40, 44-60. DOI: https://doi.org/10.1108/03090560610637301

[13] Lindman, M. T. Open or closed strategy in developing new products? A case study of industrial NPD in SMEs. *European Journal of Innovation* 2002, 5, 224-236. DOI: https://doi.org/10.1108/14601060210451180.

[14] Pitta, D. From market entry to new product development in China: Environmental Systems Control. *Journal of Product & Brand Management* 2005, 14, 119-122. DOI: https://doi.org/10.1108/10610420510592608.

[15] Fantazy, K. A.; Salem, M. The value of strategy and flexibility in new product development. *Journal of Enterprise Information Management* 2016, 29, 525-548. DOI: https://doi.org/10.1108/JEIM-10-2014-0102.

[16] Song, T. S.; Ghobakhloo, M. IT investments and product development effectiveness: Iranian SBs. *Industrial Management & Data Systems* 2013, 113, 265-293. DOI: https://doi.org/10.1108/02635571311303578.

[17] Hwang, C.L.; Yoon, K. Multiple Attribute Decision Making: Methods and Applications. New York: Springer-Verlag 1981.

[18] Saisse, R.; Lima, G. Similarity modeling with ideal solution for comparative analysis of projects in the context of the additional brics proposal. *Brazilian Journal of Operations & Production Management* 2019, 16, 659-671. https://doi.org/https://doi.org/10.14488/BJOPM.2019.v16.n4.a11.

Textile electrodes for bioimpedance measuring

Judith Tabea Meding[1,*], Khorolsuren Tuvshinbayar[1], Christoph Döpke[1] and Ferdinand Tamoue[2]

[1] Bielefeld University of Applied Sciences – Working Group Textile Technologies, Bielefeld, Germany
[2] KOB GmbH, Wolfstein, Germany; Ferdinand.Tamoue@kob.de
[*] Corresponding author E-mail address: Judith_tabea.meding@fh-bielefeld.de

INFO

ABSTRACT

This article deals with the development and comparison of eight different electrodes made out of a cotton fabric substrate, a silver coated yarn and partly conductive finishes, i.e. a PEDOT:PSS Orgacon ICP 1050 dip-coating and a Powersil coating. The purpose is the application especially in the medical field of angiopathy like for bioimpedance measurements during compression therapies. To be able to compare the suitability of the electrodes, various tests have been performed of the coating abrasion resistance, the stability of electrical resistance values, as well as resistance and bioimpedance measurements. Significant differences between the electrodes regarding their resilience and resistance that are visualized in a value-added analysis were found, with one hand-embroidered, one machine-sewn and one commercial electrode showing optimum properties.

1 Introduction

Bioelectrical impedance analysis (BIA) is commonly used as a significant tool in medical diagnosis. Several BIA applications in health monitoring are widely known and new approaches emerge from recent research. Innovative approaches are also being made in the textile medical engineering. There is an increasing amount of research on smart textiles [1,2]. These are based on data transmission within the textiles, so that formerly external measuring devices and output devices can be integrated in medical textiles. This requires robust and flexible data or power wiring to be integrated into the textiles.

Bioelectrical impedance analysis is a diagnostic tool for physicians and scientists in medical engineering. It is used to determine the body cell mass, total body water, fat free mass, fat mass and other information of the human body [3-5]. For this, four suitable skin electrodes, commonly Ag/AgCl

electrodes, are attached to the hand and foot of the right body side. A constant, imperceptible alternating current is introduced into the body via a pair of electrodes, usually at a fixed frequency of 50 kHz. The second pair of electrodes is used to measure the voltage drop caused by the body and to derive the impedance, the total resistance of the body. At the same time the phase shift of the introduced alternating current is determined, which is mainly dependent on the body cell mass. An LCR meter (inductance (L), capacitance (C), resistance (R)) in 4-wire sensing mode is used to perform the measurement. Changes to this common measurement setup can be made in order to focus on specific details. For example, it is possible to alter the measurement path through the body.

A new aspect developed and explored in this paper is the usage of textile electrodes [6,7]. These are required for certain applications where the use of gel-based electrodes is not possible. Gel-based electrodes have the disadvantage that they are made for single measurements. If the patient has these electrodes placed on his body, over time the electrodes cause skin irritation.

Another disadvantage of using electrodes that would require conductive gels is that compression bandages are sometimes applied, for staying on a limb for several days; in that case, electrodes placed beneath the bandages would not be accessible after the bandages application and would become dry with time. To make sure continuous measurements are possible, electrodes capable of functioning without any lubrification and overwhelming the skin dryness must be chosen for the BIA.

As soon as textiles are fitted with sensors or electrodes, the electrodes are exposed to a variety of strain, unlike disposable gel electrodes; the electrodes have to be adapted to clothing's usability constraints. This means that they cannot be thrown away after each measurement. Instead, they become part of the clothing and must perform measurements over a long period of time. For this, they are regularly washed in the washing machine and must still make reliable contact even after numerous washing cycles [8-11]. As Gaubert et al. [8] proved, this requires a strong resistance to water and detergents. The influence of sweat adds to the corrosion of the electrodes in frequent use and when worn for physical exercise. While this supposedly does not change measurement results [12], it can cause the electrode materials to fail over time. In addition to these influences, smart clothing creates a high stress on the integrated sensors due to the friction from body movement [13] and the internal clothing movement [11]. Zaman et al. [14] showed that different textile-based electrodes are damaged after Martindale abrasion resistance tests. The contact breaks after several cycles so that the electrodes fail.

This article deals with the development of textile electrodes for bioimpedance measurements, which are made of a durable woven fabric substrate, comprising a silver-coated yarn and a chemical treatment with two different kinds of conductive coating [15]. Electrodes with different stitch patterns were manufactured and tested for their suitability in a given medical purpose (compression therapy). This includes measurements of the resistance and various tests on how the electrodes react to abrasion, sweat and washing. Finally, a set of bioimpedance measurements was performed to test the response of textile electrodes beneath a fine stocking. Our goal was to develop reusable dry bioimpedance electrodes prototypes, which are simple to produce and consist of materials with acceptable cost. Thus, it should be easy to replicate the electrodes without having to buy special equipment.

Our measurement setup differs from the usual one used for bioimpedance measuring in terms of electrode placement and medical functionality. In the experimental case, we positioned the four electrodes in pairs of two onto the lower leg. One pair was closer to the knee and the other pair was closer to the ankle. This way, the electric current only runs through the leg instead of the trace from hand to foot. We performed a multiple frequency bioimpedance measurement to test the suitability of the electrodes.

2   Materials and Methods

At first, it is described how the textile electrodes are produced, and afterwards, how they have been tested and rated.
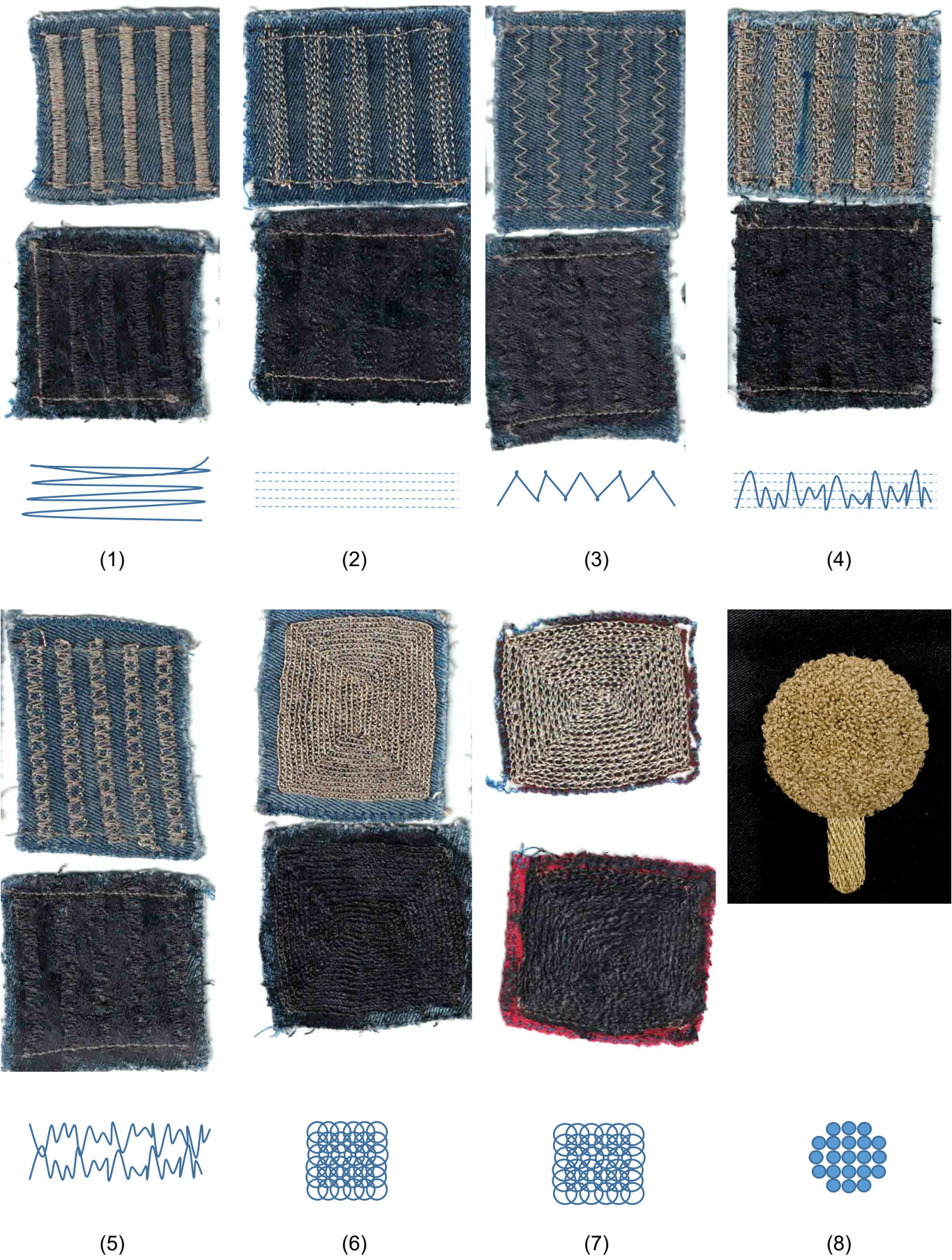
Fig. 1. Electrodes and sewing methods. Pure (upper images) and Powersil coated electrodes (lower images).

In total, eight different kinds of textile electrodes were developed (Figure 1); each type consisting of three variations (besides electrode 8): the untreated electrode (X.3) and two electrodes with different coatings. The eighth electrode is an industrially manufactured moss-embroidered non-coated electrode by the company ZSK Stickmaschinen GmbH, Krefeld, Germany and deals as an industrial comparison. The electrode has a diameter of 20 mm. The yarn is the Shieldex 33/10 dtex with < 4 kΩ/m.

The ground material of electrodes 1-6 is a cotton denim fabric with the dimensions of 55 mm x 45 mm. Electrode 7 is a thinner cotton fabric patch with the same dimensions. Electrodes 1 to 5 consist of five machines stitched (W6 model N1800) rows of conductive yarn that are 5 mm x 35 mm big and have a gap of 5 mm between them. The rows are connected on both sides with the same yarn on their ends. Electrodes 6 and 7 are hand stitched.

The stitching yarn is silver coated yarn (Shieldex 235/34 dtex 2-ply HC+B) with specific linear electrical resistivity <100 Ω/m. In Table 1, the settings and thread tensions of the machine-made electrodes are listed.

Table 1. Sewing program and distance of the electrodes.

Electrode No.	Sewing program of the sewing machine W6 N1800	Seam distance (machine specific units, motor rotations
1	C (zigzag stitch)	0.2
2	A (backstitch)	2.2
3	C (zigzag stitch)	2.8
4	A + E (backstitch plus elastic blindstitch)	3.0 + 1.0
5	E (elastic blindstitch)	1.0
6	Handmade: "Zuu Orookh" (Mongolian stitching method "needle wrapping") [16]	-
7	Handmade: "Khonin Kholboo" (Mongolian stitching method "sheep formation") [17]	-

To increase their conductivity, the electrodes X.1 were dip-coated with 2.4 mg/cm² PEDOT:PSS Orgacon ICP 1050 with a sheet resistance of 120 Ω (manufacturer information) and hardened for 4 hours at 60 °C. PEDOT:PSS is a conductive polymer, which is applied in liquid form. Through the oxidation, the polymer first enters the textile and then hardens and works like a hole conductor. Variation X.2 is a Powersil coating of 20.2 mg/cm², applied in two layers with a squeegee and hardened for 4 hours at 60 °C as well. Powersil is a silicon with integrated graphite and carbon black and is applied as a paste.

To find the most suitable electrode for bioimpedance measurements, a variety of stress tests and electrical measurements were performed and evaluated among each other with the value-added rating scale. At first, resistance tests were made to compare the general suitability as an electrode. For this, the multimeter Mastech PM334 was used. The electrodes were measured with crocodile clamps at the first, middle and last row.

To find out how stable and durable the electrodes are against machine washing, they were washed 30 times at 40 C, with detergents for fine laundry and wool, in a laundry bag, followed by spin cycling at 1000 rotations per minute. After each washing process, the electrodes were air dried and then resistance was measured with the multimeter.

The abrasion tests were performed with a Martindale abrasion tester according to the standard DIN EN ISO 12947-1:2007-04. Each electrode was measured after 10, 20, 50, 100, 200, 500 and 1000 cycles with the multimeter.
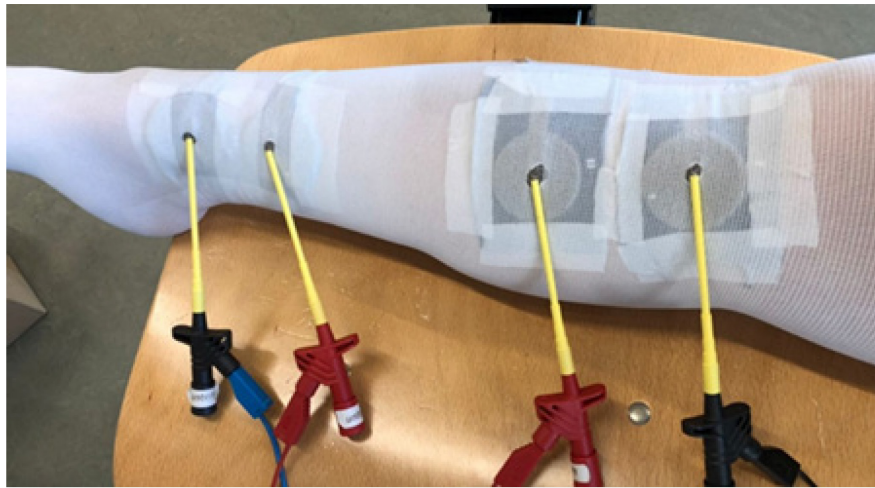
Fig. 2. Bioimpedance measurement with four electrodes.

The last test is the bioimpedance measurement. A four-point measurement at the calf was made, as shown in Figure 2, with the HP 4284A Precision LCR Meter, within a frequency range of 0 - 200 kHz. The outer electrodes inserting an electric current into the lower leg to were placed at a distance of 5 cm from the inner electrodes from which the voltage was measured. These criteria are based on experimental testing methods which are commonly used for physiological evaluation of body fluid [18,19].

3   Results and discussion

First, the resistance of the electrodes was measured, as shown in Fig. 3. Therefore, three electrodes of each type, i.e. three samples of each electrode and each coating variance, were measured on three different positions on the electrode, connecting a multimeter by crocodile clips.

A low resistance is an indicator for good conductance. In the field of textile electrodes, resistances under 10 Ω are good values. Electrodes 2, 4 and 8 are especially well conductive.
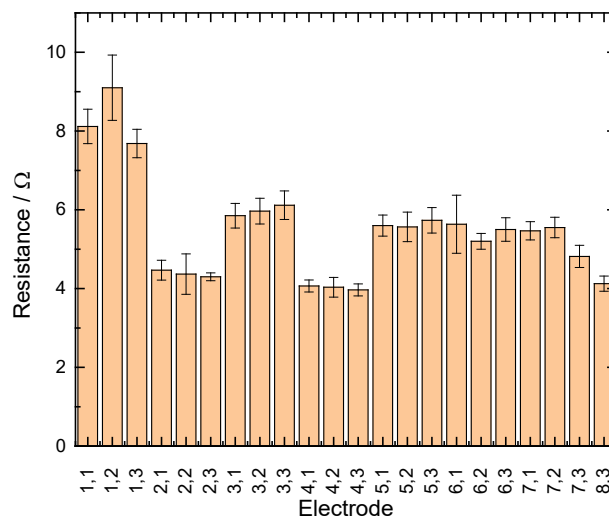

Fig. 3. Resistance measurements of the samples for the eight types of electrodes, whereas X.1 is coated with PEDOT:PSS, X.2 is coated with Powersil and X.3 is uncoated.

The next step is washing, drying and measuring the resistance. The results are presented in Fig. 4. Each electrode was produced three times and each of them were measured three times on different positions (see above) then. Electrodes 1, 3, 5 and 7 were destroyed after ten washing cycles. The remaining electrodes have been washed 30 times in total. We can observe the following results:
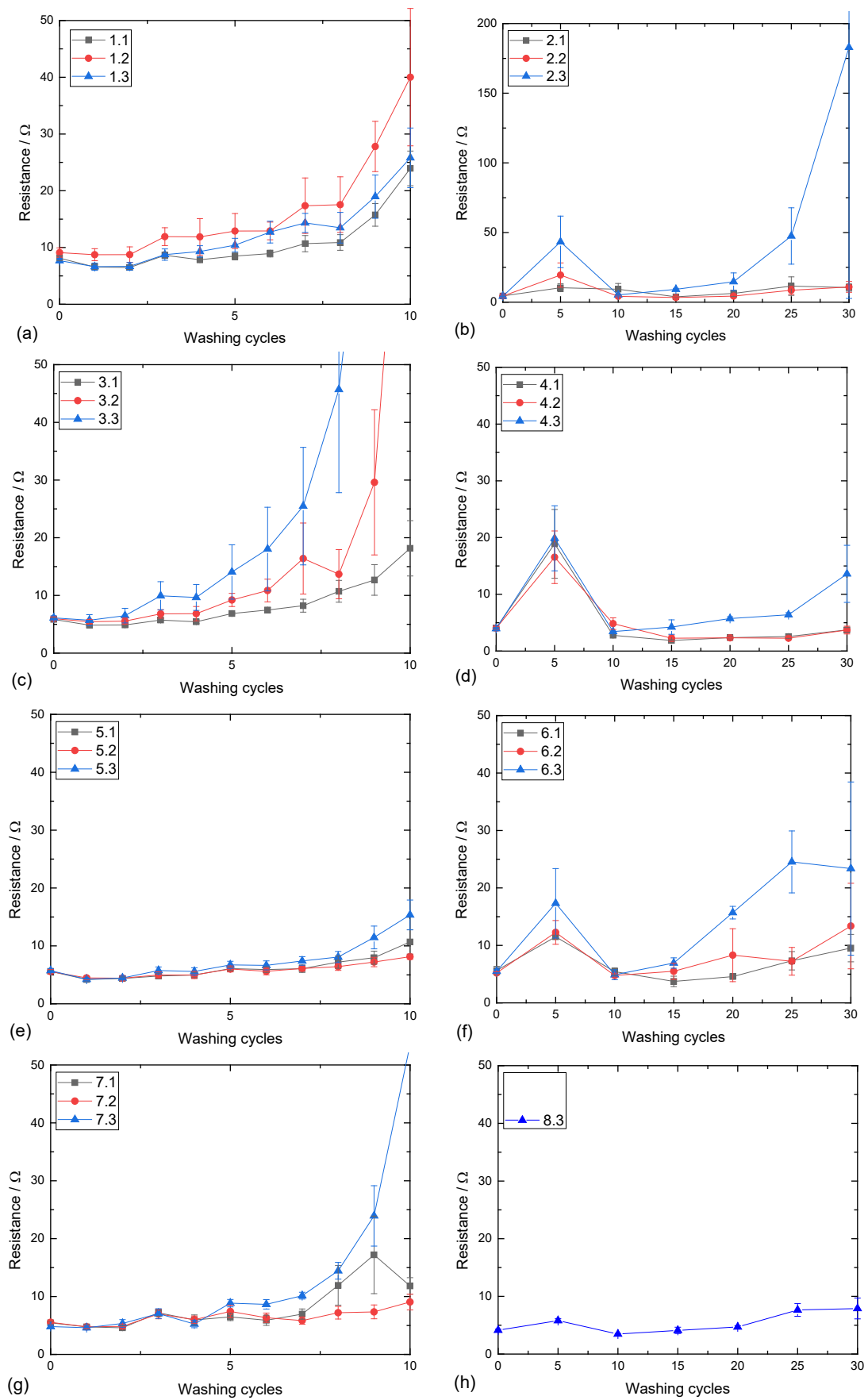
Fig. 4. Resistance measurements of the respective samples for identical wash cycles: (a) electrode 1, (b) electrode 2, (c) electrode 3, (d) electrode 4, (e) electrode 5, (f) electrode 6, (g) electrode 7, (h) electrode 8.

First, the resistances within the same electrode group yield relatively similar values except for (c) and (g), where the resistance value for (c) PEDOT:PSS coated electrode remains quite stable and low, i.e. close to a value of about 15 Ω. The last measurement of the PEDOT:PSS coated electrodes reaches a high value close to 110 Ω, rising sharply from the previous value of 20 Ω. Therefore, we can exclude this one point for the moment in order to get stable and reliable values of resistance. Sample (h) (electrode 8) is an untreated electrode. Thus, the graph depicts only one result for each measurement, and values remain between 3 Ω and 6 Ω.

Second, the resistance value of the untreated sample (g) develops relatively high values after several washing and measuring cycles, which indicates that the resistance has been deteriorated.

Third, the best electrode so far is sample 4 (Fig. 4d) where all resistance test values are lower than 5.5 Ω. This allows us to conclude that washing has little or no significant effect on their resistance. In summary, the resistance of the uncoated and the coated electrodes was compared to find out the impact of the coating and possible advantages or disadvantages through it.

Next, we carried out abrasion resistance tests and with a Martindale abrasion tester machine (Fig. 5). The resistance is measured after 0, 10, 20, 50, 100, 200, 500 and 1000 Martindale cycles. We can see large differences between the electrodes 3 and 4 (Figs. 5c and 5d). While electrode 3 starts with about 60 Ω, it rises above the multimeter range of 30 MΩ after 1000 Martindale cycles.

The electrodes 4 (Fig. 5d) and 8 (Fig. 5h) do not reach 4 Ω and do not show a clear effect of abrasion. This indicates that the denser the sewing, the more durable the sample becomes, and it is highly likely to be useful from a practical perspective. This means that the denser the seams are, the more resistant the electrodes are against abrasion and washing impacts and therefore the quality is steady in the long-term usage.

We found that electrodes 4 and 8 perform best in abrasion tests. Electrode 6 shows a nearly linear resistance increase and doubles its resistance after about 500 cycles. Nevertheless, its abrasion test results are still better than other ones.

The magnitude of the complex impedance, |Z|, evaluated by bioimpedance measurements, is depicted in Fig. 6. Criteria for the suitability of bioimpedance measurements are on one hand values higher than 10 Ω, which implies a good skin contact, and on the other hand the values should lie within a range of 30 Ω to 60 Ω at 50 kHz. Therefore, electrodes 4, 6 and 8 seem to be most suitable. Electrode 2 is only usable with a PEDOT:PSS coating but shows a high impedance in comparison to the mentioned electrodes in Figure 6.

Generally, these measurements are made with a common impedance measuring device. Its input impedance is not matched with the high contact resistance between the textile electrode and the human skin. This is the reason for the large error bars, which depend on the contact resistance. In the future, special bioimpedance measuring devices are especially developed for these textile electrodes and the error of the contact resistance will be included into the development. Nevertheless, electrodes 6.1, 6.3 and 8.3 lead to suitable values anyway. We emphasize that the measurement did not intend to measure the fluid content in the body segment.
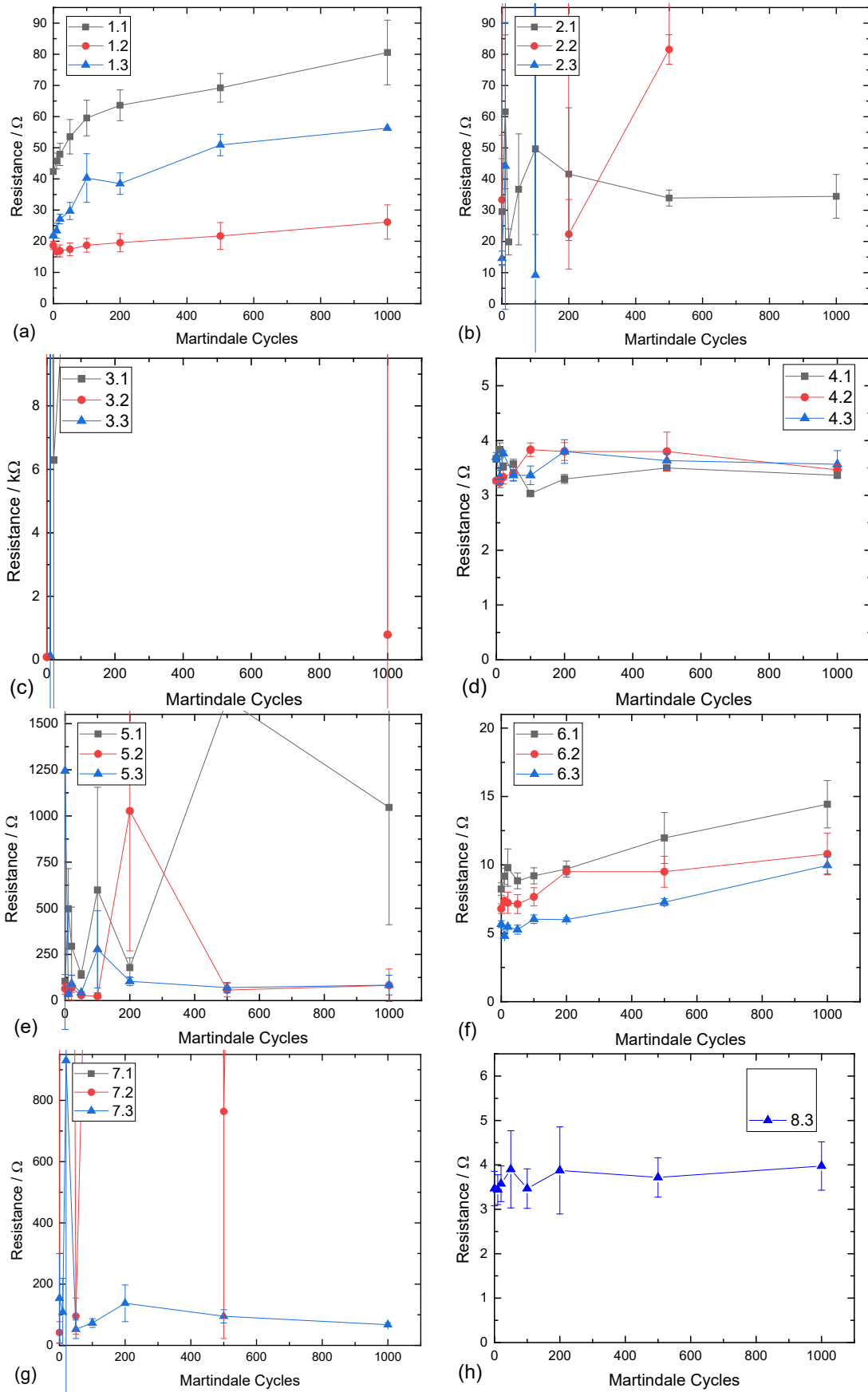
Fig. 5. Resistance measurements of the respective samples abrasion processes: (a) electrode 1, (b) electrode 2, (c) electrode 3, (d) electrode 4, (e) electrode 5, (f) electrode 6, (g) electrode 7, (h) electrode 8.
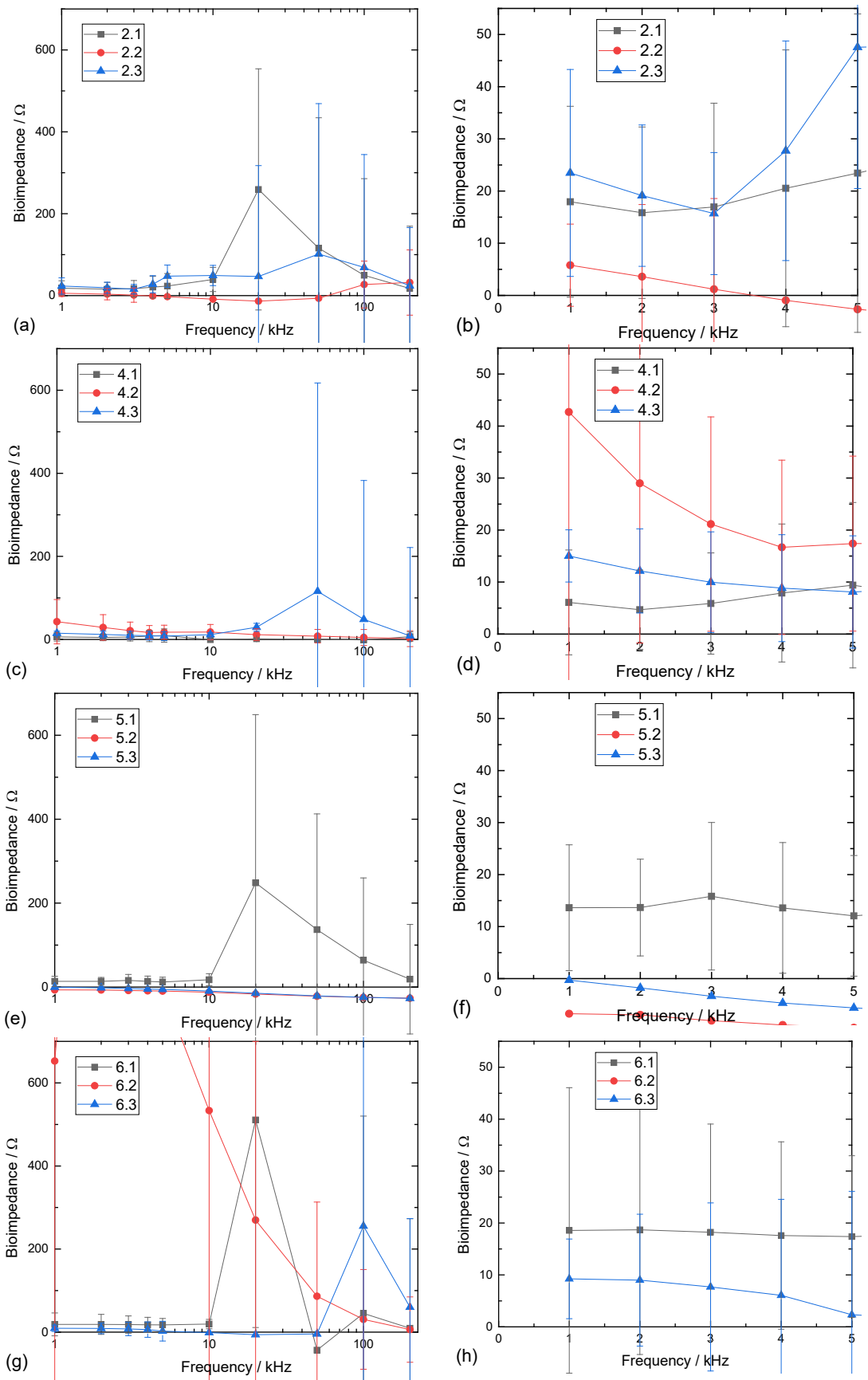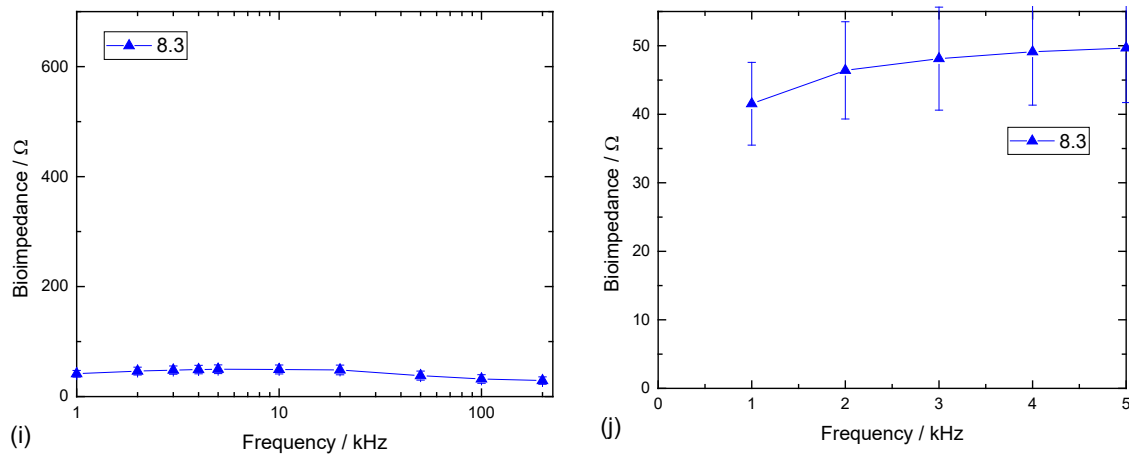
Fig. 6. Cont.

Fig. 6. Bioimpedance measurements |Z| with our textile electrodes on one person: (a) and (b) electrode 2, (c) and (d) electrode 4, (e) and (f) electrode 5, (g) and (h) electrode 6, and (i) and (j) electrode 8. The graphs on the right side depict the magnified view of the graphs from the left side in the range of 0 to 5 kHz and up to 55 Ω.

Table 2 presents the score of each electrode based on its performance. The highest score represents the best results for each or total test. We apply the rating scale using weighted value analysis to determine the most suitable electrode. Criteria include the resistance, the washability, the abrasion resistance, and the suitability for bioimpedance measurements. Since no large differences are visible for specimens with and without coating, all specimens belonging to one sample number are evaluated together. For example, Electrode No. 1-1, No. 1-2, No. 1-3 will be now averaged as electrode #1.

The most important criterion is the resistance, which was weighted with 35%. Washability and bioimpedance suitability were equally weighted with 25 % and the abrasion resistance was weighted with 15%. For each electrode, the first row indicates the rating for the criterion on a scale from 0-10; the second row is the product of the multiplication of the first row and the weighting. It is called the weighted rating. For example, electrode No. 1 received a score of 1.23 for the resistance. This value was calculated from the resistance, which has a weighting percentage of 35%, and a score of 3.5. To achieve the weighted value, the weighting percentage and score were multiplied, resulting in a value of 1.23.

Table 2. Value added analysis of the electrodes

Criteria	Resistance	Washability	Abrasion resistance	Bioimpedance suitability	Σ
Weighting	35%	25%	15%	25%	100%
#1	3.50	6.00	7.00	0.00	16.50
	1.23	1.50	1.05	0.00	3.78
#2	9.00	9.00	5.00	5.00	28.00
	3.15	2.25	0.75	1.25	7.40
#3	5.50	0.05	0.00	0.00	5.50
	1.93	0.13	0.00	0.00	2.05
#4	10.00	9.00	10.00	8.00	37.00
	3.50	2.25	1.50	2.00	9.25
#5	6.00	8.50	4.00	10.00	28.50
	2.10	2.13	0.60	2.50	7.33
#6	10.00	9.00	9.00	9.00	37.00
	3.50	2.25	1.35	2.25	9.35
#7	8.50	6.50	0.00	0.00	15.00
	2.98	1.63	0.00	0.00	4.60
#8	10.00	10.00	9.00	10.00	39.00
	3.50	2.50	1.35	2.50	9.85

The highest scores were obtained for electrodes no. 4, 6 and 8, as shown in Table 1. We can conclude that the score of electrode No. 8 is the highest as compared to the other electrodes. Electrode no. 8 received the highest weighted score with a value of 9.85 out of 10. Electrodes no. 4 and no. 6 are the following preferred electrodes with weighted total scores of 9.25 and 9.35, respectively.

4   Conclusions

To sum up, electrode No. 8 meets the requirements best. It does not only prove a good range in the resistance, but also is durable against washing and abrasion. The bioimpedance measurements can be performed as desired, too. A disadvantage about this type of electrode are the high production costs. On the other hand, it already has industrial standard, so that a mass production of these electrodes might reach the same quality easily. Electrodes no. 4 and no. 6 are also suitable for medical application electrodes.

For most aspects, the coating seems to be unimportant, besides for the bioimpedance, where it leads to a better skin contact. There we can see that the PEDOT:PSS coating leads to the perfect measuring range.

In the long-term, the electrodes should be machine-made for quicker production processes. In this case, the hand-stitched electrodes might be machine-made too and analyzed again.

Acknowledgment

References

[1]   Acar, G.; Ozturk, O.; Golparvar, A.J.; Elboshra, T.A.; Böhringer, K.; Yapici, M.K. Wearable and Flexible Textile Electrodes for Biopotential Signal Monitoring: A review. *Electronics* 2019, 8, 479. DOI: https://doi.org/10.3390/electronics8050479.

[2]   Schwarz-Pfeiffer, A.; Obermann, M.; Weber, M. O.; Ehrmann, A. Smarten up garments through knitting. *IOP Conf. Ser. Mater. Sci. Eng.* 2016, 141, 012008. DOI: https://doi.org/10.1088/1757-899X/141/1/012008.

[3]   Khalil, S.F.; Mohktar, M.S.; Ibrahim, F. The theory and fundamentals of bioimpedance analysis in clinical status monitoring and diagnosis of diseases. *Sensors* 2014, 14, 10895-10928. DOI: https://doi.org/10.3390/s140610895.

[4]   Mialich, M. S.; Sicchieri, J. M. F.; Junior, A. A. J. Analysis of body Composition: A critical review of the use of bioelectrical impedance analysis. *Int. J. Clin. Nutr.* 2014, 2, 1-10. DOI: https://doi.org/10.12691/ijcn-2-1-1.

[5]   Hoffer, E. C.; Meador, C. K.; Simpson, D. C. Correlation of whole-body impedance with total body water volume. *J. Appl. Physiol.* 1969, 27, 531-534. DOI: https://doi.org/10.1152/jappl.1969.27.4.531.

[6]   Pola, T.; Vanhala, J. Textile electrodes in ECG measurement. Proceedings of the 3rd International Conference on Intelligent Sensors, Sensor Networks and Information, Melbourne, Australia, 3-6 December 2007; 635-639.

[7]   Medrano, G.; Ubl, A.; Zimmermann, N.; Gries, T.; Leonhardt S. Skin electrode impedance of textile electrodes for bioimpedance spectroscopy. IFMBE Proceedings of the 13th International Conference on Electrical Bioimpedance and the 8th Conference on Electrical Impedance Tomography, Graz, Austria, 29 August-2 September 2007; Scharfetter H., Merwa R., Eds.; Springer: Berlin/Heidelberg, Germany, 2007.

[8]   Gaubert, V.; Gidik, H.; Bodart, N.; Koncar, V. Investigating the impact of washing cycles on silver-plated textile electrodes: A complete study. *Sensors* 2020, 20, 1739. DOI: https://doi.org/10.3390/s20061739.

[9]   Ankhili, A.; Zaman, S. U.; Tao, X.; Cochrane, C.; Koncar, V.; Coulon, D. Washable embroidered textile electrodes for long-term electrocardiography monitoring. *Text. Leath. Rev.* 2019, 2, 126-135. DOI: https://doi.org/10.31881/TLR.2019.27.

[10] Zaman, S. U.; Tao, X.; Cochrane, C.; Koncar, V. Market readiness of smart textile structures – reliability and washability. *IOP Conf. Ser. Mater. Sci. Eng.* 2018, 459, 012071. DOI: https://doi.org/10.1088/1757-899X/459/1/012071.

[11] Özdil, N.; Kayseri, G. Ö.; Mengüç, G. S. Analysis of abrasion characteristics in textiles. In *Abrasion Resistance of Materials*; Adamiak, M., Ed.; IntechOpen Limited: London, England, 2012; pp. 119-146, ISBN 978-953-51-0300-4.

[12] Bîrlea, S. I.; Breen, P. P.; Corley, G. J.; Bîrlea, N. M.; Quondamatteo, F.; ÓLaighin, G. Changes in the electrical properties of the electrode-skin-underlying tissue composite during a week-long programme of neuromuscular electrical stimulation. *Physiol. Meas.* 2014, 35, 231. DOI: https://doi.org/10.1088/0967-3334/35/2/231.

[13] Cho, G.; Jeong, K.; Paik, M. J.; Kwun, Y.; Sung, M. Performance evaluation of textile-based electrodes and motion sensors for smart clothing. *IEEE Sens. J.* 2011, 11, 3183-3193. DOI: https://doi.org/10.1109/JSEN.2011.2167508.

[14] Zaman, S. U.; Tao, X.; Cochrane, C.; Koncar, V. Understanding the washing damage to textile ECG dry skin electrodes, embroidered and fabric-based; set up of equivalent laboratory tests. *Sensors* 2020, 20, 1272. DOI: https://doi.org/10.3390/s20051272.

[15] Schäl, P.; Juhász Junger, I.; Grimmelsmann, N; Ehrmann, A. Development of graphite-based conductive textile coatings. *J. Coat. Technol. Res.* 2018, 15, 875-883. DOI: https://doi.org/10.1007/s11998-017-0024-5.

[16] Myagmarjav, O. 11-анги. Дизайн технологи. Зүү ороох оёдол. Багш Ж.Доржханд. Available online: https://www.youtube.com/watch?v=b-dsEzPfDd8 (accesses on 03.05.2021).

[17] Нийслэлийн ЕБ-ийн лаборатори 14-р сургууль. 6-р анги дизайн технологи. Гоёлын оёдол. Багш Ж.Доржханд. Available online: https://www.youtube.com/watch?v=hiwMtNg7qOw (accessed on 03.05.2021).

[18] Trenz, F. Anwendung dielektrischer Materialcharakterisierung auf die Detektion physiologisch relevanter Dehydrationseffekte (Application of dielectric material characterization on the detection of physiologically relevant dehydration effects). Dissertation thesis, Friedrich-Alexander University Erlangen-Nuremberg, Germany 2019.

[19] Tamoue, F; Ehrmann, A; Blachowicz, T. Predictability of sub-bandage pressure in compression therapy based on material properties. *Text. Res. J.* 2019, 89, 4410-4424. DOI: https://doi.org/10.1177/0040517519833969.

The effect of fabric's structure on the breathability and the drying rate properties

Mohamed Ghaith Chakroun*, Sofien Benltoufa, Faten Fayala

LESTE (Laboratoire d'étude des systèmes thermiques et énergétiques), National Engineering School of Monastir, University of Monastir, Tunisia.
*Corresponding author *E-mail address:* medghaithchakroun@gmail.com

INFO

ABSTRACT

Many parameters affect sportswear comfort. Therefore, we selected five sportswear fabrics designed for jogging and hiking T-shirts to study their structural characteristics and to investigate the influence of these characteristics on the clothing comfort properties. The areal weight, the thickness, the loop length and the course and wales densities were calculated. Investigations were performed on air permeability, water vapor resistance and drying time/rate properties of selected fabrics. We found that an increase in the mass per square meter and in thickness decreases the air permeability and increases the water vapor resistance of knitted fabrics. The air permeability is proportional to the loop length, while the water vapor resistance is inversely proportional to the loop length. Finally we did not find any significant relation between the fabric's structure characteristics and the drying time/rate.

1 Introduction

The human need of comfort is a way to improve the quality of life. It is fulfilled by providing a satisfactory and pleasant environment, foremost improving clothes, since we are dressed up all the time. The clothing comfort may be defined as a human psychological perception related to clothing ensemble, which is an outcome of the complex linkages between individual sensory stimuli received by brain, evaluation and weighing of all these stimuli to formulate subjective perception of overall comfort based on wear experience [1]. Comfort is a crucial requirement of clothing, which can be categorized into four aspects: physiological comfort, tactile comfort, ergonomic comfort and psychological comfort. Physiological comfort is a very complicated aspect, because it depends on the physical activity of the

wearer (sleep, rest, walk, run) and the environment surrounding it (cold, warm, humid). Following this change, the physiological responses and the clothing interactions with the human body change too.

During sports activities, several intense physiological mechanisms of heat loss are activated to prevent an excessive rise in body temperature and maintain thermal comfort [2]. The excess heat must first be transported from inside the body to the skin where heat can be lost through heat exchange with the environment. Once metabolic heat is transferred to the skin, there are different ways it is lost to the environment. Heat can be transferred within clothing in the form of conduction, convection, radiation and latent heat transfer by moisture transport. Conduction, convection and radiation are dominated by the temperature difference between skin surface and the environment and are therefore grouped as a dry heat transfer. On the other hand, latent heat transfer is achieved by moisture transmission related to water vapor pressure between the skin surface and the environment [3]. The clothes and the still air entrapped between the skin and the fabric's inner layer form a barrier that influences the heat loss processes of the body. So the garment must have properties that promote the natural phenomena of the human body to avoid body hyperthermia and have a state of discomfort that could pass into a pathological state. Furthermore, the accumulation of liquid sweat on the skin or the fabric's inner surface affects the physiological and tactile comfort of the wearer. Thus, studying and improving the thermal behavior governed by the air permeability and the water vapor resistance property of fabrics serves to enhance the clothing comfort.

The properties must be explained by the structure; many research groups have studied the influence of the fiber's, the yarn's and the fabric's structure on thermal and moisture management properties. Esra and Binnaz [4] investigated the thermal resistance, absorptivity and conductivity, air permeability and moisture management properties of fabrics made of different types of polyester yarns. The results showed that textured polyester yarn knitted fabrics had the highest air permeability values as compared to moisture management polyester with the same yarn count and knit structure. Lower filament number fabrics showed higher thermal resistance values in the same yarn count of fabrics. Moisture management polyester knitted fabrics showed the highest top absorption and one-way transport index value.

Mikučionienė et al. [5] studied the influence of the loop length on air permeability of single jersey knitted fabrics. They found that an increase in the loop length of the knit increases their permeability to air. Similar results were found by Ebru [6] who investigated the influence of the knitting structure on water vapor and air permeability. Results showed that an increase in the loop length increased the permeability to air and an increase in the linear density of yarns decreased the water vapor permeability of the knits.

Figen and Yıldıray [7] used FX3300-III air permeability tester instrument and SDL Atlas MMT Moisture Management Tester to investigate the air permeability and moisture management properties, respectively, of knitted fabrics with different knit type, yarn count and mass. They revealed that air permeability decreased not proportionally to the mass of fabrics, Rib fabrics had higher air permeability values as compared to single jersey fabrics, single jersey and rib fabrics' moisture management properties decreased as the fabrics' mass increased, and wetting time and absorption rate increased as the single jersey fabrics' mass increased.

Esra et al. [8] investigated the effect of fiber cross sectional shape on the thermal properties, water vapor and air permeability. Four type of fiber were used – round, hollow round, trilobal and hollow trilobal – to prepare two types of weaves: plain and twill. They found that the thermal conductivity increased in the fabrics woven with hollow fibers when compared to those woven with solid fibers, contrary to the water vapor and air permeability. The fabrics woven from trilobal fibers had lower thermal conductivity and thermal absorption and higher water vapor and air permeability values than those woven from round fibers.

Sampath et al. [9] made five different fabrics from 150 denier polyester yarns constituting different numbers of filaments. They investigated their wetting, vertical wicking, transverse wicking, and moisture vapor transfer. They concluded that when the filament fineness in the fabric increased, wicking rate and

wicking height first increased and then decreased, while the wicking rate and wicking height increased with time for all fabrics. In transverse wicking, when the filament fineness increased, the area of water spread increased and correspondingly the time taken to reach saturation point also increased.

In this study, we measured first the mass, loop length, thickness, course and wale density of five knitted fabrics made for sportswear, and then we studied the air permeability, water vapor resistance and drying time/rate as a function of the structure parameters.

2   Experimental methods

The specimens were cut at least 10 cm away from the selvage and creases and folds have been avoided. 24 h conditioning of the specimens and all experiments were carried out in a standard atmosphere of (65 ± 2) % relative humidity and (20 ± 2) °C temperature for testing. The mass per unit area was measured according to the test method EN 12127. The thickness was determined in accordance with the standard ISO 5084-1996 with 0.1 kPa pressure. Course and wale density values per cm were taken into account for the study in conformity with standard EN 14971:2006 method A. The loop length of 100 needles was measured according to EN 14970:2006. The TEXTEST Air Permeability Tester FX 3300 LABOTESTER III was used for accurate determination of the air permeability with a 100 kPa pressure difference and 20 cm² test area according to ISO 9237:1995. The air flow through the test specimen is measured with a variable orifice. The air permeability of the test specimen is determined from the pressure drop across this orifice, and is digitally displayed in the selected unit of measure for direct reading [10]. To measure the water vapor resistance, the PERMETEST Sensora instrument was used in accordance with ISO 11092. The Permetest instrument is also called skin model, which simulates dry and wet human skin in terms of its thermal feeling [11].

The drying time was measured using an internal test method. Initially, the fabric sample's (circular specimen size 100 cm²) mass was measured and recorded. Then, a (20 ± 2) mg distilled water drop was placed on the digital scale, immediately the specimen was placed (back side down) gently on the drop, the drop must be at the specimen's center. At this moment the chronometer was launched. The mass was recorded at 2 minutes intervals until the mass has returned to the original fabric sample mass. The time when the mass has returned to the fabric initial mass is defined as the drying time. As shown in Fig. 1, the air can penetrate to the glass box from the top, the right and the left side in the test apparatus. The test is carried out in the normal conditioning atmosphere as mentioned above and without air flow, i.e. the air velocity through the exposed faces must not exceed 0.1 m/s.
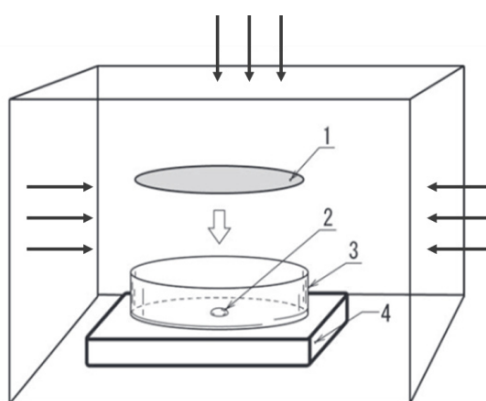
Key :
1) Specimen
2) Drop of distilled water   → : Air flow
3) Petri dish
4) Digital scale

Fig. 1 The test apparatus for determining the drying time/rate.

In this internal test method, it is not mentioned how we calculate the drying rate, which is a key factor in the study of the drying phenomena of fabrics. So we referred to the international standard ISO 17617:2014 for the determination of the drying rate. First, we calculated the percentage of water loss by mass L_t according to equation (1).

$$L_t(\%) = \frac{M_0 - M_t}{M_D} \times 100, \qquad\qquad (1)$$

where:

- M_0: mass of the wetted sample at t=0.

- M_t: mass of the wetted sample at t.

- M_D: mass of the water drop.

The mass unit used for all mass values in equation (1) is gramm (g).

Then, the regression line of the water mass loss as a function of time is determined and the drying rate is defined according to the ISO 17617 as the slope of this linear curve. For each fabric three test specimens were considered in the measurement of the drying time and rate and their mean value was considered for this investigation.

Figure 2 shows the evolution of water mass loss in time of the V93 fabric. The equation of the regression line is "y = 0.0323 x/min + 0.0172", consequently the slope is equal to 0.0323/min. The drying rate of V93 is 3.23 %/min.
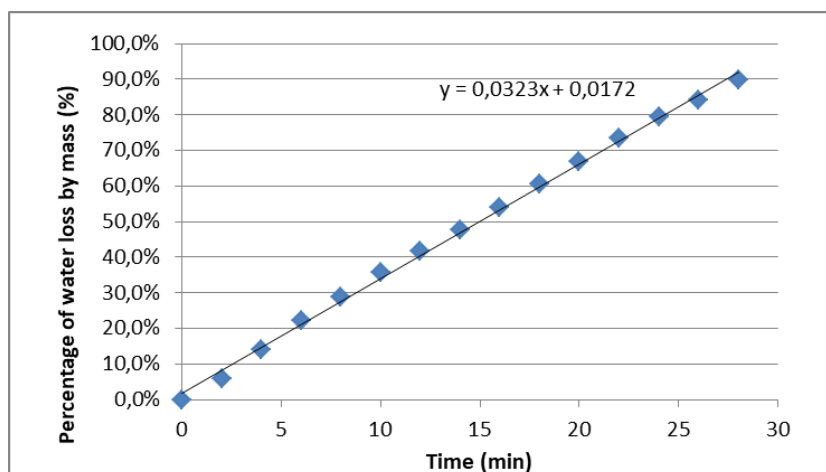

Fig. 2 Evolution of water mass loss as a function of time of V93.

3   Materials

Five types of knitted fabrics for sportswear were selected for this study. The knitting, dyeing and finishing were accomplished in VTL group (Société Tunisienne de Vêtement de Travail et de Loisir) in Tunisia. The yarns used in the study made with a natural fiber, wool merino, and man-made fibers with circular cross sectional shape: polyamide (PA) and polyester (PES). Four kinds of man-made yarns were employed: 100% PES, 100% PA, PA/PES mixture and PES COC. PES COC is a COCONA® polyester yarn made with polyester fibers that have 37.5® technology. They work through permanently integrated active particles that capture and release water vapor and actively react to body heat. The particles use the body's infrared energy to accelerate the movement of vapor and evaporation of liquid.

All fabrics were made on a single jersey machine, gauge E 28. Details of the knitted hoses made are given in Table 1.

Table 1. Details of the knit hoses.

Code	Pattern	Composition	Fiber fraction (%)	Linear density (dtex)
V06	Jersey crepe	PES	43	83/72
		PES COC	43	83/42
		Elasthane	14	22
V93	Jersey crepe	PES	50	83/72
		PES COC	50	83/42
V05	Jersey crepe	PES	50	83/72
		PES COC	50	83/42
V16	Honeycomb	Wool merino	67	138
		PES	33	55/24
V19	Mesh	57% PA / 43% PES	96	77/82
		PA	4	22/7

As presented in Table 1, Fabrics V06, V93 and V05 have the same pattern and they are made with the same yarns except in fabric V06 which is plated with an elasthane yarn. The difference between V93 and V05 is the loop length. All fabrics were washed and dyed on industrial scale. Finishing treatments and heat settings were done on a stenter machine which is a specialist oven used in the textile industry for drying and heat treating fabric after wet processing. V93, V05, V16 and V19 underwent a hydrophilic treatment using ULTRPHIL® which is a moisture management agent, padded at a speed of 20 m/min with a liquor pick of 50%, bath temperature of approximately 20 °C and a drying temperature of 120 °C. Structure characteristics of the finished fabrics are presented in Table 2.

Table 2. Structure characteristics of the finished fabrics. CV = coefficient of variation.

Code	Areal mass (g/m²)	CV (%)	Thickness (mm)	CV (%)	Course density (course/cm)	CV (%)	Wale density (wale/cm)	CV (%)	Loop length (cm)	CV (%)
V06	133.08	1.2	0.670	2.1	16.0	0	25.0	0	21.6	2.9
V93	66.99	1.6	0.564	1.6	14.8	4.4	15.2	2.9	25.0	1.2
V05	108.56	2.9	0.572	2.9	17.5	2.9	23.8	4.2	17.1	2.0
V16	120.96	1.1	0.924	2.6	18.0	0	32.0	0	Wool 23	3.3
									PES 17.2	2.5
V19	89.89	0.9	0.524	1.7	17.3	0	22.8	0	PA/PES 21.3	1.9
									PA 13.6	1.1

For a better understanding of the finished fabric's structure and design, we took microscopic images of the front and back side of each one, as illustrated in Figure 3. The magnification scale of all fabrics images is x 51 except for V16 where we put a microscopic image less magnified then the other fabrics (x 32) to visualize clearly the honeycomb unit structure which is larger than the other samples.
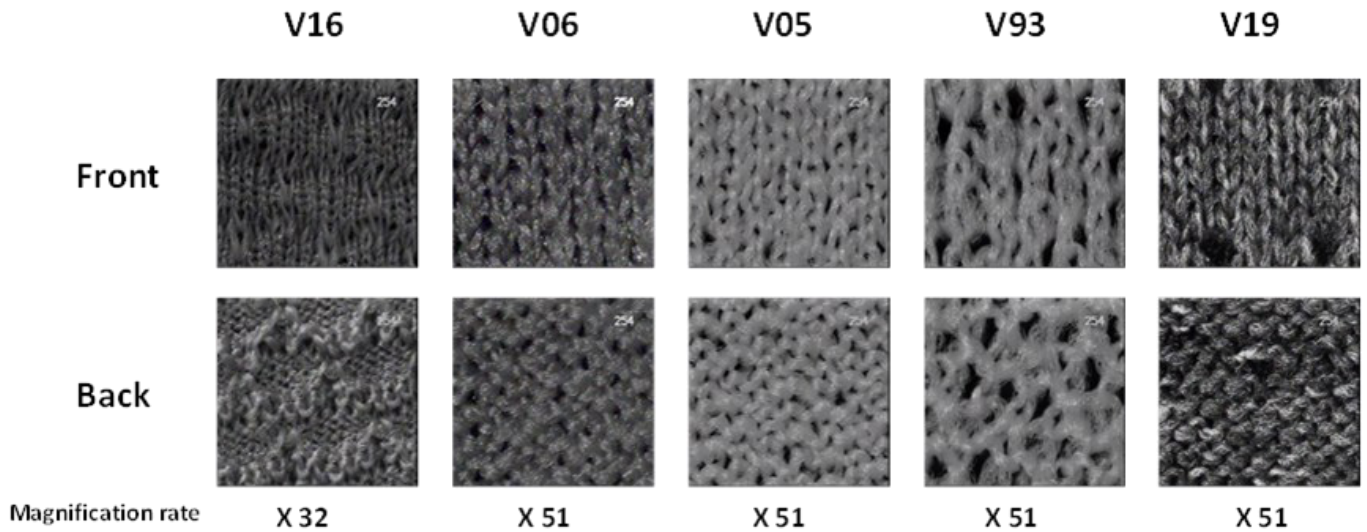
Fig. 3 Microscopic images of the two sides of the finished fabrics.

4 Results and discussion

We plotted the error bars in all the charts of this section, to indicate the uncertainty of the reported measurements. Also the coefficient of variation (CV) has been found beneath 4% in the air permeability test, beneath 5% in the water vapor resistance measurements and beneath 6% in the drying time and the drying rate determination.

4.1 The influence of fabric's structure on the air permeability

Air permeability is the rate of air flow passing perpendicularly through a known area under a prescribed air pressure differential between two surfaces of a material [12]. Air permeability values of fabrics used in the experiments are compared in Figure 4.
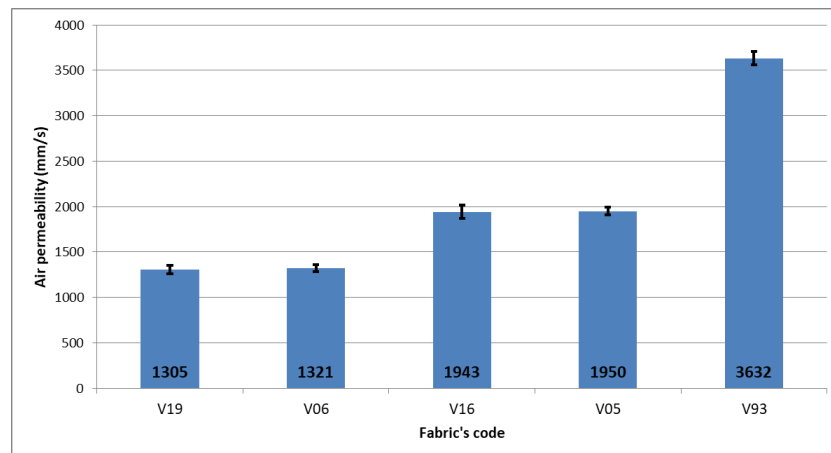

Fig. 4 Air permeability of used fabrics.

The highest air permeability value (V93) was noticed in the highest loop length and lowest course and wale densities, and consequently the lowest mass per unit area. The lowest air permeability values were found in fabric V19; this may be explained by the reduced number of macro pores through which most of the airflow permeates.

When comparing V093, V05 and V06, the heaviest and thickest fabric V06 shows the lowest air permeability value. This is explained by the presence of Lycra yarn, which made the structure tighter and reduces the spaces within yarns, hence decreasing the airflow passing through the fabric. So an

increase in the mass per unit area and the thickness leads to a decrease in the air permeability of fabrics.

When comparing V093 and V05, we found that air permeability increased significantly when the loop length increased. The air permeability is proportional to the loop length and inversely proportional to fabric's mass per unit area and thickness.

4.2   The influence of fabric's structure on the water vapor resistance

Water vapor resistance is the fabric's resistance to transport the moisture (in vapor form) away from the skin. Fabrics have to evacuate this vapor before it becomes liquid, avoiding the fabric to get wet and reducing the uncomfortable sensation of the wearer [13]. According to Figure 5, the highest water vapor resistance was seen in V16 which is the thickest fabric and has the highest stitch density. The lowest water vapor resistance is visible in V93 which has the highest air permeability value, which is explained by the high porosity of this fabric that allows both the air flow and the water vapor to permeate through the fabric layer effectively.

Comparison of jersey crepe knitted fabrics V93, V05 and V06, the highest water vapor resistance value was seen in V06. Similar to the air permeability, the heaviest and thickest fabric has the highest water vapor resistance. So, heavy and thick fabrics do not promote heat loss by evaporation. Accordingly, the water vapor resistance is proportional to the fabric's square mass and thickness. From comparing V93 and V05 we can say that an increase in loop length decreases the water vapor resistance of fabrics.
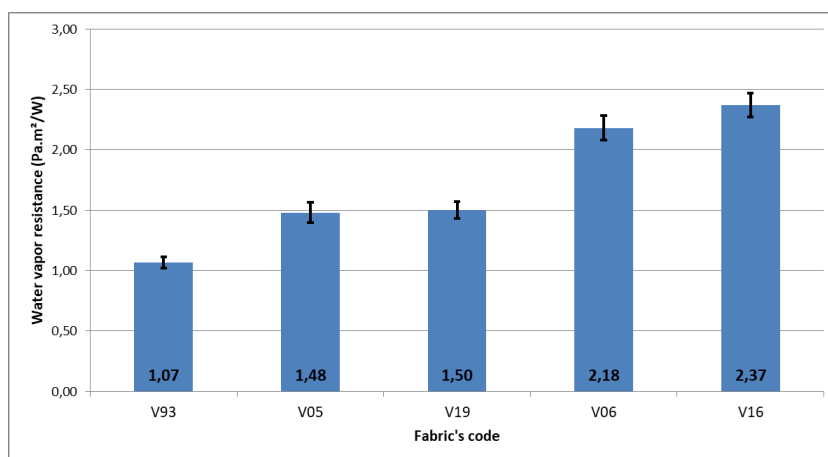

Fig. 5 Water vapor resistance of used fabrics.

4.3   The influence of fabric's structure on the drying rate/time

Drying rate is defined as the required time to dry a known mass of moisture from a textile fabric. It is expressed in drying percent per unit time. Another parameter related to drying is the drying time defined as the time for which 100% of applied water loss occurs [14]. The drying rate and time of all fabrics are compared in Figure 6. It is evident that the fabric having the highest drying rate is the fastest one to dry. The lowest drying rate was seen in V16 which contains the wool yarn. The absorption of water by the wool fibers makes the loss of water by evaporation more difficult than the hydrophobic man-made fibers where the water remains on the fiber's surface.

The highest drying rate among jersey crepe fabrics was seen in V05 which have the lowest loop length. Nevertheless, the drying rate cannot be explained by the loop length, since a great loop length difference between V05 (17.1 cm) and V93 (25 cm) shows an approximately same drying rate. Thus, there is no significant influence of the loop length on the drying rate.
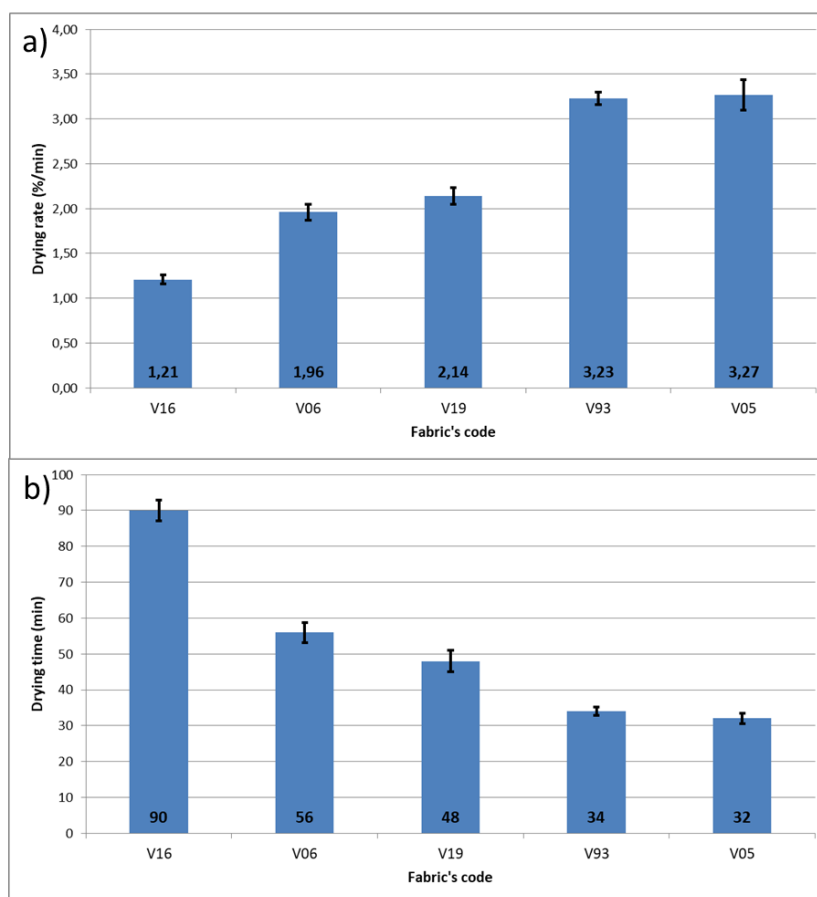
Fig. 6 (a) Drying rate; (b) drying time of fabrics used in the experiments.

5 Conclusion

The main conclusions drawn from this work are: First, air permeability is low in tight fabrics. Second, an increase in the mass per unit area and the thickness leads to a decrease in the air permeability and an increase in the water vapor resistance of knitted fabrics. Third, the air permeability is proportional to the loop length. Fourth, the water vapor resistance is inversely proportional to the loop length. Fifth, the presence of a hydrophilic fiber affects the water vapor resistance and the drying behavior of fabrics. Sixth, there is not a significant relation found in this investigation of the fabric's structure characteristics on the drying behavior of these fabrics.

Breathability, moisture vapor transmission and fast drying are crucial in determining the comfort in high activity and sportswear clothes. Therefore, the most suitable fabric among the five knitted ones investigated is V93 and in second place we found V05. On the other hand, V06 and V16 are the two fabrics which behaved worst in maintaining a comfort sensation during activities. V19 can be improved by increasing the pore volume by increasing the loop length, for example.

There must be a further investigation of the fiber's and yarn's composition and structure properties for a better understanding of the factors that affects the drying rate of textiles, and likewise, knowing the wetting and wicking behavior of textile structure.

References

[1] Apurba Das and Ramsamy Alagirusamy. 2010. Science in Clothing Comfort, Vol. 2: Psychology and Comfort, Woodhead Publishing India Pvt. Ltd.

[2] Daniel Wendt, Luc van Loon and Wouter van Marken Lichtenbelt. Thermoregulation during exercise in the heat strategies for maintaining health and performance. *Sports Med.* 2007, 37, 669-682.

[3] Dinesh Bhatia and Urvashi Malhotra. 2016. Thermophysiological wear comfort of clothing: an overview. *J. Textile Sci. Eng.* 2016, 6, 1000250. DOI: https://doi.org/10.4172/2165-8064.1000250.

[4] Esra Taştan Özkan and Binnaz Meriç Kaplangiray. Investigating thermophysiological comfort properties of polyester knitted fabrics. *J. Textile Eng. Fashion Technol*. 2019, 5, 50-56.

[5] Daiva Mikučionienė, Laima Milašiūtė, Rimvydas Milašius. Influence of knits structure on flammability and comfortability. *AUTEX Res. J.* 2014, 14, 226-232. DOI: https://doi.org/10.2478/aut-2014-0022.

[6] Ebru Çoruh. Optimization of comfort properties of single jersey knitted fabrics. *FIBRES & TEXTILES in Eastern Europe* 2015, 23, 66-72. DOI: https://doi.org/10.5604/12303666.1152728.

[7] Figen Selli, Yıldıray Turhan. 2017. Investigation of air permeability and moisture management properties of the commercial single jersey and rib knitted fabrics. *Tekstil ve Konfeksiyon* 2017, 27, 27-31.

[8] Esra Karaca, Nalan Kahraman, Sunay Omeroglu and Behcet Becerir. Effects of fiber cross sectional shape and weave pattern on thermal comfort properties of polyester woven fabrics. *FIBRES & TEXTILES in Eastern Europe* 2012, 20, 67-72.

[9] M. B. Sampath, Senthilkumar Mani and Govindan Nalankilli. Effect of filament fineness on comfort characteristics of moisture management finished polyester knitted fabrics. *J. Ind. Text.* 2011, 41, 160-173. DOI: https://doi.org/10.1177/1528083711400774.

[10] Air Permeability Tester FX 3300 LABOTESTER III; ARTEC TESTNOLOGY manual.

[11] Lubos Hes. Non-destructive determination of comfort parameters during marketing of functional garments and clothing. *Indian Journal of Fibre & Textile Research* 2008, 33, 239-245.

[12] Banu Özgen and Sevda Altaş. The investigation of thermal comfort, moisture management and handle properties of knitted fabrics made of various fibres. *Tekstil ve Konfeksiyon* 2014, 24, 272-278.

[13] Amel Boughattas, Sofien Benltoufa and Faten Fayala. Moisture management properties of double face denim fabrics. *International Journal of Applied Research on Textile* 2019, Special Issue Cirat-8, 38-43.

[14] ISO 17617:2014 Textiles — Determination of moisture drying rate.

The comfort of knitted fabric: interaction of sportswear and athlete's body

Ivana Salopek Čubrić[1], Goran Čubrić[1,*], Vesna Marija Potočić Matković[1], Alenka Pavko Čuden[2]

[1] University of Zagreb, Faculty of Textile Technology, Zagreb, Croatia
[2] University of Ljubljana, Faculty of Natural Sciences and Engineering, Ljubljana, Slovenia
*Corresponding author *E-mail address:* goran.cubric@ttf.unizg.hr

INFO

ABSTRACT

The properties of the material used for the production of sportswear directly affect the heat exchange and sweat transfer that occurs at the interface between the skin and the environment. Thermography is a valuable method that provides insight into the patterns of temperature distribution on the surface of human skin that change during sports training or intense exercise. Such patterns can be further used to improve the design of sportswear. The experiment presented in this paper focuses on studying the changes in body temperature of the participating subjects during two typical types of training in football (condition training and tactical training). The duration of each training session was 60 minutes and measurements were taken after each of the total 10 training sessions. A thermal camera was used to measure the upper body temperatures of the players and professional software was used for further processing of the thermal images. In the analysis of the thermal data, the average temperatures for 9 anterior and 9 posterior zones of the upper body were obtained. The results related to the changes in average temperature for each observed anterior and posterior zone and two types of football training are presented and discussed.

1 Introduction

Research related to football includes various topics such as sociological studies, physiological, psychological, technical and tactical elements of the sport, coaching, and the prevalence of injuries.

Physiological thermoregulation, triggered by temperature signals from the body and skin during athletic activity, attracts research. During athletic activity, the core temperature of the body increases, a limited amount of energy is converted to mechanical energy, while the rest is converted to thermal energy. The body has the ability to lose heat through evaporation of moisture on the skin. Thermoregulation is related to the thermal comfort of clothing [1]. Therefore, there is a growing interest in the thermal properties and moisture management of fabrics for sportswear, as well as in the properties of the fibers and yarns from which they are made.

Thermography as a noninvasive and rapid measurement is widely used in sports science. The validity and reliability of this method for measuring skin temperature has been documented in a number of sports. Thermography for measuring thermoregulation of football players was used in the study by Dębiec-Bąk et al. [2]. The results of the study indicate better effectiveness of thermoregulatory processes in football players compared to students. In another study, a novel injury prevention program based on infrared thermography was established and its influence on injury incidence in professional soccer players was investigated [3]. The incidence of injuries was reduced by identifying players potentially at risk, and injury severity and days lost were also reduced.

The relationship between energy expenditure and skin temperature during swimming protocol (front crawl and backstroke) was investigated by Seixas et al. [4]. Both swimming techniques increased skin temperature, but with different thermal patterns. Thermography was used in cycling to investigate the effects of saddle height on thermoregulation [5]. The aim of this study was to investigate whether different cycling postures, caused by different knee flexion angles, could affect skin temperature. In another experiment, thermography was used to investigate the changes in body temperatures of participating divers due to different wetsuit thickness and thermal environment [6]. The thermography showed the great influence of the environmental temperature, wetsuit thickness and physiology of the divers on the changes of skin temperature during immersion over time. In a study of runners, thermography was compared with thermal contact sensors to define the methodology for further research [7]. The stationary sensor showed a higher skin temperature after running than infrared thermography. Another study on runners investigated the relationship between skin temperature changes and muscle fatigue [8]. Correlation analysis performed to quantify the relationship between performance and temperature change over time showed that there was a significant negative correlation between the increase in skin temperature and the decrease in performance of the exercising quadriceps. A systematic literature review on the use of thermal imaging for the diagnosis of musculoskeletal injuries was conducted and found that infrared thermal imaging is a good diagnostic tool for musculoskeletal injuries [9]. Interestingly, no significant relationship was found between measured skin temperature and subjective assessment of muscle soreness in junior athletes [10].

Technical developments in the field of sportswear, high performance textiles and knitted fabrics for sportswear are also attracting increasing research attention. Knitted fabrics are preferred for sportswear due to their water vapor permeability, air permeability, thermal conductivity and moisture management as well as better elasticity and stretchability as compared to woven fabrics. Thermography was used by Salopek et al. to develop suggestions for sportswear for futsal players based on thermal body mapping [11]. The results of the study showed the importance of adapting the construction and fit of the clothing to the type of training. Heat and moisture transfer and air permeability in single jersey knitted garments and their influence on comfort were studied by Gupta et al. [12]. Finer yarns and higher loop lengths of knitted fabrics were more permeable to air and water vapor, making them more suitable for humid conditions. Nemeckova et al. used the method to measure moisture transport on knitted fabrics using thermographic and micro-thermographic systems [13]. Three types of knitted fabrics with the same raw material composition and fineness but different construction were studied, of which the interlock structure was shown to give the best results in terms of liquid absorption and transfer. In another study, thermography was used to observe the influence of different yarn types on the total drying time of knitted fabrics, which directly affect human comfort [14]. The results showed significant differences in total drying time between fabrics and the influence of elastane yarn on total drying time.
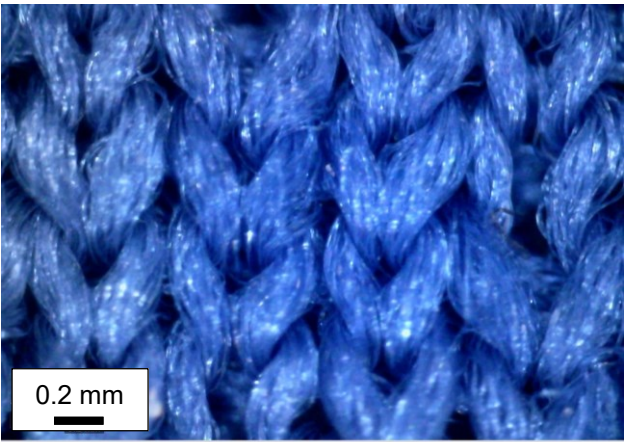
Synthetic fabrics are generally considered a better alternative for sportswear than natural fibers because they provide good heat and moisture management, allowing body temperature to be regulated. Polyester (PES) is the most commonly used fiber in sportswear because it is dimensionally stable, very durable, easy to care for, wrinkle resistant, and highly stain resistant. Hes and Ursache [15] investigated the cooling effect of knitted fabrics under simulated sweating conditions. They found that the highest cooling effect occurred with fabrics made of PES filaments with a grooved surface, which conduct moisture along the fabric. When polyamide or cotton fibers were present in the structure, the cooling effect was lower. The thermal resistance and air and water vapor permeability of various commercially available PES yarns were studied by Souza et al. [16]. The knitted fabrics with the highest thermal resistance values and the lowest heat absorption capacity and heat flow were those with higher air content in the fabric structure, which slowed down the heat transfer process. The air permeability of the fabrics seemed to depend on the fiber morphology. In terms of moisture management, Coolmax yarns achieved the best performance and Airclo and Seacell showed the best performance in terms of thermal regulation. The water vapor transport behavior of PES knitted fabrics with different thicknesses, densities, porosities and fiber cross-sectional properties was investigated by Prahsarn et al. using upright cup method, guarded sweating hot plate method and dynamic sweating hot plate apparatus [17]. The primary design criterion for a fabric for high water vapor transport performance is a structure that is both thin and open.

In this study, thermography was used to observe the changes in skin temperature of football players wearing PES knitted sportswear. A FLIR E6 thermal camera was used for the measurements [18].

2 Methods and Materials

The experiment presented in this manuscript focuses on studying the changes in body temperature during two typical football training sessions. A T-shirt (size L, in blue color, manufactured by Fotex company, Croatia) used as part of the official football clothing was selected for the study. The characteristics of the weft knitted fabric used for the production of T-shirts and the microscopic image are given in Table 1. The breaking force and breaking elongation of fabric were tested using the tensile tester Statimat M (Textechno Herbert Stein GmbH & Co. KG, Mönchengladbach, Germany). The gauge length of the tensile tester was (100 ± 1) mm and the dimensions of specimen (50 ± 0.5) mm x (200 ± 0.5) mm. Specimen were cut in the direction of wales and courses.

Table 1. Characteristics of knitted fabric. Dh/Dv = density horizontal/vertical.

Microscopic image	Fabric property	Measured value
0.2 mm	Fiber composition	100% polyester
	Average surface mass	145.20 g/m^2
	Average thickness	0.56 mm
	Fabric density (Dh/Dv)	18/cm / 22.5/cm
	Average breaking force in the direction of courses	233.41 N
	Average breaking elongation in the direction of courses	228.77%
	Average breaking force in the direction of wales	473.73 N
	Average breaking elongation in the direction of wales	72.61%

The participants were four male veteran footballers in good health who had no health disorders, such as cardiovascular or metabolic disorders, and were assessed as healthy by completing a general health questionnaire. All were non-smokers and not taking any medication. The participants were (42 ± 3) years

old, had a body weight of (82 ± 5) kg and a height of (180 ± 5) cm. The research with the participation of volunteers was approved by the Ethics Committee of the University of Zagreb, Faculty of Textile Technology. The volunteers were advised not to eat one hour before the training sessions and not to consume alcoholic beverages 24 h before. During the training sessions, the volunteers wore the predetermined T-shirt as well as shorts, socks, and sneakers. They wore the same outfit during the measurements (both before and after training). They were further advised to take the usual amount of water. Before and after the training sessions, temperature measurements were taken on the entire upper body of the player. The experiment focused on two types of typical football training: condition training (further referred to as Tr1) and tactical training (further referred to as Tr2). The duration of each training session was 60 minutes and measurements were taken after each of the total 10 training sessions. Training sessions were held at 1-2 day intervals. The main difference between these two types of training is that tactical training is performed with the ball, while condition training is performed without the ball. Both types of training start with warm-ups and end with stretching. Condition training includes running, push-ups, crunches, burpees, etc., while tactical training includes ball control and passing, turning and facing, cone weaving, etc. Between each series of exercises, the volunteer had breaks of 30 to 60 seconds to refresh himself.

The FLIR E6 thermal camera (Flir Systems Inc, USA) was used to measure the upper body temperatures of the players at a distance of 2 m, always at the same location. The specifications of the camera used are: IR resolution 120 × 90 pixels; thermal sensitivity <0.10 °C, field of view 45° × 34°, temperature range 0 °C to 150°C (standard range is -20 °C to +250 °C), emissivity correction: variable from 0.1 to 1.0 (set to 0.98 in these measurements). The camera was held vertically and all measurements were performed by one person according to the suggestions given in ISO 18434-1:2008 [19]. The example of thermograms for the anterior and posterior body is shown in Figure 1. The measurement was performed indoors with a controlled temperature of (21 ± 0.5) °C and relative humidity of (50 ± 5)%, without ventilation. Measurements were taken in the afternoon, during the spring season, just before the start of training and just after the end of training. The professional software FLIR Tools® (Flir Systems Inc, USA) was used for further processing of the thermal images.

(a)   (b)

Fig. 1. Example of a thermal images taken before training for: (a) anterior part of the body; (b) posterior part of the body.

In the analysis of thermal data, average temperatures were defined for 9 anterior and 9 posterior zones of the upper body, as depicted in Table 2. The variation of measured temperatures between participating footballers was up to 5% for a single observed zone.

Table 2. Observed body zones.

Anterior body zones		Posterior body zones	
Designation	Description	Designation	Description
z1a	Right upper arm	z1p	Right upper arm
z2a	Right chest	z2p	Right upper back
z3a	Mid chest	z3p	Mid upper back
z4a	Left chest	z4p	Left upper back
z5a	Left upper arm	z5p	Left upper arm
z6a	Right abdomen	z6p	Right lower back
z7a	Mid abdomen	z7p	Mid lower back
z8a	Left abdomen	z8p	Left lower back
z9a	Anterior pelvis	z9p	Posterior pelvis

3   Results and discussion

The results in terms of differences in absolute temperature between the measured pre-training body temperatures and the post-training body temperatures are shown in Figures 2 and 3. The results are presented for each observed anterior and posterior zone and two types of football training, i.e. condition training (Tr1) and tactical training (Tr2).

Figure 2a shows that after condition training the body temperature in the anterior upper arm and chest zones drops by up to 2 K. The situation is quite different after tactical training, where the body temperature in the anterior chest area increases by up to 1 K, while it decreases in the upper arms. There is also a difference in temperature change between the left and right upper arms.

As can be seen in Figure 2b, body temperature decreases in the anterior right and mid abdominal and pelvic zones after condition training, while it increases in the anterior left abdominal zone. The temperature decrease in the anterior right abdominal zone is more than 3 K. The difference in temperature change between the left and right abdominal sides of the body is even greater than in the upper arms. After tactical training, body temperature decreases by up to 2 K in the anterior left and middle abdominal zones. Again, the difference in temperature change between the left and right abdominal sides of the body sides is clear.

Figures 3a and 3b show that after both condition and tactical training, body temperature decreases by 1.2-3.7 K in all posterior body zones. The decrease is most pronounced in the right chest and mid abdominal zones. The differences in temperature change between left and right side of the body are also significant.

From the comparison of Figures 2 and 3, the significant differences between the absolute temperatures in the anterior and posterior body zones can also be seen.
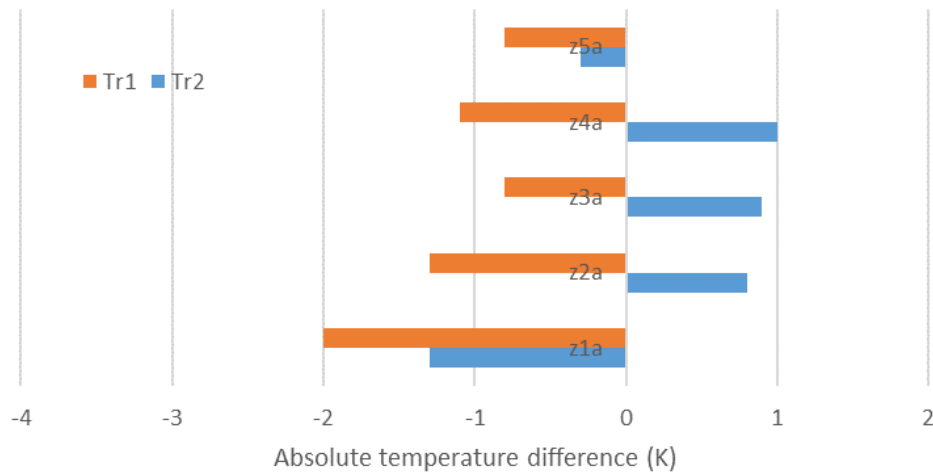
(a)
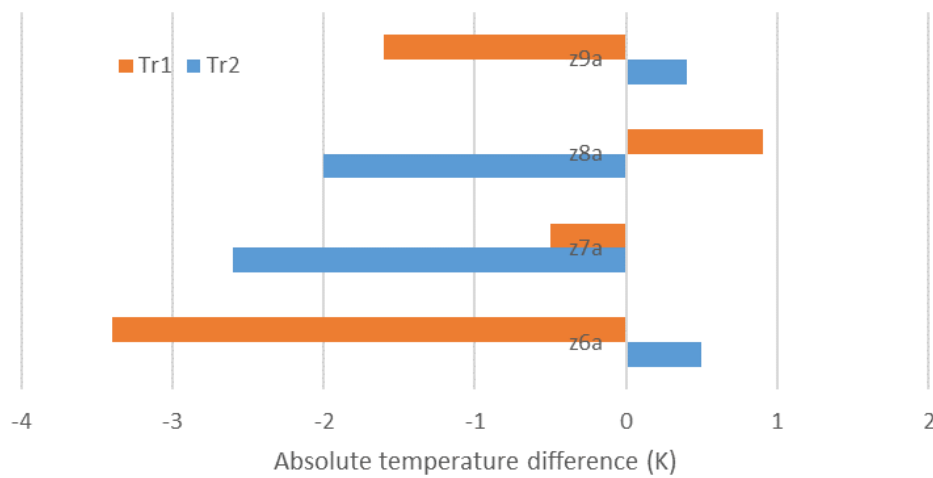
(b)

Fig. 2 Absolute temperature difference for anterior body zones (a) zones z1a-z5a; (b) zones z6a-z9a.

The decrease in skin temperature over the selected muscle zones of the upper body seems to be related to the cooling effect of sweat evaporation. Sweating is the main thermoregulatory response by which heat balance is maintained after a rise in body temperature during exercise-induced heat load. Evaporation of sweat from the skin surface has a cooling effect because evaporation is an endothermic process [20]. It is important to consider other factors that could influence differences in skin temperature between body regions [21]. Body movement causes air movement around the body and could increase heat consumption and lead to lower local skin temperatures. Thermal insulation of clothing and obstruction of sweating may also cause differences in different body zones. On the other hand, sweating may moisten the clothing locally and evaporation may cause the local body temperature decrease. Individual characteristics of the subject (genetic and/or anthropometric and/or training factors) may also influence the skin temperature change [15,16].
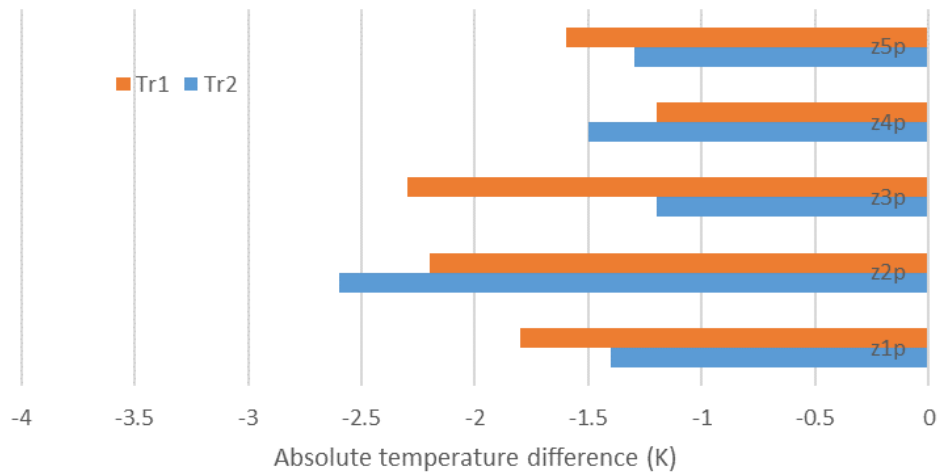
(a)
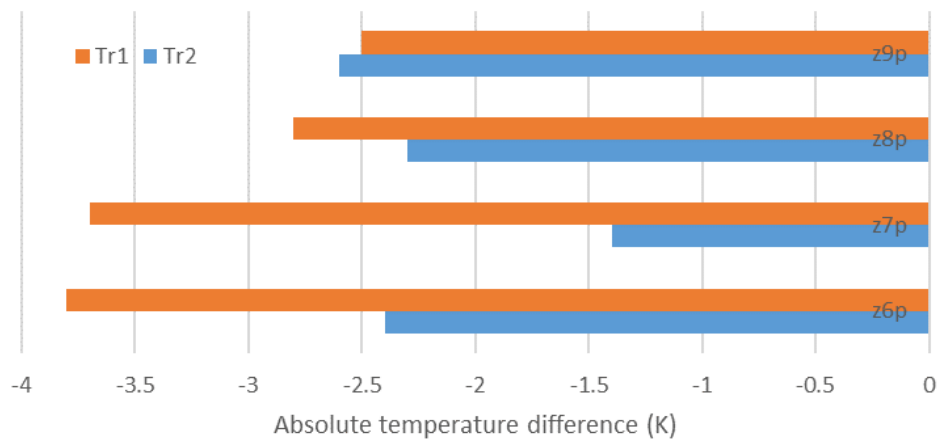
(b)

Fig. 3 Absolute temperature difference for posterior body zones (a) zones z1p-z5p; (b) zones z6p-z9p.

The type of training also affects the change in body temperature. During graded load exercise, where the load on the body progressively increases (and the blood demand of the working organs also increases), the mean skin temperature decreases throughout the exercise. A continuous vasoconstrictor response, resulting in a progressive decrease in blood flow with increasing exercise intensity, is thought to be the reason for the decrease in mean skin temperature. In the case of constant load exercise, skin temperature decreases at the beginning of work due to the initial vasoconstriction of the skin and then reaches a minimum value, followed by a small and gradual increase over time. It is argued that the initial decrease and subsequent small increase in skin temperature is the net result of competition between the vasoconstrictor response, which lasts as long as the exercise continues, and the vasodilator response, which is induced by increasing body temperature [22].

The results of the unpaired t-test are determined with $\alpha = 0.05$. The test compared the values of measured body zone temperatures after the training activity for two types of training. The results are given in Table 3. According to the p-value given, the differences are considered not statistically significant. As can be seen from the same table, a significant difference ($p < 0.05$) is defined only for the posterior pelvic zone.

Table 3. Results of the t-test.

Anterior body zones

Designation	Description	p-value
z1a	Right upper arm	0.6692
z2a	Right chest	0.8621
z3a	Mid chest	0.7385
z4a	Left chest	0.9492
z5a	Left upper arm	0.6534
z6a	Right abdomen	0.5547
z7a	Mid abdomen	0.4176
z8a	Left abdomen	0.8975
z9a	Anterior Pelvis	0.9340

Posterior body zones

Designation	Description	p-value
z1p	Right upper arm	0.5782
z2p	Right upper back	0.5400
z3p	Mid upper back	0.7693
z4p	Left upper back	0.3481
z5p	Left upper arm	0.9799
z6p	Right lower back	0.6776
z7p	Mid lower back	0.7389
z8p	Left lower back	0.7697
z9p	Posterior pelvis	0.0263

Conclusions

The aim of this work was to compare the changes in temperatures of the anterior and posterior body zones of an athlete due to different types of training. The results showed that:
- after condition training, body temperature in the anterior upper arm and chest zones decreases by up to 2 K, while after tactical training, it increases by up to 1 K in the anterior chest zone;
- after condition training, body temperature decreases in the anterior right, mid abdominal and pelvic zones, while after tactical training it decreases in the anterior left and middle abdominal zones;
- after both types of training, body temperature decreases by 1.2-3.7 K in all posterior body zones;
- for a number of zones, significant differences between left and right sides of the body are observed.

The results of the study are expected to be applied in the design and development of specific sportswear for high-level professional football players. More specifically, these results can be used to design T-shirts in which individual cut parts (in specific body zones) are made of materials with different properties, especially in terms of sweat transfer.

Acknowledgement

References

[1] George Havenith. 1999. Heat balance when wearing protective clothing. *Ann. Occup. Hyg.* 43, 5, 289-296. DOI: https://doi.org/10.1016/S0003-4878(99)00051-4.

[2] Agnieszka Dębiec-Bąk, Łukasz Pawik and Anna Skrzek. 2016. Thermoregulation of football players after cryotherapy in thermography. *J. Therm. Anal. Calorim.* 126, 1, 1633-1644. DOI: https://doi.org/10.1007/s10973-016-5623-3.

[3] Pedro Gomez-Carmona, Ismael Fernández-Cuevas, Manuel Sillero-Quintana,Javier Arnaiz-Lastras, and Archit Navandar. 2020. Infrared Thermography Protocol on Reducing the Incidence of Soccer Injuries. *Journal of Sport Rehabilitation* 29, 8, 1222-1227. DOI: https://doi.org/10.1123/jsr.2019-0056.

[4] Adérito Seixas, Gonjo Tomohiro, Ricardo Vardasca, Joaquim Gabriel Mendes, Ricardo Fernandes and J. Vilas-Boas. 2014. A preliminary study on the relationship between energy expenditure and skin temperature in swimming. In *Proceedings of the QIRT2014 – The 12th International Conference on Quantitative InfraRed Thermography,* July 2014, Bordeaux. DOI: https://doi.org/10.21611/qirt.2014.097.

[5] Jose Ignacio Priego Quesada, Felipe P. Carpes, Rosario Salvador Palmer, Pedro Pérez‑Soriano and Rosa M. Cibrián Ortiz de Anda. 2016. Effect of saddle height on skin temperature measured in different days of cycling. *SpringerPlus* 5, 205, 1-9. DOI: https://doi.org/10.1186/s40064-016-1843-z.

[6] Vesna Marija Potočić Matković and Ivana Salopek Čubrić. 2018. Performance of neoprene wetsuits in different underwater thermal environments. In *Proceedings of 7th International Ergonomics Conference – Ergonomics 2018*, June 13-16, 2018, Zadar, Croatia.

[7] Jose Ignacio Priego-Quesada, Alvaro S. Machado, Marina Gil-Calvo, Irene Jimenez-Perez, Rosa M. Cibrian Ortiz de Anda, Rosario Salvador Palmer and Pedro Perez-Soriano. 2020. A methodology to assess the effect of sweat on infrared thermography data after running: Preliminary study. *Infrared Physics & Technology* 109, 103382. DOI: https://doi.org/10.1016/j.infrared.2020.103382.

[8] Vedran Hadžić, Brane Širok, Aleš Malneršič and Milan Čoh, 2019. Can infrared thermography be used to monitor fatigue during exercise? A case study. *Journal of Sport and Health Science* 8, 1, 89-92. DOI: https://doi.org/10.1016/j.jshs.2015.08.002.

[9] Priscila dos Santos Bunn, Maria Elisa Koppke Miranda, Allan Inoue Rodrigues, Ravini de Souza Sodré, Eduardo Borba Neves and Elirez Bezerra da Silva, 2020. Infrared thermography and musculoskeletal injuries: A systematic review with meta-analysis. *Infrared Physics & Technology* 109, 103435. DOI: doi.org/10.1016/j.infrared.2020.103435.

[10] Thomas W. Jones, Barry C. Shillabeer, and Marco Cardinale. 2020. Skin temperature, training load, and subjective muscle soreness in junior endurance athletes: A case study. *International Journal of Sports Physiology and Performance* 15, 9, 1349-1352. DOI: https://doi.org/10.1123/ijspp.2019-0748.

[11] Ivana Salopek Čubrić, Goran Čubrić and Vesna Marija Potočić Matković. Development of ergonomic sportswear based on thermal body mapping. In *Proceedings of the 8th International Ergonomics Conference,* December 2-5, 2020, Zagreb, Croatia. Springer International Publishing, ISBN: 978-3-030-66937-9.

[12] Deepti Gupta, Vijay Kumar Kothari and Yamini Jhanji. 2014. Heat and moisture transport in single jersey plated fabrics. *Indian Journal of Fibre & Textile Research* 39, 2, 115-121.

[13] Renata Nemcokova, Viera Glombikova and Petra Komarkova. 2015. Study on liquid moisture transport of knitted fabrics by means of MMT, thermography and microtomography systems. *AUTEX Research Journal* 15, 4, 233-242. DOI: https://doi.org/10.1515/aut-2015-0022.

[14] Ivana Salopek Čubrić, Goran Čubrić and Vesna Marija Potočić Matković. Use of thermography to analyze the influence of Yarn properties on fabric drying. In *Proceedings of 7th International Conference on Textile*, November 10-11, 2016, Tirana, Albania.

[15] Lubos Hes and Mariana Ursache. 2011. Effect of composition of knitted fabrics on their cooling efficiency at simulated sweating. *Indian Journal of Fibre & Textile Research* 36. 3, 281-284.

[16] Jefferson M. Souza, Sandra Sampaio, Welter C. Silva, Sidney G. de Lima, Andrea Zille and Raul Fangueiro. 2018. Characterization of functional single jersey knitted fabrics using non-conventional yarns for sportswear. *Textile Research Journal* 88, 3, 275-292. DOI: https://doi.org/10.1177/0040517516677226.

[17] C. Prahsarn, R. L. Barker and B. S. Gupta. 2005. Moisture vapor transport behavior of polyester knit fabrics. *Textile Research Journal* 75, 4, 346-351. DOI: https://doi.org/10.1177/0040517505053811.

[18] Flir. FLIR E6. Retrieved from https://www.flir.com/products/e6/.

[19] ISO 18434-1: Condition monitoring and diagnostics of machines – Thermography – Part 1: General procedures.

[20] Zofia Drzazga, Mariusz Binek, Ilona Pokora and Ewa Sadowska-Krepa. 2018. A preliminary study on infrared thermal imaging of cross-country skiers and swimmers subjected to endurance exercise. *Journal of Thermal Analysis and Calorimetry* 134, 701-710. DOI: https://doi.org/10.1007/s10973-018-7311-y.

[21] Jose Ignacio Priego Quesada, Natividad Martínez, Rosario Salvador Palmer, Agnes Psikuta, Simon Annaheim, René Michel Rossi, José Miguel Corberán, Rosa M. Cibrián Ortiz de Anda and Pedro Pérez-Soriano. 2016. Effects of the cycling workload on core and local skin temperatures. *Experimental Thermal and Fluid Science* 77, 91-99. DOI: https://doi.org/10.1016/j.expthermflusci.2016.04.008.

[22] Giovanni Tanda. 2015. The use of infrared thermography to detect the skin temperature response to physical activity. *Journal of Physics: Conference Series* 655, 1, 1-10. DOI: https://doi.org/10.1088/1742-6596/655/1/012062.

Haptic virtualization of surfaces: feeling textiles on your phone

Tung Le, Christopher Martin, Annerose Braune*

Chair of Automation Engineering, Technische Universität Dresden, Germany
*Corresponding author *E-mail address:* annerose.braune@tu-dresden.de

INFO

ABSTRACT

The haptic impression of textile surface properties has a decisive influence on its evaluation and ultimately on its acceptance and usability. Many solutions are used to replicate a static contour or shape, e.g. to feel controls on common touch displays. In contrast, this project investigates whether it is possible to simulate the roughness or friction behavior of a textile surface using a commercially available mobile device.

1 Introduction

The importance of virtual reality applications continuously increases e.g. in the field of online shopping. Yet, potential buyers have not been able to perceive product properties throughout the haptic modality, e.g. in textile industries. Humans have haptic sensors to feel the properties when swiping over the textiles. In case of virtual reality, however, humans do not interact with the real textile, but with a device. Now this device must represent the textile and has to simulate textile properties as far as possible in such a way that realistic sensations are generated.

In several research projects, devices have already been developed that simulate textile properties [1,2]. The reproduction of static contours and shapes is already being used, for example, to feel control elements on touch displays [3]. These shapes represent static elements as virtual elevations on a flat screen. However, if you want to feel the texture, the roughness or the friction behavior of a textile surface by stroking your fingertip over it, the contours to be simulated are microscopically small. In this article, we will now investigate whether normal commercial touch displays in mobile devices can be used for this purpose.

Typical mobile devices have features for vibration alarms. They act as an alternative signal transmitter if the acoustic signal is perceived as disturbing during a call or the visual display cannot be perceived immediately. For the user it is only necessary to distinguish certain vibration patterns from each other or to perceive a vibration haptically at all. The engines of the mobile phones are not designed for a large variation of vibration intensities and therefore only a low resolution of the intensity exists. However, due to the widespread use and the easy accessibility of smartphones and tablets, the "misappropriation" for textile surfaces will be discussed.

The following chapter 2 therefore first describes the human sensors for haptic perception on the finger and their essential capabilities. Chapter 3 presents existing haptic devices for user interfaces both in terms of the haptic properties to be displayed and from the aspect of accessibility. Chapters 4 and 5 subsequently describe the developed mobile application and a user study conducted with it. Chapter 6 evaluates the results and derives conclusions about usability.

2 Human haptic perception

When evaluating the importance of each human sensory organ, one approach is to analyze the number of receptors and the amount of information perceived. Whereas most information is processed through the visual channel, the human skin comes out as the second most important sensory organ, being about 1000 times larger than the other ones [4]. The skin's sensors are distributed over the entire human body and the receptor density depends on the part of the body. For example, the fingers can detect extremely fine structures (down to 2.5 mm [5,6]), while at the back, the resolving capacity is lower, so that structures can no longer be distinguished that well [5].

Haptic perception is described as all sensory and motoric functions that are responsible for the sense of touch (*tactile perception*) and movement (*kinaesthetic perception*). While tactile perception is perceived through the skin's mechanoreceptors, kinaesthesia describes activity and perception of the muscles, tendons, and joints [7]. Haptic perception describes the process of actively exploring objects and surfaces including both perception receptors (Fig. 1). Important tactile receptors are

- Merkel cells: **S**lowly **A**dapting type 1 (SA-I)
- Ruffini corpuscles: **S**lowly **A**dapting type 2 (SA-II)
- Meissner's corpuscles: **R**apidly **A**dapting (RA) resp. **F**ast **A**dapting type 1 (FA-I)
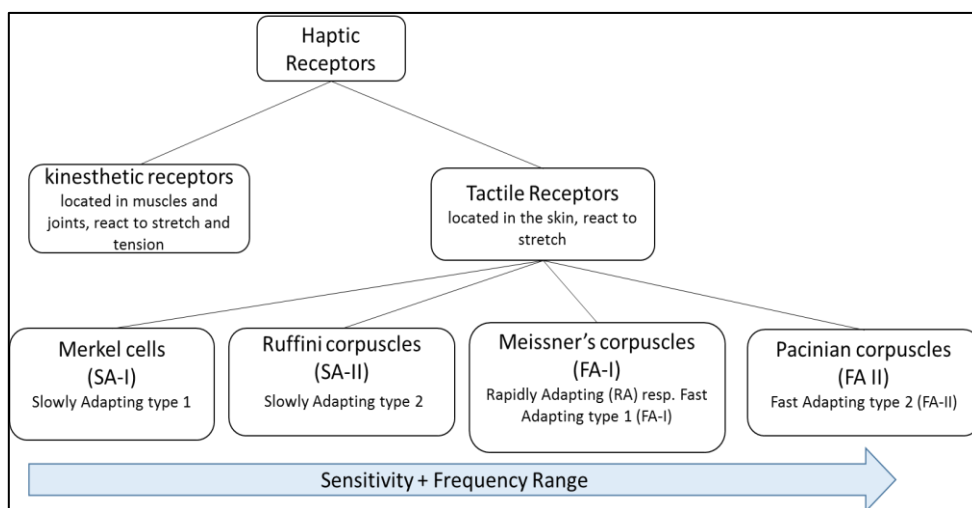- Pacinian corpuscles: **F**ast **A**dapting type 2 (FA-II)

Figure 1: Classification of haptic sensors, following [7]

The slowly adapting receptors (SA-I and SA-II) detect the strength of the deformation, i.e. the depth of the skin's stretching. They are mainly responsible for perceiving more static deformation [5]. Fig. 2 summarizes

the tactile perception by displaying the frequency ranges which each tactile sensor responds to. Furthermore, the figure provides the absolute threshold area for each receptor type. The average displacement threshold for the SA receptors is detected at about 50 µm (dashed line in Fig. 2) and they have their highest sensitivity at less than 20 changes per second (10 Hz). The rapidly adapting sensors (RA and FA) adapt very quickly to changing deformations. However, their sensitivity to stimuli decreases again after a short time. They therefore tend to detect rapidly changing stimulus patterns and are thus used to detect relative movements of objects on the skin and mechanical vibratory deformation. These sensors can sense vibrations at around 200 to 300 Hz with an amplitude starting from 10 µm. This is an indicator for the higher degree of sensitivity for the RA resp. FA sensors.
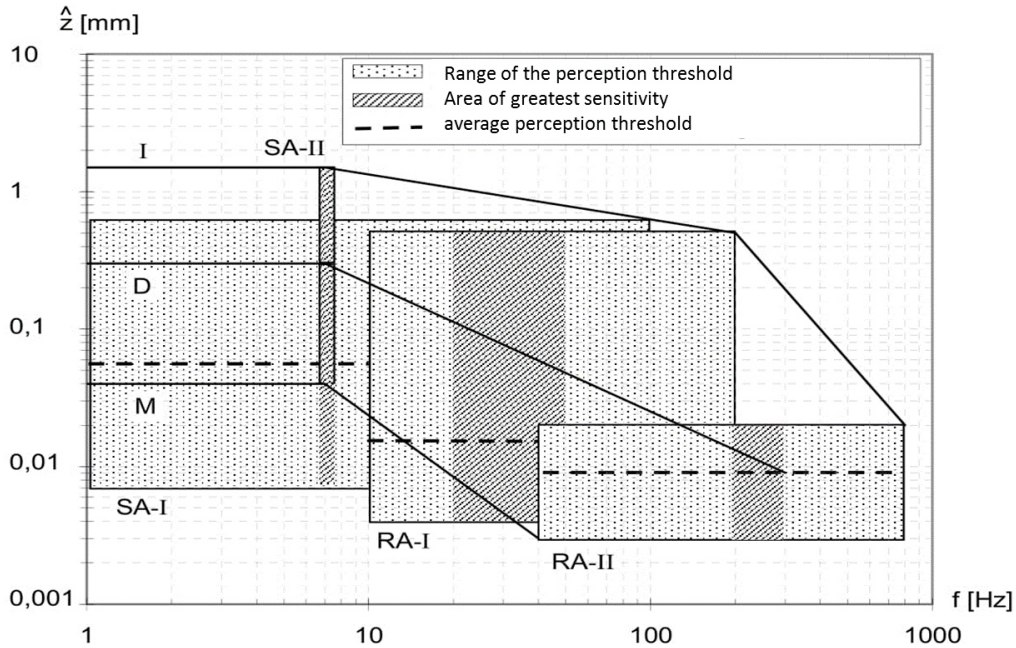

Fig. 2: Frequency dependent perception thresholds of tactile receptors [27]

The neurophysiological point of view is not ideally applicable to the human perception. Sensory stimuli may be filtered, but also combined for a more sensitive perception. Psychophysics, as in [6], discusses the effects of physical stimuli on the subjective sensation and perception. The detection threshold for a non-moving fingertip, e.g., is about 1 mm [8], whereas active haptic perception can detect bumps down to 0.85 µm [9]. This allows distinguishing the roughness level of textile surfaces for evaluating its comfort.

3 Haptic Devices

With the biological concepts of haptic perception in mind, devices can be designed to target the sensor types as described in the previous chapter. According to Fig. 1, haptic devices can be divided into those that stimulate kinaesthetic receptors and those that stimulate tactile receptors. Kinaesthetic devices stimulate the receptors in muscles, tendons and joints. They use the feedback of force to interact with users. Such force feedback devices are often used as virtual training simulation cockpits or robotic assisted teleoperations [10]. But in this paper, we restrict the applicable domain to textile surfaces. Those are primarily sensed by skin receptors, which leads to an in-depth look for tactile devices.

3.1   Concepts of Tactile Devices

For contact-based mechanical stimulation there are two common approaches. The first one can be described as static displacement. Such devices replicate the shape and surface of an object as close-to-reality as possible. The virtualization process requires multiple actor pins arranged in a matrix (pin-array). By giving each pin a separately controllable displacement output, different surface forms can be applied onto the device. This approach can be achieved, for example, piezo-electrically [11] or with electro- or

magnetorheological fluids [12]. A high spatial resolution array, with pins being about 0.5 mm apart from each other, was accomplished by using thermal-sensitive hydrogels [13].

The second approach can be described as vibrotactile. These devices do not aim for replicating the static shape of the surface itself. Instead they focus on giving a realistic impression and sensation of haptic surface properties, when feeling a virtualized object. This approach is supported by means of vibration [5,7] to stimulate FA receptors (cf. Chapter 2). Vibrotactile output of these devices is rendered through position tracking of the human contact area, such as the fingertip. Although not necessarily required, this method can be used in conjunction with previously described pin-arrays (e.g. [14-16]). Adding vibrotactile elements to pin-arrays vastly improves user experience [17].

More recent advances for tactile stimulation for consideration are non-contact stimulation via ultrasonic waves [18], generating friction with electrostatic fields [19] or electrotactile displays that directly induce current into the receptor's nerve endings [20]. These technologies are especially useful for low-noise devices over motoric actuators.

3.2   Mobile consumer devices as haptic user interfaces

Using previously described concepts, several haptic devices were developed, often as a result of research projects. These devices were not designed from the point of usability, but for very specific applications and further scientific studies. Their technical design usually requires additional equipment, making them therefore often quite large, heavy and thus uncomfortable for consumers and for transport. These research products are generally not easily accessible on the consumer market.

In contrast mobile consumer devices, such as smartphones and tablets, are prevalent around the world. Leading corporations are striving to equip common displays with tactile functionality. This enables feeling control elements such as buttons intuitively on displays through haptic feedback. The simulation of tactile surface properties creates significantly higher requirements.

Mobile devices utilize a vibrotactile approach (cf. Chapter 2) with two widespread technical implementations: eccentric rotating mass (ERM) and linear resonant actuator (LRA). ERM's rotating unbalance causes the device casing to vibrate on the rotational plane. Due to their simple nature, ERM technology is still more dominant on the mobile device market. However, if the haptic user experience is to be improved, manufacturers prefer newer LRA implementations. LRAs work similar to voice-coil principles of loudspeakers. Their dynamic properties are characterized by faster response times than ERM actuators [21]. LRAs are installed, e.g., in newer iPhone models with Apple's *Taptic Engine* [22] or in the Sony Xperia XZ2 device for enhancing media playback experience by additionally providing haptic feedback (*Dynamic Vibration System – technology*) [23].

3.3   Conclusion

The spatial pin densities of tactile pin arrays vary from 2 mm to 3 mm per pin (e.g. [12,14-16]), but can be reduced to 0.5 mm with manufacturing processes for semiconductors (cf. Section 3.1). When used as static displacement devices, this would be sufficient since the pin density meets the fingertips spatial threshold (cf. Chapter 2). However, textile surfaces generally have far more defined contours, where distances between surface levels are possibly within microns. In addition to a swiping movement, this results in a vibration from a finger's point of view. As human receptors can sense vibratory skin displacement up to 800 Hz (cf. Fig. 2), they can distinguish finer surface structures, such as textiles. Therefore, a vibrotactile approach is preferred over static displacement, to precisely stimulate FA receptors.

Since mobile devices, such as smartphones or tablets, are widely used, their suitability for a haptic user interface is the central task of this paper. Conventional built-in vibration motors oscillate at 7.000 to 12.000 rpm (rounds per minute) [7] and thus specifically target Pacinian corpuscles (cf. Chapter 2). Since they

provide visual and auditive feedback, a multimodal aspect may be included, enhancing user experience by targeting multiple perception channels.

With these aspects in mind, we would like to test the following scenarios: Is it possible to feel the texture and roughness of the textile surface, the friction behavior and, to a certain extent, the softness of the textile surface when swiping over the display of a mobile device? Consequently, a mobile application is proposed, that is tested on *Sony Xperia XZ3* mobile phone, the successor of the *Sony Xperia XZ2* model on an Android operating system. With the integrated LRA, the haptic virtualization application substantially benefits from better transient response, as stated earlier.

4. Mobile Application
4.1. Haptic rendering

While the main purpose of mobile devices' vibrations is silent alerts, a haptic inspection process requires a precise control of the vibrating device. In this paper, the procedure of exploring a textile surface with a fingertip is virtualized by replacing the inspected surface with a smartphone's display. While the finger swipes over the touch screen, the application generates a vibration pattern according to the surfaces' contour, giving the impression of an actual textile by its property *roughness*.

In this section, we introduce an algorithm for continuous adaption of haptic feedback depending on the finger trajectory. For this purpose, the textile surfaces are measured and digitalized by 3D scans. The resulting point cloud serves as a function $z = f(x, y)$, with x, y spanning the surface plain and z being the corresponding height level (Fig. 3).
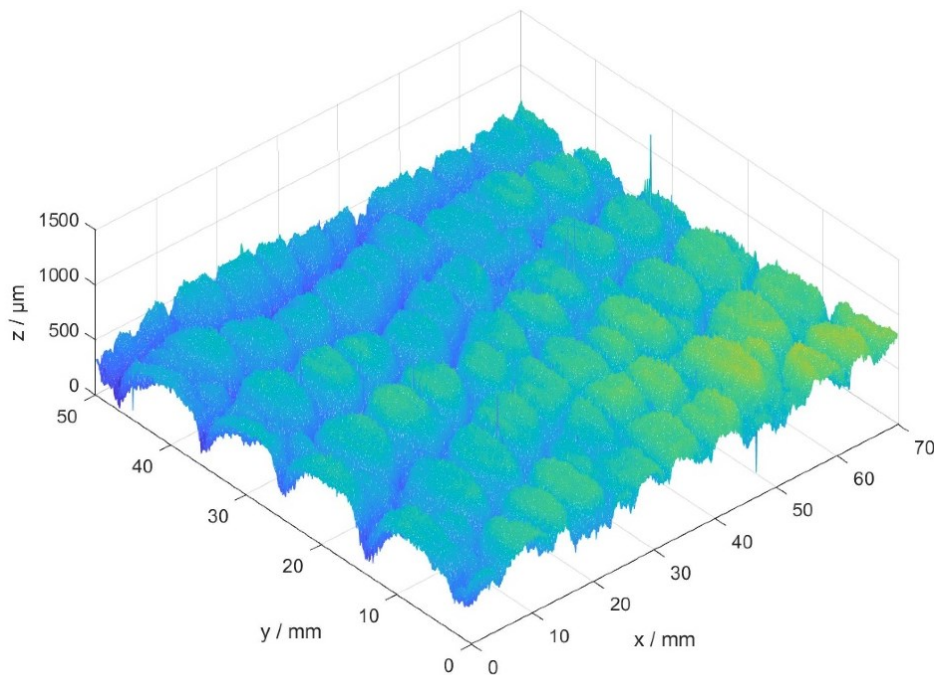

Fig. 3: 3D scan example of a textile surface

This function may be encoded within a grayscale image, with z matching to the image's pixel values. Now, by tracking the finger's movement $[x(t) \quad y(t)]^T$ and combining it with previously described height function results in a temporal height function:

$$z(t) = f(x(t), y(t)) \tag{1}$$

Having the surface height variation history, this function is processed by a haptic feedback algorithm to set a proper output on the vibration element. Due to similarities in the auditory and haptic perception, the

input data are pre-processed by means of Fourier transformation (Equation 2), a common approach implemented in haptic applications [14,24].

$$F(\omega) = \mathcal{F}\{z(t)\} \tag{2}$$

After performing Fourier analysis, a convenient amplitude must be applied onto the vibrating device. Allerkamp et al. [14] proposed a generalized haptic signal, consisting of two base frequencies at 40 Hz and 320 Hz, thus targeting both SA and FA sensors (cf. Chapter 2). With a suitable superposition of the two frequencies, one tries to stimulate any haptic feeling. A similar basic idea underlies the RGB model. Here, too, any other color is generated by superposition of the 3 basic colors, i.e. by the superposition of the different wavelengths respectively the corresponding frequencies. However, our selected hardware in conjunction with its underlying vibration API [25] is limited to oscillate at a single pre-set frequency. As stated earlier, the concept is not to exactly replicate the surface contour, but to stimulate a comparable tactile impression. For this purpose, a weighted root mean square (RMS) is calculated from the discrete Fourier spectrum $F(\omega_i)$, as seen in Equation (3). An RMS emphasizes dominant frequencies over multiple minor frequencies and assesses them a higher value.

$$P = c_v \sqrt{\frac{1}{n} \sum [c_{rec}(\omega_i) \cdot F(\omega_i)]^2} \tag{3}$$

P describes the input parameter of Android's vibration API [25], representing the oscillation amplitude. Equation (3) includes a frequency-dependent weight factor c_{rec} that resembles different sensitivities of each sensor type (cf. Chapter 2). Values for c_{rec} are selected according to the relative average detection threshold (cf. Fig. 2Fig. 2). Consequently, sensors operating in higher frequency bands (FA-I, FA-II) are given a higher weight factor, as seen in Equation (4).

$$c_{rec}(\omega) = \begin{cases} 1/6, & \text{for} & \omega < 10 \text{ Hz} \\ 1/2, & \text{for} & 10 \text{ Hz} \leq \omega < 40 \text{ Hz} \\ 1, & \text{for} & 40 \text{ Hz} \leq \omega < 800 \text{ Hz} \\ 0, & \text{else} \end{cases} \tag{4}$$

Before P can finally be applied onto the vibration motor, Equation (3) still contains an unknown variable c_v. As the mobile device's displacement parameter are neither found in its data sheet, nor can it be reliably determined by internal sensory, this amplification constant will be discussed in a follow-up perception study (cf. Chapter 5).

4.2 Android App

Our approach was implemented by developing an app for Android-based handhelds. The app including the mobile device hardware serves as the haptic user interface, whereas textile-related information is stored on an external database. The app accesses the database by sending HTTP requests over the internet to its web service. The server provides a catalogue along with a property set (e.g. type of fabric, materials), containing textile surfaces being available for inspection. After browsing and on item selection, the app fetches the necessary data for tactile rendering from the web service, including the item's surface profile.

When developing an Android app, its interfaces (such as Wi-Fi, touchscreen, or sensors) can only be accessed throughout the operating system API that may cause limitations on the user interface. Input-wise, the retrieval of a finger's trajectory is controlled by the Android framework with efficiency purposes [26]. On the one hand, input data is delivered at undeterminable timestamps (being around 15 ms to 70 ms apart, depending on the rate of input change). On the other hand, multiple samples are batched together. Equation (2) from Chapter 4.1 is practically implemented by Fast Fourier Transformation (FFT). This algorithm though requires temporal equidistant sample data in contradiction to Android's motion data. In

order to perform the FFT algorithm, additional samples are computed by means of linear interpolation (cf. Equation (5)), with $t_i, \vec{x}(t_i)$ being provided by the motion framework.

$$\begin{pmatrix} x(t) \\ y(t) \end{pmatrix} = \vec{x}(t) = \frac{\vec{x}(t_{i+1}) - \vec{x}(t_i)}{t_{i+1} - t_i} \ (t - t_i) + \ \vec{x}(t_i) \quad \text{with } t_i \le t < t_{i+1} \tag{5}$$

On the output-wise limitations it was discovered that sending a vibration request to the device's API causes the LRA module to halt, before oscillating with the desired amplitude. Too frequent updates seriously affect user experience. Therefore, a minimum update interval of 50 ms was found to feel continuous vibration and suppress perceivable stops of the actuator. A constant time interval is preferred, however, since a.) Android operating system does not provide real-time execution to guarantee specified cycle time, and b.) the algorithm could possibly miss on valuable input data. The time window for the FFT is equivalent to the current update interval and its time stamps have to be determined for each iteration.

5 User study

Finally, a user study is conducted for the mobile application. The study serves two purposes: subjective user evaluation and determining an amplification factor for c_v (cf. Equation (3)).
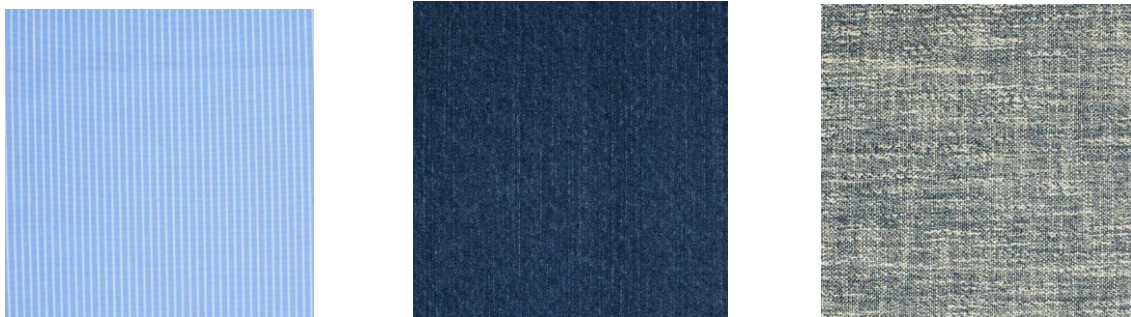
(a) H71 Shirting fabric, very smooth	(b) B1 Denim, medium rough	(c) H31 costume fabric, very rough

Fig. 4: Textile samples used in the user study with increasing roughness from left to right

The experimental setup consists of a *Sony Xperia XZ3* smartphone and three textile surfaces with their structure ranging from very smooth to very rough (cf. Fig. 4). The subjects' task was to explore the textiles by moving their fingertip over the surface. For each surface their virtual resemblance on the smartphone shall be inspected and adjusted, so that the feeling of virtual and actual textile is as close as possible to the Point of Subjective Equality (PSE), e.g., introduced in [20]. For this purpose, a modified application was installed, which included a slider to modify the vibration intensity (cf. Fig. 5).

The subjects were asked to obtain a PSE value for a slow (2 cm/s) and a fast (10 cm/s) swiping movement, which were visually monitored. The smartphone was fixated on a table to suppress the device moving and to restrain receptor stimulation to the fingertip only.

13 subjects in total, six female and seven male, in the age from 18 to 34, resp. 50 and above participated in this experiment. Subjects were asked about their textile expertise, ranging from beginner to expert, where two declared as advanced and the remaining as beginners. None of them had experience in haptic human-machine interaction. Participants were given an introductory training phase with the total experiment duration lasting approx. 30 minutes.
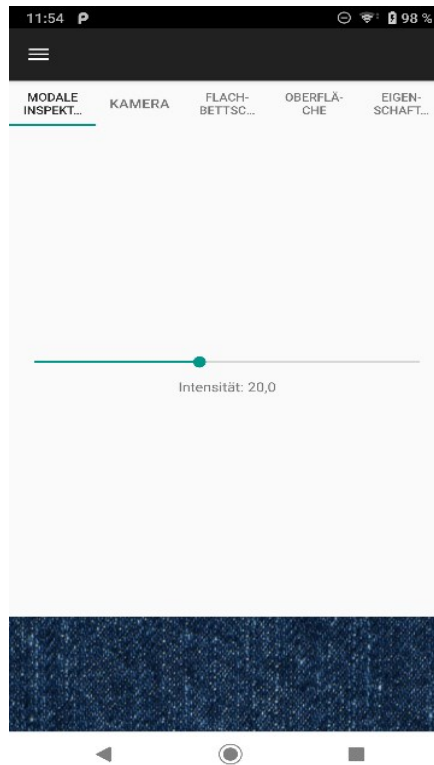
Fig. 5 : Textile inspection view of the user study's application

For each sub experiment the average PSE value resp. standard deviation from all participants are presented in Fig. 6. The medium rough textile B1 denim achieved the lowest relative standard deviation, meaning a high level of agreement from all subjects. B1's surface is mainly perceived by means of friction, rather than its structures and contours. The mobile device's oscillation direction parallel to the finger's motion proves to be advantageous over vertical displacement, when stimulating a friction effect. This result complies with the participants' comments: H71's shirting fabric surface was too smooth, when swiping over the real textile, complicating the replication on the handheld's glass surface. PSE values were set on the individual perception threshold, rather than identifying equal points of tactile feels. The H31 costume fabric on the other hand displayed strongly defined textures even in a static context, which cannot by imitated by the plain glass surface. Often the PSE values were set to maximum intensity, which exceeded the vibration's output range. Therefore, the mobile device as a haptic user interface may function with textiles within a specified roughness range, as surface virtualization for both too smooth and too rough surfaces collide with device limitations.
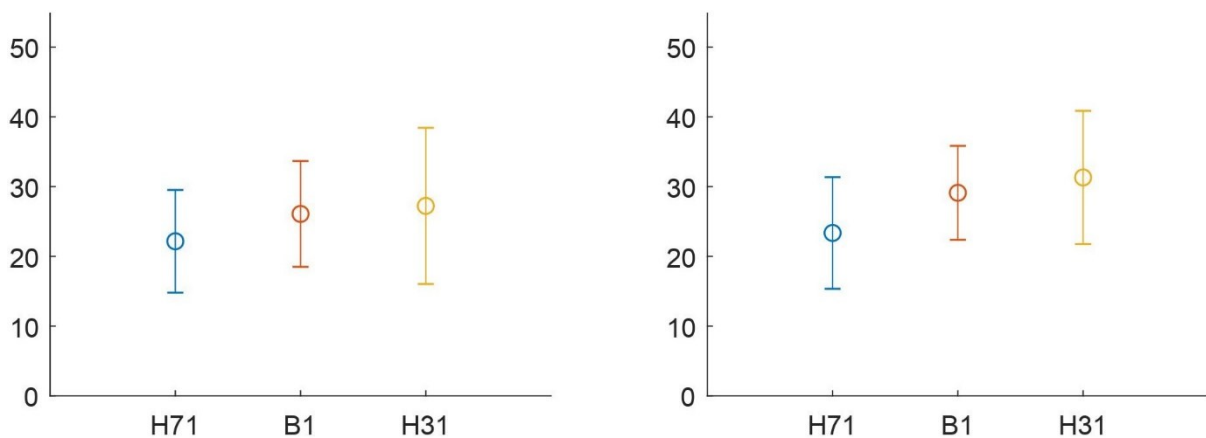

Fig. 6: Mean PSE values with standard deviations for slow movement (left) and fast movement (right)

The algorithm described in Section 4.1 proves to be a suitable approach, but requires refinement, e.g. including textile properties (such as stiffness), since the PSE mean values show discrepancies among each sub-experiment while having the earlier discussed device restraints in mind.

The rather high standard deviations illustrate a highly individual perception, which requires a user-specific scaling factor. This could be determined by an initialization run with a few common reference textiles.

6 Conclusions

The aim of this project was to test whether properties of a textile surface such as roughness and friction behavior can be realistically simulated with the help of a mobile consumer device (cf. Section 3.2). For this purpose, it is helpful to be able to use measured and thus objectively detectable data.

In our case, the surfaces of the textiles were measured using a 3D scanner. From this, roughness parameters were determined according to DIN EN ISO 4287:2010-07 and serve as the basis for the haptic algorithm which controls the motor in the mobile device. Fig. 7 shows the output of the described haptic algorithm (x-axis) and the measured roughness values (y-axis). The plot shows the expected high degree of correlation between the considered quantities, since both characteristics were derived from the same measured value, the 3D scan. The correlation coefficients are 0.92 for the center roughness, 0.93 for the profile depth and 0.95 for the maximum roughness depth.

The results of the user study show that the algorithm described in Section 4.1 proves to be a suitable approach, but requires refinement, since the PSE mean values show discrepancies among each sub experiment. For a further improvement of the sensation, a consideration of additional objectively measurable parameters in the algorithm is also conceivable. For example, fiber stiffness is not yet taken into account by the 3D scan of the textile.
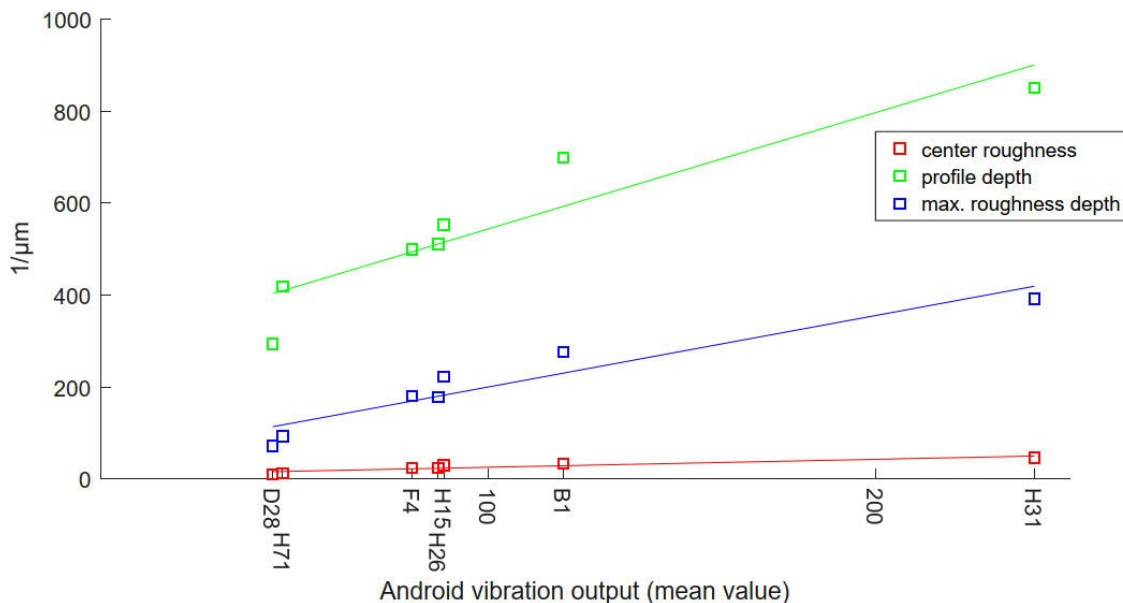

Fig. 7: Correlation between optical roughness and vibration output

However, the smartphone's surface and the haptics engine's properties proved to be limiting. The hardware's shortcomings were particularly evident on very smooth and heavily textured surfaces. The motor's non-centered placement also falsifies the user's sensation.

Several test persons registered a heat development of the display as annoying when brushing over the hard glass surface. The heat development should therefore be taken into account in future developments. Sweat on the fingers also affects the sensation. Other surfaces or a cover could help.

Finally, subjects were asked whether this application would influence their online shopping behavior. Despite the limitations, five replied, such a device would probably support their shopping decision, with three more being undecided.

Acknowledgements

References

[1] N. Magnenat-Thalmann, P. Volino, U. Bonanni, I. R. Summers, M. Bergamasco, F. Salsedo and F.-E. Wolter. 2007. From physics-based simulation to the touching of textiles: the HAPTEX project. The International Journal of Virtual Reality 6, 3, 35-44.

[2] Tanvas Inc. Sample Applications – Tanvas. 2021. Retrieved May 7, 2021 from https://tanvas.co/sample-applications.

[3] Haptische Displays: Die Zukunft fühlbarer Tasten auf flachen Bildschirmen. Retrieved April 20, 2020 from https://www.trendsderzukunft.de/haptische-displays-die-zukunft-fuehlbarer-tasten-auf-flachen-bildschirmen/.

[4] D. Zühlke. 2012. *Nutzergerechte Entwicklung von Mensch-Maschine-Systemen: Useware-Engineering für technische Systeme* (2nd ed.) Springer-Verlag, Berlin and Heidelberg.

[5] M. Grunwald. 2008. *Human Haptic Perception: Basics and Applications.* Birkhäuser Verlag, Basel, Berlin and Boston.

[6] G. A. Gescheider. 1997. *Psychophysics: The Fundamentals* (3. ed.). Lawrence Erlbaum Associates, New Jersey and London.

[7] T. A. Kern and M. Matysek. *Entwicklung haptischer Geräte: Ein Einstieg für Ingenieure* (7. ed.). Springer-Verlag, Berlin and Heidelberg.

[8] K. O. Johnson and J. R. Phillips. 1981. Tactile spatial-resolution. I. Two-point discrimination, gap detection, grating resolution, and letter recognition. *Journal of Physiology* 46, 6, 1171-1191.

[9] K. A. Kaczmarek and P. Bach-y-Rita. 1995. Tactile Displays. In W. Barfield and T. A. Furness III (Eds.). *Virtual environments and advanced interface design*. Oxford University Press, New York, 349-414.

[10] Intuitive Surgical Inc., Intuitive | da Vinci Robotic Assisted Surgical System. 2019. Retrieved May 27, 2019 from https://www.intuitive.com/.

[11] V. G. Chouvardas, A. N. Miliou and M. K. Hatalis. 2008. Tactile displays: Overview and recent advances. *Displays* 29, 185-194. DOI: https://doi.org/10.1016/j.displa.2007.07.003.

[12] H. Böse, H. Ermert, A. Tunayar, G. Monkman, M. Baumann, W. Khaled, S. Reichling, O. T. Bruhns, H. Freimuth and S. Egersdörfer. 2004. A novel haptic sensor-actuator system for applications in virtual reality. *Proc. 4th Internat Conf. EuroHaptics* 2004, 88-93.

[13] G. Paschew. 2020. Intermodale Displays auf Basis intrinsisch aktiver Polymere, Technische Universität Dresden.

[14] D. Allerkamp, G. Böttcher, F.-E. Wolter, A. C. Brady, J. Qu and I. R. Summers. 2007. A vibrotactile approach to tactile rendering. *The Visual Computer* 23, 97-108. DOI: https://doi.org/10.1007/s00371-006-0031-5.

[15] Y. Ikei and M. Shiratori 2002. TextureExplorer: A Tactile and Force Display for Virtual Textures. In *Proceedings of the 10th Symposium on Haptic Interfaces for Virtual Environment and Teleoperator Systems*, Washington.

[16] G.-H. Yang, K.-U. Kyung, M. A. Srinivasan and D.-S. Kwon. 2006. Quantitative tactile display device with pin-array type tactile feedback and thermal feedback. In *Proceedings 2006 IEEE International Conference on Robotics and Automation* ICRA 2006.

[17] K.-U. Kyung, M. Ahn, D.-S. Kwon and M. A. Srinivasan, 2005. A compact broadband tactile display and its effectiveness in the display of tactile form. In *First Joint Eurohaptics Conference and Symposium on Haptic Interfaces for Virtual Environment and Teleoperator Systems. World Haptics Conference*.

[18] E. Freeman, R. Anderson, J. Williamson, G. Wilson and S. A. Brewster. 2017. Textured Surfaces for Ultrasound Haptic Displays. In *Proceedings of the 19th ACM International Conference on Multimodal Interaction*, New York, USA.

[19] O. Bau, I. Poupyrev, A. Israr und C. Harrison. 2010. Teslatouch: Electrovibration for Touch Surfaces. In *UIST'10: Proceedings of the 23nd annual ACM symposium on User interface software and technology*, New York, USA.

[20] M. E. Altinsoy and S. Merchel. 2012. Electrotactile feedback for handheld devices with touch screen and simulation of roughness. *IEEE Transactions on Haptics* 5, 6-13. DOI: https://doi.org/10.1109/TOH.2011.56.

[21] Texas Instruments. 2013. Haptics: Solutions for ERM and LRA Actuators. Retrieved June 6, 2019 from http://www.ti.com/lit/ml/sszb151/sszb151.pdf.

[22] AppleInsider. 2016. Inside the iPhone 7: Apple's Taptic Engine, explained. Retrieved Jung 6, 2019 from: https://appleinsider.com/articles/16/09/27/inside-the-iphone-7-apples-taptic-engine-explained.

[23] Sony Mobile Communications. 2018. Meet the Makers: Die Macher hinter der Unterhaltungsrevolution – Sony Mobile (Deutschland). Retrieved Jung 21, 2019 from https://blogs.sonymobile.com/de/2018/05/25/meet-makers-dynamic-vibration-system/.

[24] E. Steinbach, M. Strese, M. Eid, X. Liu, A. Bhardwaj, Q. Liu, M. Al-Ja'afreh, T. Mahmoodi, R. Hassen, A. E. Saddik and O. Holland. 2019. Haptic codecs for the tactile internet. *Proceedings of the IEEE* 107, 447-470. DOI https://doi.org/10.1109/JPROC.2018.2867835.

[25] Google Inc. 2019. Vibrator | Android Developers Retrieved July 17, 2019 from https://developer.android.com/reference/android/os/Vibrator.html.

[26] Google Inc. 2019. MotionEvent | Android Developers. Retrieved June 18, 2019 from https://developer.android.com/reference/android/view/MotionEvent.

[27] M. Jungmann. 2004. Entwicklung elektrostatischer Festkörperaktoren mit elastischen Dielektrika für den Einsatz in taktilen Anzeigefeldern. Dissertation Thesis, Technische Universität Darmstadt.

Auxetic structures from 3D printed hybrid textiles

Subin Shajoo[1], David Schmelzeisen[2], Christopher Pastore[3,*]

[1] Department of Design, Politecnico di Milano, Italy.

[2] Institut für Textiltechnik der RWTH Aachen University (ITA), Germany

[3] Thomas Jefferson University, Philadelphia, USA

* Corresponding author *E-mail address:* Chris.Pastore@Jefferson.edu

INFO

ABSTRACT

Auxetic structures have been produced using 3D printing and knitted textile materials. A review of other auxetic textiles is presented along with the new materials. A range of configurations were developed, prototyped, and tested to demonstrate significant auxetic response, including Poisson's ratio up to negative one. The concept of 4D textiles was employed to create environmentally responsive hinges in some structures, allowing the material to change shape in response to thermal stimulus.

1 Introduction

When a material is subject to an applied tensile extension in a given direction (ε_a), the material will demonstrate an extension in the other orthogonal, transverse, directions (ε_t). Poisson's ratio ν for a given material is defined as the negative ratio of these two values [1]: $\nu = -\varepsilon_t/\varepsilon_a$. For most materials, Poisson's ratio is positive. There are a few materials that have negative Poisson's ratios, as a result of their molecular structure. These tend to be highly porous foam-like structures [2]. In fact, the behavior comes from the microstructural geometry of the foam [3]. Materials with negative Poisson's ratios are called auxetic.

Expanding the auxetic microstructure to a larger scale, there is a well-established field of research to evaluate structural systems that demonstrate auxetic behavior through the use of structural elements at a much larger scale than molecules or pores, by combining triangles [4], squares [5], or auxetic hexagons [6].

There are a range of applications for auxetic materials, including biomedical [7], sports [8], and textiles [9]. One of the interesting properties is the ability of auxetic materials and structures to form synclastic shapes (including domes and spheres), as opposed to traditional materials which form anticlastic

(positive Poisson's ratio) or even monoclastic surfaces (high shear modulus), as illustrated in Fig. 1. A synclastic curve is formed from an increase in dimensions in both direction and shearing of the surface, monoclastic requires no stretch and no shear, and anticlastic one has shearing as well as an increased length in one direction and decreased length in the other.
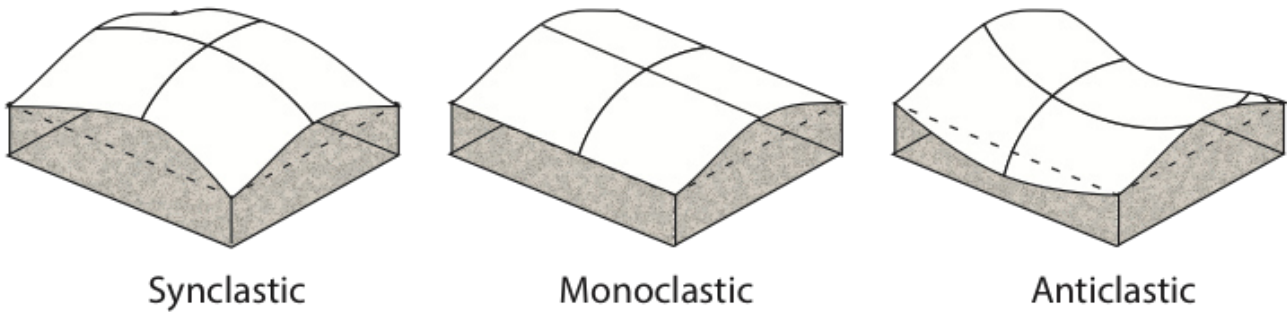

Fig. 1. Classification of curved surfaces as synclastic, monoclastic, or anticlastic.

Design and modeling of novel auxetic materials and structures is a developing field. In this paper, we are examining a methodology for creating auxetic membrane structures using 3D printing combined with textile materials. The result is a quick method of producing auxetic structures that are durable and suitable for a range of applications.

2 Auxetic shapes

The classic example of an auxetic structure is a hinged hexagonal system. If we consider a framework produced in a hexagonal, honey-comb type of shape, assuming it is a pin jointed truss where the members are stiff and the joints have no resistance to rotation, we create a structure that has a traditional behavior, as shown in the top of Fig. 2 [10].
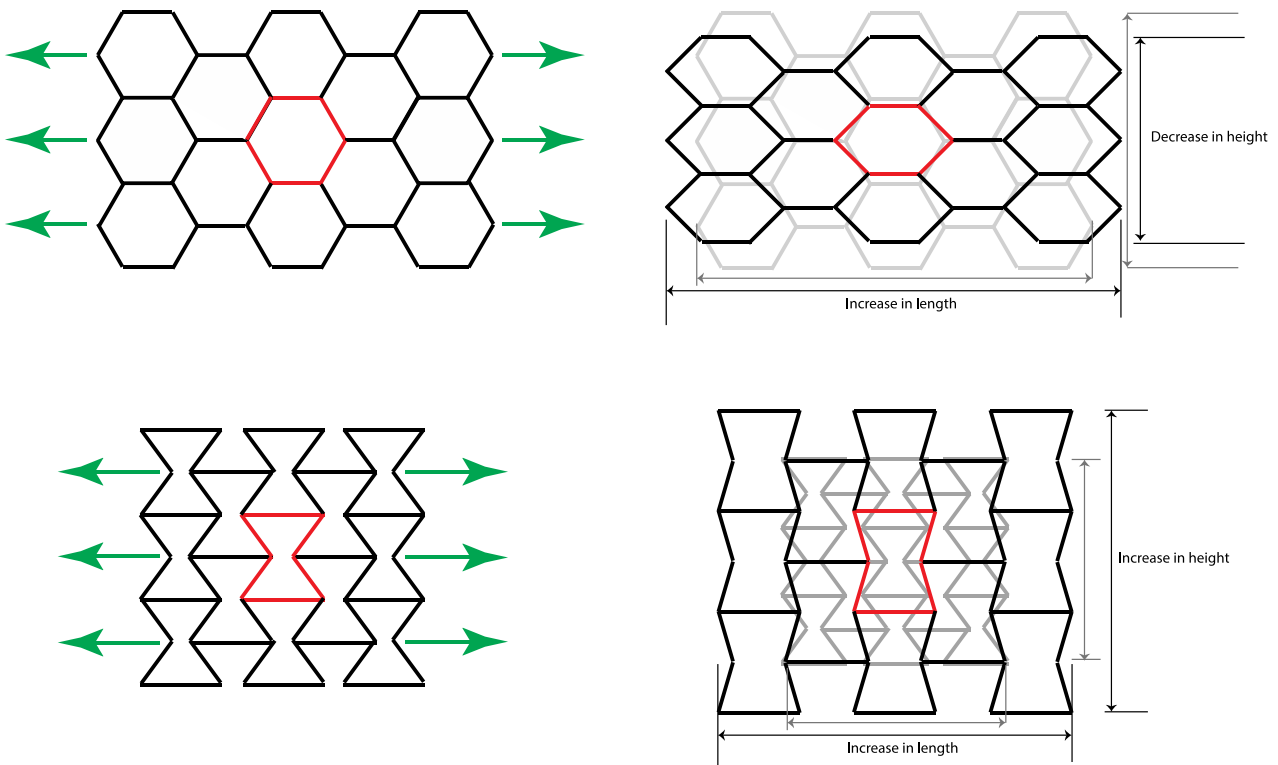

Fig. 2. Comparison of traditional honeycomb shape with positive Poisson's ratio (top) and an auxetic structure formed from an inward facing hexagon demonstrating a negative Poisson's ratio, thus an auxetic material (bottom).

But changing that hexagon to a convex, inward facing one, as illustrated in the bottom of Fig. 2, the behavior of the structure changes dramatically. This is due to the orientation of the structural elements. In order for the inward facing arms of the hexagons to extend horizontally, they must rotate around their joints, resulting in an increase in the height of the structure. The specific Poisson's ratio of this structure depends on the relative length of the horizontal elements to diagonal elements, and the angle of orientation of the inward facing diagonals.

It should be noted that this behavior is easy to demonstrate and model for an idealized (perfect) truss with no resistance to joint rotation [10]. In an actual material system, the behavior is not perfect.

There are many different geometries that can accomplish auxetic structural behavior. The key component is the rotation of individual structural elements that interact with each other to create the auxetic behavior.

Investigators have considered a range of possible systems, such as star shaped inclusions, to create auxetic composites [11], interlocking hexagons [6], or trilobal inclusions in foam [8], or other types of "missing rib" structures embedded in foam [12].

2.1 Auxetic yarns

Auxetic behavior has also been demonstrated in linear systems, such as yarns [13]. The principle here is a bit different than the auxetic structures identified above. The idea is to make a yarn structure that increases in average diameter when stretched in the axial direction. This is accomplished through the use of two different yarn systems, one notably stiffer than the other. In a structure often termed helical auxetic yarn [14], or HAY, the stiff element is wrapped around a core of the less stiff element, as shown in Fig. 3. Upon application of axial load, the stiffer wrapper resists elongation and uses the applied energy to move to the center rather than extend. The lower modulus core element can deform and move into an outer spiral.
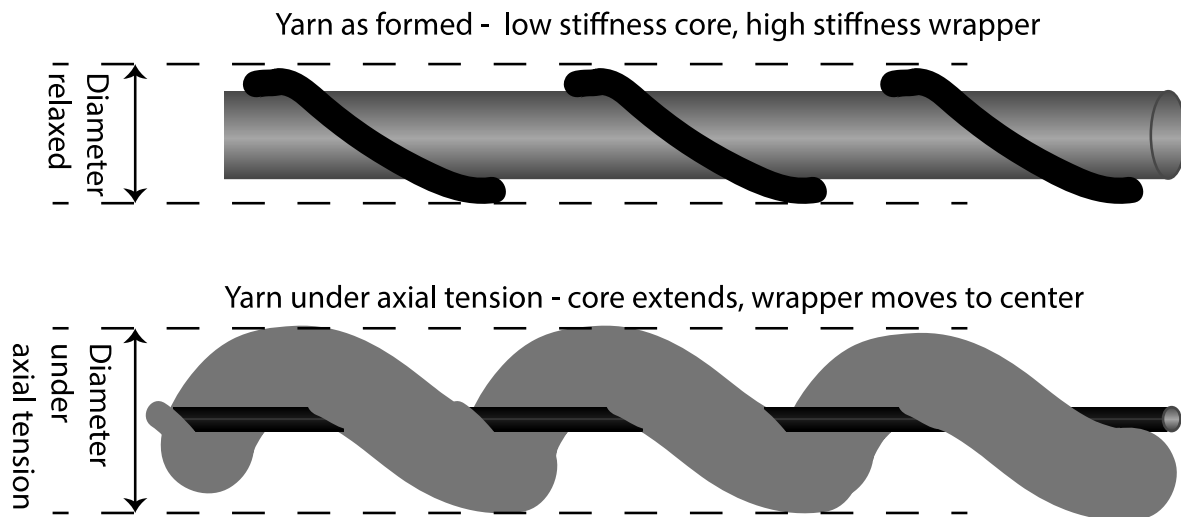

Fig. 3. Schematic illustration of an auxetic yarn (helical auxetic yarn) showing relaxed state (top) with a low stiffness core and a high stiffness wrapper, the same yarn under axial tension (bottom) wherein the low stiffness core has stretched and moved to the outside while the high modulus wrapper moves to the center, creating an increase in the effective diameter of the yarns.

The exchange of positions between core and wrapper result in an auxetic yarn, i.e. in an increase in the effective diameter of the yarn. In general terms, the effective diameter of the relaxed yarn D_r can be estimated in terms of the core diameter, d_c, and the wrapper diameter, d_w:

$$D_r = d_c + 2d_w \tag{1}$$

When it is fully extended, the diameter D_e can be approximated as

$$D_e = 2d_c + d_w \tag{2}$$

Thus, the diameter of the composite yarn varies by approximately $(d_c - d_w)$, depending on the applied load. The magnitude of that change depends on the starting diameters of the two elements.

It is important to note that, as illustrated in the drawings, this is the effective diameter. The entire volume is not filled with yarn, but rather the projection of the diameter along the axis of the yarn shows the auxetic behavior.

2.2 Auxetic textiles

There is also a significant amount of research in ways to create auxetic textiles [15,16]. One approach is creating fabrics using the HAY systems described above. This is not a particularly effective method, as the yarns themselves, carrying the load, will try to resist the negative Poisson effect, as illustrated in Fig. 4. Further, the yarns in the perpendicular direction will resist the expansion in that direction.
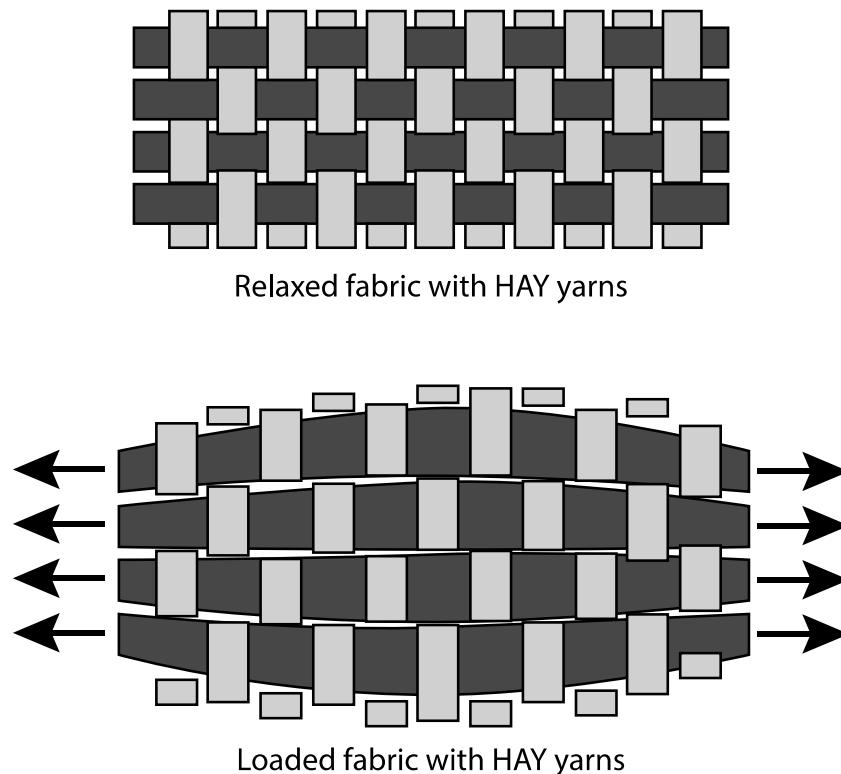

Relaxed fabric with HAY yarns

Loaded fabric with HAY yarns

Fig. 4. Schematic illustration of a woven fabric with HAY yarns, relaxed in the top image and under load in the bottom image.

When the yarns in Fig. 4 expand due to the negative Poisson's ratio, they need to move out of their original position because of the expansion of the neighboring yarns. In order to carry the load, the individual yarns must be held in some position. Thus, the motion of the expanding yarns attempts to make a curved path rather than the original straight path. This creates compressive forces at the sides of the yarn and these forces attempt to reduce the expansion of the yarns.

Although woven fabrics made from HAY yarns are not particularly auxetic in practice, they do change permeability and porosity significantly when under load making them good for applications such as blast protection [14].

A number of researchers have explored the potentials of incorporating auxetic shapes (see above) into warp knitted fabrics so that the yarns formed into auxetic patterns [17,18]. These structures appear to provide the auxetic behavior, relying on the use of elastic yarns in addition to stiffer yarns to make the transition. Most of the configurations only have the negative Poisson effect in the first loading, and are not reversible [19]. However, some work has been done attempting to create reversible warp knitted fabrics that demonstrate auxetic behavior [20].

Nonwoven fabrics can be designed to produce auxetic behavior in the thickness direction only through proper needle punching [21].

A different approach to inducing auxetic behavior in textile structures is through folding techniques, inspired by origami arts [22-24]. The basic concept is to make the fabric in a highly folded configuration and in effect the material oriented in thickness direction reorients into the transverse direction, resulting in a negative Poisson's ratio in the transverse planar direction, but a highly positive value in the thickness direction [25]. A typical origami folding pattern is shown in Fig. 5. This technique has been used to fold textiles, holding the creases through an ironing or pressing procedure. Variations on the folding patterns exist, and all generally can create auxetic behavior in the plane of the folded system.
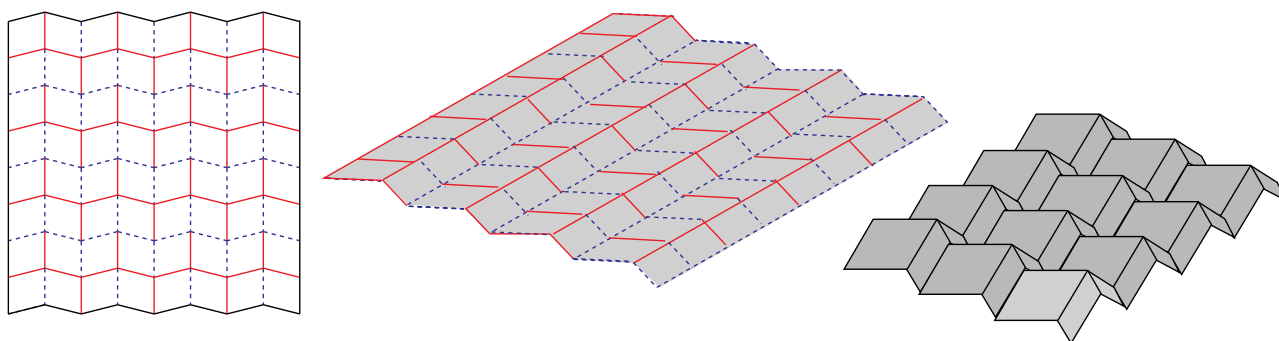

Fig. 5. Schematic illustration of an origami folding pattern that creates auxetic structures used for paper or textile materials.

3   3D printing on textiles

There has been a rapid growth in research regarding 3D printing in recent years driven by the low cost and material efficiency of the technology. Combining 3D printing and textile materials is still a relatively new research area [26-28]. This method offers the promise of "4D Textiles" – hybrid textile/3D printed structures that can change structural form with time [29,30]. The adhesion between substrate and printed polymer is important for long-term stability of the developed structure [31].

Because the textile material is highly flexible, as opposed to the relative stiffness of the printed polymer, in the hybrid system the textile acts as a unifying hinge and structural reinforcement that can permit and restrain both flexure and torsion.

In the process described here, an elastic knitted fabric was used as the textile substrate. This allows pre-stretching of the fabric prior to printing, in which case the textile is a repository of stored elastic energy. This method of storing energy is commonly employed in 4D textiles [32], typically to create curvature or to provide a mechanism for assisting shape transformation. In the process described, a pre-strain level of 50% in two orthogonal directions was applied to the knitted fabric prior to printing. This opens the pores of the fabric, but also provides some energy that pulls the structure towards the center, as illustrated in Fig. 6.
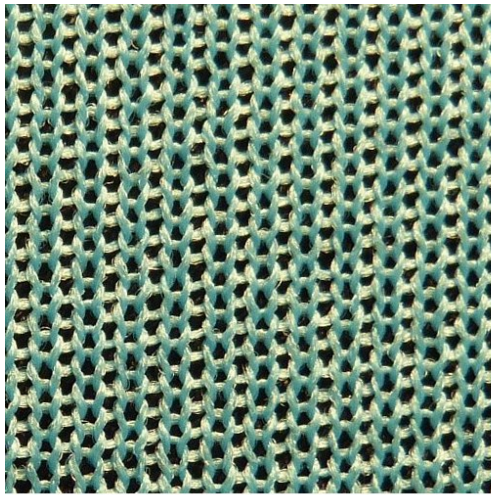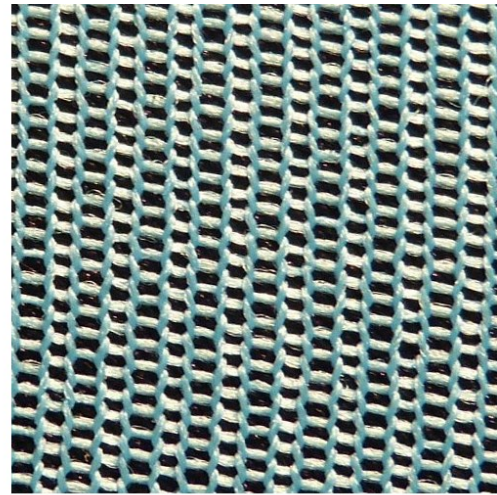
Fig. 6. Photomicrograph of elastic Jersey knit with no stretch (left) and after 50% stretch in both x- and y-directions (right).

The fabric stretch is maintained during printing with a flat metallic plate that has pins at the sides, as shown in Fig. 7. The fabric is measured and marked prior to stretching on the plate to ensure the proper dimensions are achieved. The pins do not provide a perfect boundary condition, as can be seen, but near the center of the fabric the strain field is relatively uniform as was demonstrated in Fig. 6.

Fig. 7. Weft knitted fabric stretched and held in place on a plate prior to 3D printing. Pins at the edges of the plate hold the fabric still during the processing.

In this research, the polymer was printed onto the fabric surface using a Mass Portal Pharaoh XD® printer using a 0.4 mm nozzle. This printer uses 1.75 mm thermoplastic filaments with two filament feeds and a heater capable of printing at 300 °C. The auxetic forms used for printing were designed with SolidWorks®. After exporting them as STL files, G-codes of the sliced model was developed using Simplify3D®. During the slicing process, all printing parameters, such as printing velocity, layer thickness, flow rate, etc. could be defined. The G-codes were sent to the 3D printer and used to print the structure. Details of these printing parameters are contained in Appendix A.

3.1   Auxetic structures on textile substrates

For example, as illustrated in Fig. 8, a structure such as the corner joined squares could be printed onto a textile material. The flexible nature of the textile should allow the structural shapes to create the auxetic behavior. The initial goal was to develop a 3D print/textile hybrid that demonstrated the auxetic behavior shown below.
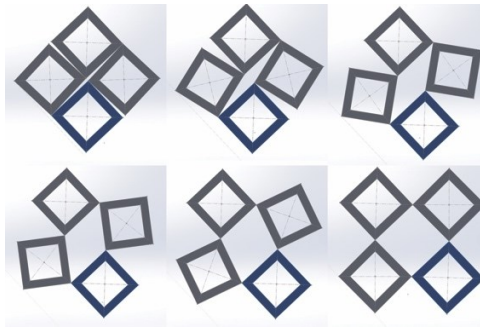
Fig. 8. Simulation of rectangular auxetic structures joined at corners showing auxetic in-plane behavior.

The 3D print/textile hybrid requires two elements – the 3D printing design and execution and the selection of an appropriate textile substrate. In order to get this structure printed onto a textile, it is necessary to create a model of the print. There are several critical aspects of the print model:

- Design a joint for the corner which is capable of repeated flexing.
- Ensure the polymer bonds well with the textile substrate.
- Provide sufficient stiffness to the frame element.

To accomplish this, the design employed used two different polymers during the printing process. A polylactic acid (PLA) was used as a soft material to provide the corner hinge. This was also used as a base layer for the entire structure because the low viscosity PLA provides a good infiltration with the textile substrate.

For the structural square, acrylonitrile butadiene styrene (ABS) was printed. This has a much higher stiffness and higher glass transition temperature than the PLA. The print pattern was two layered – first a layer of PLA and then a selective layer of ABS, as illustrated in Fig. 9. During printing, the ABS and PLA were each provided in the form of a filament with diameter of 1.75 mm.
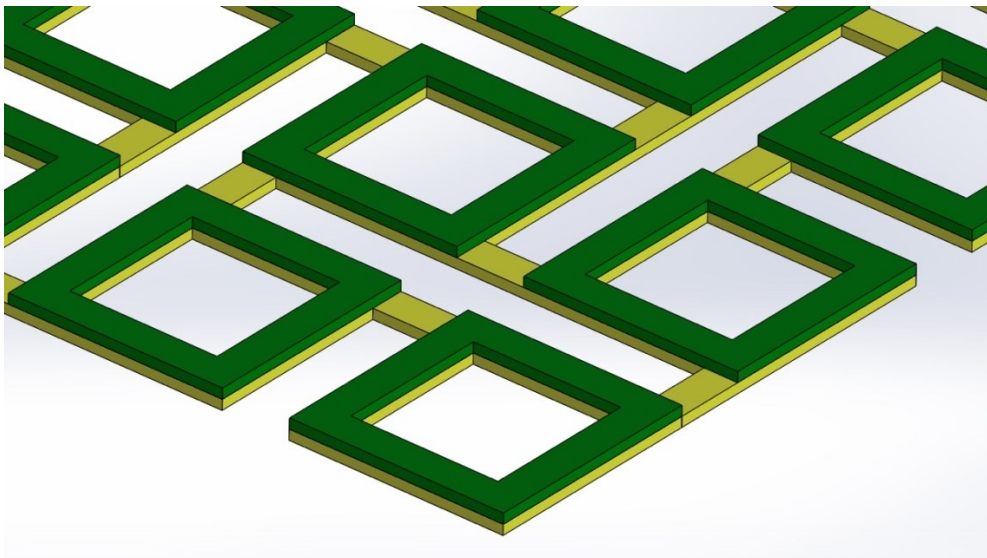

Fig. 9. CAD drawing used to control the printer for the two-layer system. In this illustration dark green represents the ABS and light green represents the PLA.

As mentioned previously, the substrate needs to be able to rotate at the joint. The localized shear strain field on the textile will be quite high, and thus a highly extensible, low shear modulus fabric is needed. An elastic jersey knit, formed from polyester yarns with Spandex, was used. This fabric has low shear modulus, high extensibility, and good elastic recovery.

Initial experiments involved printing acrylonitrile butadiene styrene (ABS) onto the pre-stretched jersey knit fabric (formed of polyester/Spandex yarns). After printing rectangular shapes onto the fabric, the

fabric was slit selectively to allow the fabric to function as a rotational hinge for the structure. If the fabric was not slit, the tensile modulus of the fabric would fight against the expansion in the transverse direction. By slitting the fabric, the knit functions primarily as the hinge material in addition to providing a protective membrane inside the printed squares.

A sample of a 3x3 printed auxetic square structure is illustrated in Fig. 10. The resulting structure had a very strong auxetic behavior, and a tendency to returning to the original form. However, repeated loadings resulted in delamination of the ABS from the knit fabric, particularly at the corners of the squares where stresses are highest.
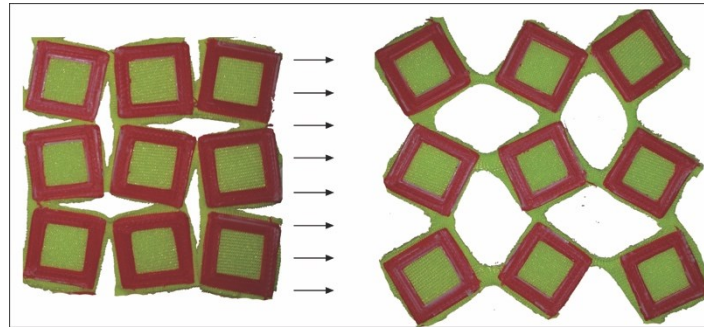

Fig. 10. Experimental study of a 3x3 rectangular auxetic formed from ABS printed onto polyester/Spandex jersey knit fabric. The fabric was slit to create space for rotation (left) and after extension the auxetic behavior is quite clear and dramatic (right).

Larger structures using smaller squares were also explored. Fig. 11 shows a 7x7 print, again slit between the squares, demonstrating significant auxetic behavior and also the ability to form into synclastic surfaces. The Poisson's ratio calculated from the example below is -0.9.
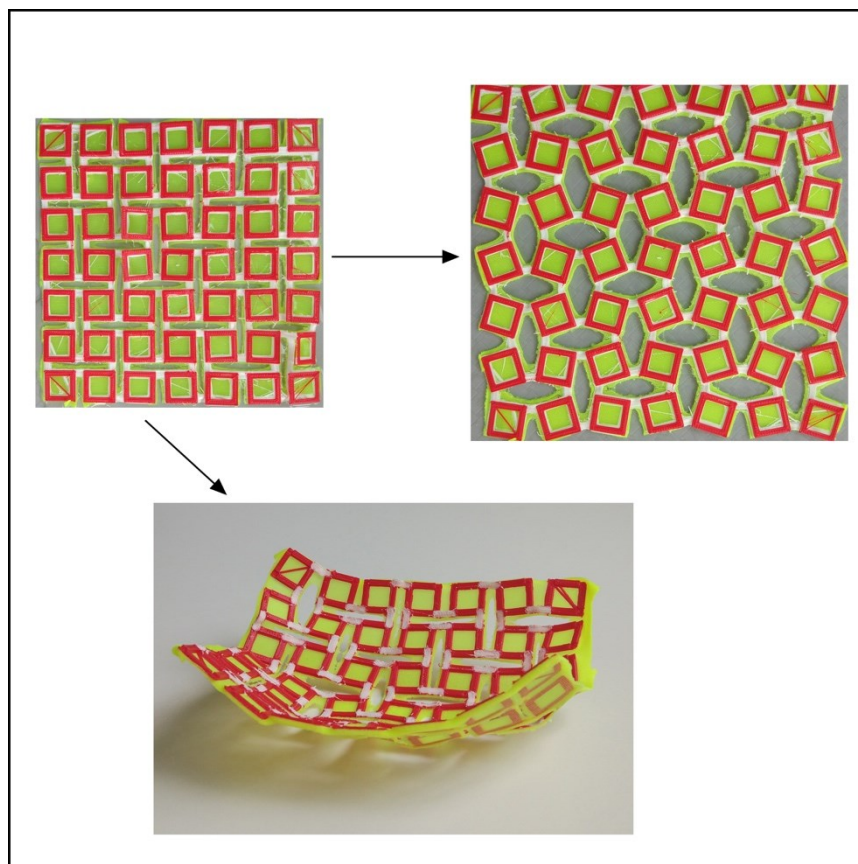

Fig. 11. 7x7 printed auxetic square structure on elastic jersey knit showing auxetic behavior with a Poisson's ratio of -0.9 (right) and also ability to form synclastic surfaces (bottom).

An alternative triangular auxetic form was also printed. The fabric was slit at the sides of the triangles to allow maximum extension in the transverse direction. The auxetic textile shown in Fig. 12 demonstrated a Poisson's ratio of -1.05 under simple extension.
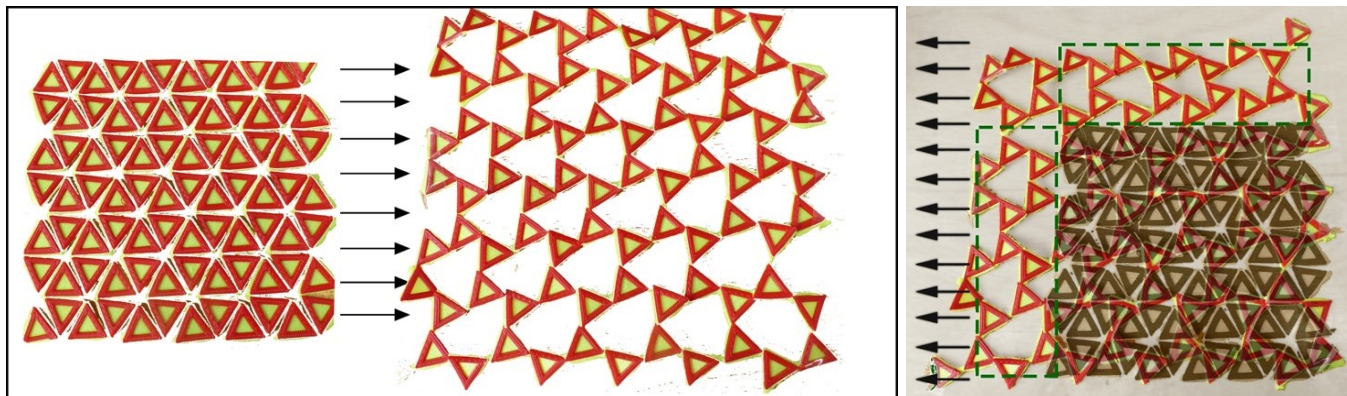

Fig. 12. Triangular auxetic structure printed onto elastic jersey knit showing an auxetic behavior with a Poisson's ratio of -1.05.

3.2   Triggered response

The use of PLA as the hinge material provides an additional interesting feature potential. Because the PLA has a relatively low glass transition temperature T_G, approximately 60-65° C, it is possible to heat the PLA above T_G but still stay below the T_G of the ABS (which is approximately 105° C). When above T_G, the PLA has extremely low modulus and can be deformed to a very high level. The structure can be heated above the PLA T_G, deformed, and then cooled. In this way the structure will maintain the deformed shape to a large extent.

In this way, one can manufacture a wrap which can form synclastic shapes when heated above 60 °C and retain that shape when cooled. This could be useful for any number of wraps, including casts for limbs, molds, prosthesis and more. Particularly when a synclastic shape is desired, these auxetic textile hybrids can provide such geometries without wrinkling or folding.

The wrap formed in this way will also return back to its original shape on heating, allowing reusability. When the structure is heated above the PLA T_G, the PLA acts as a rubbery material, enabling the squares to freely rotate. When the structure heated without applying any external force, the stored energy in the fabric will return it back to the original printed shape. Fig. 13 shows a time sequence of an auxetic textile hybrid. The original structure is that shown in Fig. 11 – a 7x7 printed square system. The hybrid was heated above 60 °C and extended then cooled. The image shown in the top left of Fig. 13 is the structure at room temperature. The PLA "froze" into place in the extended form. Warm water (60° C) was poured over the hybrid system and the next 7 images show the system over a period of less than one minute. The PLA gets above its T_G and then the stored energy in the knitted substrate returns the structure to its original shape. A reusable, synclastic structure is thus produced.
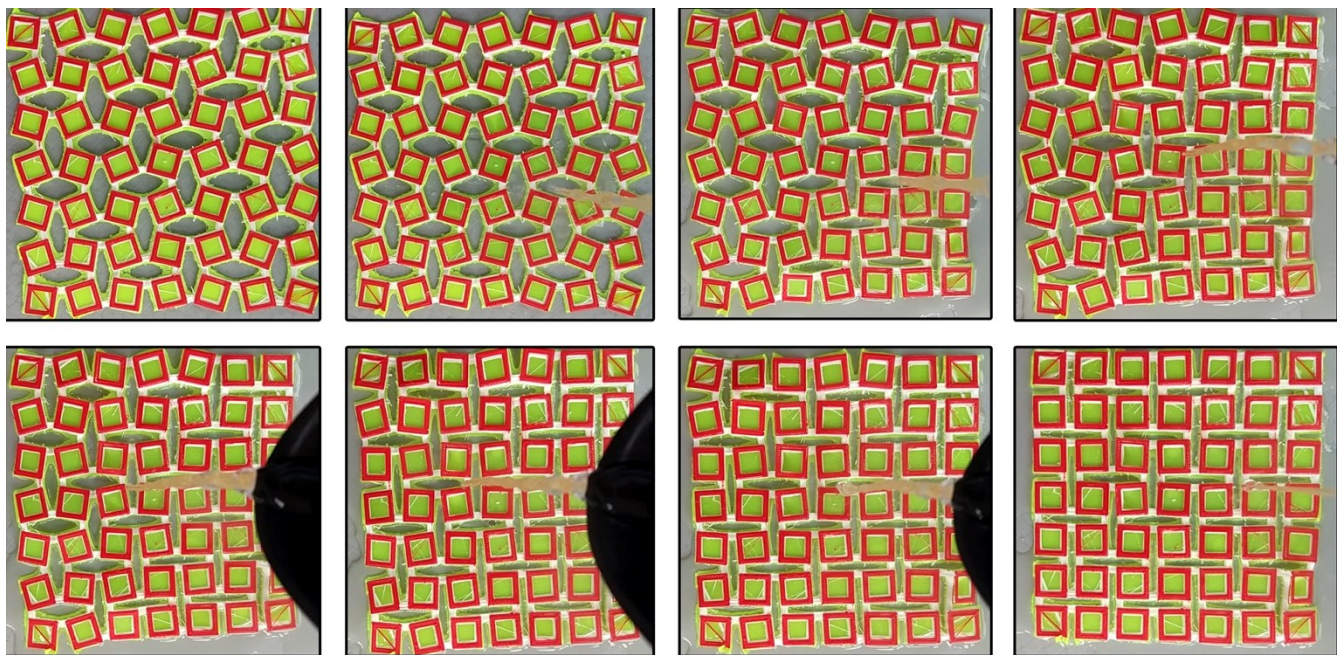
Fig. 13. A time sequence of an auxetic textile hybrid that was frozen into an extended shape (top left) and then introduced to 60 °C water. As the images progress from left to right on top, and then on the bottom from left to right, the structure changing shape back to the as-printed form can be seen.

4   Conclusion

Initially two different auxetic forms, rotating squares and rotating triangles, were printed on the pre-strained fabric to study the auxetic properties. Slits were made on the fabric in such a way that the fabric would act as a hinge for the rotating shapes. Rotating squares were chosen based on the ease to design and make slits.

PLA hinges were added to the structure because for a structure to function as a support wrap, it was necessary that wrap retained the necessary shape. The low glass transition temperature of PLA enabled the structure to change shape or form synclastic shapes when heated to temperature of 65° C because at temperatures above 60° C the modulus of rigidity of the PLA falls, enabling the squares to rotate freely when stretched.

References

[1]   S.D. Poisson. 1827. Note sur l'Extension des Fils et des Plaques élastiques. *Annales de Chimnie et Physique* 36, 384-387.

[2]   R. Lakes. 1987. Foam Structures with a Negative Poisson's Ratio. *Science* 235, 4792, 1038.1040. DOI: https://doi.org/10.1126/science.235.4792.1038.

[3]   K. E. Evans. 1991. Auxetic polymers: a new range of materials. *Endeavour* 15, 4, 170-174. DOI: https://doi.org/10.1016/0160-9327(91)90123-S.

[4]   J.N. Grima and K.E. Evans. 2006. Auxetic behavior from rotating triangles. *Journal of Materials Science* 41, 10, 3193-3196. DOI: https://doi.org/10.1007/s10853-006-6339-8.

[5]   J.N. Grima and K.E. Evans. 2000. Auxetic behavior from rotating squares. *Journal of Materials Science Letters* 19, 17, 1563-1565. DOI: https://doi.org/10.1023/A:1006781224002.

[6]   N. Ravirala, A. Alderson, and K.L. Alderson. 2007. Interlocking hexagons model for auxetic behaviour. *Journal of Materials Science* 42, 17, 7433-7445. DOI: https://doi.org/10.1007/s10853-007-1583-0.

[7]   M. Mir, M. N. Ali, J. Sami, and U. Ansari. 2014. Review of Mechanics and Applications of Auxetic Structures. *Advances in Materials Science and Engineering* 2014, 753496. DOI: https://doi.org/10.1155/2014/753496.

[8]   M. Sanami, N. Ravirala, K. Alderson, and A. Alderson. 2014. Auxetic Materials for Sports Applications. *Procedia Engineering* 72, 453-458. DOI: https://doi.org/10.1016/j.proeng.2014.06.079.

[9]   Z. Wang and H. Hu. 2014. Auxetic materials and their potential applications in textiles. *Textile Research Journal* 84, 15, 1600-1611. DOI: https://doi.org/10.1177/0040517512449051.

[10] Y. Prawoto. 2012. Seeing auxetic materials from the mechanics point of view: A structural review on the negative Poisson's ratio. *Computational Materials Science* 58, 140-153. DOI: https://doi.org/10.1016/j.commatsci.2012.02.012.

[11] G. E. Stavroulakis. 2005. Auxetic behaviour: appearance and engineering applications. *physica status solidi (b)* 242, 3, 710-720. DOI: https://doi.org/10.1002/pssb.200460388.

[12] C. W. Smith, J. N. Grima, and K. E. Evans. 2000. A novel mechanism for generating auxetic behaviour in reticulated foams: missing rib foam model. *Acta Materialia* 48, 17, 4349-4356. DOI: https://doi.org/10.1016/S1359-6454(00)00269-X.

[13] M. R. Sloan, J. R. Wright, and K. E. Evans. 2011. The helical auxetic yarn – A novel structure for composites and textiles; geometry, manufacture and mechanical properties. *Mechanics of Materials* 43, 9, 476-486. DOI: https://doi.org/10.1016/j.mechmat.2011.05.003.

[14] J. R. Wright, M. K. Burns, E. James, M. R. Sloan, and K. E. Evans. 2012. On the design and characterisation of low-stiffness auxetic yarns and fabrics. *Textile Research Journal* 82, 7, 645-654. DOI: https://doi.org/10.1177/0040517512436824.

[15] D. Rant, T. Rijavec, and A. Pavko-Çuden. 2013. Auxetic Textiles. *Act Chimica Slovenica* 60, 4, 715-723.

[16] S. C. Ugbolue, Y. K. Kim, S. B. Warner, Q. Fan, C.-L. Yang, O. Kyzymchuk, and Y. Feng. 2010. The formation and performance of auxetic textiles. Part I: theoretical and technical considerations. *Journal of the Textile Institute* 101, 7, 660-667. DOI: https://doi.org/10.1080/00405000902733790.

[17] C. Ugbolue, S., K. Kim, Y. and B. Warner, S. 2012. Engineered Warp Knit Auxetic Fabrics. *Journal of Textile Science & Engineering* 2, 1, 1000e103. DOI: https://doi.org/10.4172/2165-8064.1000e103.

[18] M. Starbuck, S. C. Anand, N. Ravirala, K. Alderson, and A. Alderson, 2008. Fabrics having knit structures exhibiting auxetic properties and garments formed thereby. Patent No. US 20080011021 A1, Jan. 17, 2008.

[19] Z. Wang and H. Hu. 2017. Tensile and forming properties of auxetic warp-knitted spacer fabrics. *Textile Research Journal* 87, 16, 1925-1937. DOI: https://doi.org/10.1177/0040517516660889.

[20] S. C. Anand and D. Skertchly. 2010. Auxetic knitted fabric. Patent No. WO 2010125397 A1, Nov. 4, 2010.

[21] P. Verma, M. L. Shofner, A. Lin, K. B. Wagner, and A. C. Griffin. 2015. Inducing out-of-plane auxetic behavior in needle-punched nonwovens. *physica status solidi (b)* 252, 7, 1455-1464. DOI: https://doi.org/10.1002/pssb.201552036.

[22] S.M. Felton, M. T. Tolley, B. Shin, C. D. Onal, E. D. Demaine, D. Rus, and R. J. Wood. 2013. Self-folding with shape memory composites. *Soft Matter* 9, 32, 7688. DOI: https://doi.org/10.1039/c3sm51003d.

[23] E. A. Peraza-Hernandez, D. J. Hartl, R. J. Malak Jr,, and D. C. Lagoudas. 2014. Origami-inspired active structures: A synthesis and review. *Smart Materials and Structures* 23, 9, 094001. DOI: https://doi.org/10.1088/0964-1726/23/9/094001.

[24] V. Turk. 2015. Space Origami Could Pack Big Structures into Tiny Satellites. Retrieved August 14, 2021 from https://www.vice.com/en/article/ezp4mm/space-origami-could-pack-big-structures-into-tiny-satellites.

[25] Y. Liu, H. Hu, J. K. C. Lam, and S. Liu. 2010. Negative Poisson's Ratio Weft-knitted Fabrics. *Textile Research Journal* 80, 9, 856-863. DOI: https://doi.org/10.1177/0040517509349788.

[26] G. J. Brinks, M. M. C. Warmöskerken, R. Akkerman, and W. Zweers. 2013. The added value of 3D polymer deposition on textiles. Proc. of 13th AUTEX World Textile Conference, Dresden, Germany.

[27] E. Pei, J. Shen, and J. Watling. 2015. Direct 3D printing of polymers onto textiles: Experimental studies and applications. *Rapid Prototyping Journal* 21, 5, 556-571. DOI: https://doi.org/10.1108/RPJ-09-2014-0126.

[28] L. Sabantina, F. Kinzel, A. Ehrmann, and K. Finsterbusch. 2015. Combining 3D printed forms with textile structures - mechanical and geometrical properties of multi-material systems. *IOP Conference Series: Materials Science and Engineering* 87, 012005. DOI: https://doi.org/10.1088/1757-899X/87/1/012005.

[29] D. Schmelzeisen, H. Koch, and C. Pastore. 2018. 4D-Textiles: Hybrid textile structures that change structural form with time. In Y. Kyosev, Mahltig, B., and A. Schwarz-Pfeiffer (Eds.). *Narrow Fabrics and Smart Textiles*. Springer International Publishing.

[30] K. Simonis, D. Schmelzeisen, V. Gesché, and T. Gries. 2017. 4D textiles: application in sports industry. *Future Textiles* 2, 2, 38-39.

[31] A. Narula, C. M. Pastore, D. Schmelzeisen, S. El Basri, J. Schenk, and S. Shajoo. 2018. Effect of knit and print parameters on peel strength of hybrid 3-D printed textiles. *Journal of Textiles and Fibrous Materials* 1, 251522111774925. DOI: https://doi.org/10.1177/2515221117749251.

[32] R. Melnikova, A. Ehrmann, and K. Finsterbusch. 2014. 3D printing of textile-based structures by fused deposition modelling (FDM) with different polymer materials. *IOP Conference Series: Materials Science and Engineering* 62, 012018. DOI: https://doi.org/10.1088/1757-899X/62/1/012018.

Appendix A. Printing Parameters

The printing parameters used for this project are contained in the table below. There were slight differences in the settings used for the ABS and PLA materials.

printMaterial	PLA	ABS	units
extruderName	Extruder 1	Extruder 2	
extruderToolheadNumber	0	1	
extruderDiameter	0.4	0.4	mm
extruderWidth	0.4	0.4	mm
extrusionMultiplier	0.9	1	
extruderUseRetract	1	1	
extruderRetractionDistance	1	1	
extruderExtraRestartDistance	0	0	
extruderRetractionZLift	0	0	
extruderRetractionSpeed	1800	1800	
extruderUseCoasting	0	0	
extruderCoastingDistance	0.2	0.2	mm
layerHeight	0.2	0.2	mm
topSolidLayers	3	3	
bottomSolidLayers	3	3	
perimeterOutlines	2	2	
firstLayerHeightPercentage	90	100	
firstLayerWidthPercentage	100	100	
firstLayerUnderspeed	0.5	0.5	
internalInfillPattern	Rectilinear	Rectilinear	
externalInfillPattern	Rectilinear	Rectilinear	
infillPercentage	20	20	
outlineOverlapPercentage	15	15	
infillExtrusionWidthPercentage	100	100	
minInfillLength	5	5	
infillLayerInterval	1	1	
infillAngles	45	45	
SetpointTemperatures	190	225	°C
fanLayers	2	1	
fanSpeeds	100	0	
defaultSpeed	3600	5400	
outlineUnderspeed	0.5	0.5	
solidInfillUnderspeed	0.8	0.8	
supportUnderspeed	0.8	0.8	
rapidXYspeed	4800	4800	
rapidZspeed	1000	1000	